A Loop-Based Approach for Topological Processing of Mobility and Subsystem Rigidity in Complex Spatial Multibody Systems

Von der Fakultät für Ingenieurwissenschaften,

Abteilung Maschinenbau und Verfahrenstechnik der

Universität Duisburg-Essen

zur Erlangung des akademischen Grades

eines

Doktors der Ingenieurwissenschaften

Dr.-Ing.

genehmigte Dissertation

von

Florian Simroth

aus

Rostock, Deutschland

Referent: Prof. Dr.-Ing. Dr. h. c. Andrés Kecskeméthy

Korreferent: Prof. Mag. Dr. Dr. h. c. Manfred Husty

Tag der mündlichen Prüfung: 29. Juli 2020

To my grandfather Hans-Jürgen Brosin
who inspired me to take this path

Acknowledgements

Arriving at the end of this journey of enlightening discoveries, inspiring people, and plenty of opportunities to grow, I realize that I owe my deepest appreciation to these amazing people accompanying me along this journey, and who made the successful conclusion of this work possible in the first place.

First of all, I would like to express my sincere appreciation to my advisor Prof. Andrés Kecskeméthy for his trust, patience, immense scientific experience, and his passion for this field of research. I would also like to extend my gratitude to Prof. Manfred Husty for his active interest and thorough review of my thesis.

An extraordinary scientific and cultural experience constitutes my research at the Shanghai Jiao Tong University which would not have been possible without the friendly cooperation and warm welcome of Prof. Haidong Yu and his whole team. Especially helpful to me at this were the guidance of Canming Yi and Haoming Zhang through the Chinese culture and some peculiar dishes, as well as the thought-provoking and fruitful scientific discussions with Prof. Huiping Shen, for which I am greatly thankful.

During my time in Duisburg, I was truly fortunate that I had the opportunity to work with such a great and encouraging research team, with who I do not only share numerous enjoyable conversations and active after-lunch breaks. I also owe a greater part of the completion to their continuous support and motivation, lasting even beyond my time at the department. In this regard, I would particularly like to thank my long-term office colleague Dr. Nikolas Bufe for rewarding discussions and wise counsel in all circumstances. Working with Dr. Matthew Millard during my very first year of teaching has been a great pleasure and an inspiring time. I very much appreciate the assistance from my undergraduate and graduate students, notably the work of Jan Laufkötter.

I would like to pay my special regards to my fellow student and friend Florian Roscheck, for his invaluable comments on this thesis, spirited life advice, and his encouraging optimistic attitude.

After all, I would not have been able to go the extra mile without the unconditional support of my family and friends. I am deeply grateful for your loyalty, understanding, and patience. Thank you that you have always been there for me!

Hamburg, October 2020 Florian Simroth

Abstract

For a given system of bodies whose relative motions are described by a set of constraints, the dimension of these allowed motions can provide valuable information about the physical properties of this system. The special case of rigidity is of particular interest for multidisciplinary research, e.g., for the analysis of crystal lattices, granular packings, the definition of placement conditions in CAD systems, or the synthesis of multibody systems. This thesis is dedicated to the recognition of rigid substructures in the context of multibody systems.

The number of possible motions is characterized by the concept of the degree of freedom, for which several established classifications are reviewed, and three additional categories, namely fully, transmitted, and structurally isolated degrees of freedom are introduced. Based on this classification, it is now possible to recognize not only absolutely rigid systems, but also those that are rigid in character, yet have isolated degrees of freedom, e.g., in the form of bodies that can rotate freely between two spherical joints.

For this purpose, a multibody system consisting of rigid bodies and joints is topologically understood as a network of coupled modular multibody loops, which simplifies the recognition of efficient recursive solutions and enables a uniform consideration of planar, spatial and mixed systems. The isolated degrees of freedom are first independently identified in the individual multibody loops based on their displacement groups. Afterward, they are tracked across the couplings of the network and are classified with respect to newly introduced categories. In a graph, rigid subsystems, both with and without isolated degrees of freedom, can be identified by means of simple graph cuts. Through subsequent replacement of the determined rigid subsystems by simple bodies, the complexity of a multibody system can be reduced. Overdetermined parts that lead to false assumptions counting the degree of freedom are thus identified, enabling a better determination of the actual degree of freedom of a system. Finally, the procedure is successfully applied to well-known counter-examples in which conventional formulas for determining the degree of freedom lead to incorrect results.

Contents

1 Introduction

One of the probably most fundamental properties immanent to a mechanical system is its degree of freedom, which provides insight on the number of independent movements its components can undergo. It decides on whether a mechanism is capable of performing a particular type of motion, indicates the number of necessary actuators, or reveals that an assembly may not be able to move at all.

Thus, its correct determination has attracted researchers ever since the nineteenth century, bringing up a wide variety of different algorithms. Especially the peculiar case of an assembly with zero degrees of freedom, which is then referred to as a structure finds its application even beyond the field of mechanics. As such, in material science some macroscopic properties like material strength can be better understood by identification of underlying microscopic rigid and flexible subsystems as for covalent glass networks (Thorpe, 1985), insights on proteins and molecules can be gained (Feng and Sen, 1984; Jacobs et al., 2002, 2001; Whiteley, 2005), or granular packings can be analyzed (Bedi and Chakraborty, 2018). In the design of novel mechanisms or structural optimization for achieving kinematics with enhanced performance, automated synthesis methods were introduced for which, though, degenerate specimens containing rigid subsystems have to be detected and sorted out (Ding, 2015). When assembling complex models in computer-aided design programs, users introduce geometric constraints forming a constraint graph, for the solution of which it is important to detect not yet defined (flexible), or overconstrained subsystems leading to inconsistencies (Lee, 2008; Moinet et al., 2014).

The variety of applications explains the great interest in rigidity theory and long-lasting research in this area. While the two-dimensional case of generic rigidity has been solved by Laman (1970) for bar-and-joint systems, the spatial problem is still an open challenge, since a characterization of generic rigidity based only on combinatorics is not available (Kitson and Power, 2018).

While general counting formulas are doomed to fail as they do not account for specific topological peculiarities, pure combinatorial approaches though are in general quite performant, yet usually, apply only to specific cases such as body-bar frameworks with limited applicability to general mechanisms. Methods numerically analyzing the set of constraint equations for dependencies, in general, deliver correct results for a particular realization of a mechanism, presuming numerical values for dimensions are known. However, the full set of equations has to be established at first, particular caution has

to be exercised in the neighborhood of any singularities, and regarding only a single configuration does not permit a direct conclusion on the general degree of freedom. A remedy to these shortcomings is promised by the symbolic processing of these equations as proclaimed by Gogu (2008), which would theoretically deliver not only correct results with respect to the degree of freedom, but would even return conditions for the presence of singularities or redundant constraints. Though determining the dependence of symbolic equations is non-trivial, thus (over-) stretching the capabilities of current computer algebra systems and even for simple cases may consume a considerable amount of time. Therefore, there remains a high demand for efficient approaches tackling mobility and rigidity determination for the spatial case.

The underlying idea of the present approach is to regard a mechanism, not as an assembly of bodies and joints, but instead as a network of interconnected kinematic loops introduced by Kecskeméthy (1993b). The method proved particularly suitable to derive (possibly closed-form) efficient solutions for systems with many coupled loops whose implementation in MATHEMATICA (Wolfram Research, Inc., 2019) was presented by Kecskeméthy et al. (1997). The structural properties of each of these loops are first analyzed individually, effectively breaking down the overall system into several smaller ones, in a way that naturally spatial, spherical, and planar subsystems may be mixed, for which often efficient solutions can be found. Reconstituting these "building blocks" into a connected network and tracking the transmission of relative kinematics then allows identifying potentially rigid or overconstrained subsystems, which reduces the general search space.

For the structural analysis, a symbolic approach is pursued, for which symbolic operators express the relative kinematics by elementary rotations and translations, sufficient to describe any general rigid body displacement. By analysis of invariant properties such as points, lines, and planes, geometric characteristics can be captured to some extent without the necessity to symbolically analyze the set of in general non-linear closure conditions.

Building upon previous work by Xia et al. (2012), the main contribution of this work is an approach to track and detect subsystems with isolated degrees of freedom, which for instance, are present in spatial mechanisms of spherical joints and bars. For this purpose, three new categories of isolated degrees of freedom are proposed for the detection of which concepts of group theory are used. Necessary to that end is to automatically associate joints expressed by sequences of rotational and translational transformations to corresponding displacement subgroups, for which an appropriate method

is described. Furthermore, a quick determination of the mobility number of single-loops based on isotropy groups following the idea of Kecskeméthy and Hiller (1992) is elaborated and a universal procedure to treat multiple joints and also derive resulting non-linear coupling conditions is provided. The approach is applied successfully to well-known counterexamples to which end also "implicit" edges are of concern.

1.1 Literature Overview

In this section, an overview of different available approaches to determine the degrees of freedom of a multibody system, and consequently, to detect rigid subsystems shall be given. To this end, the following definition for degrees of freedom (or mobility) will be used, which will be discussed in more detail in sec. 2.4:

> "The mobility of a mechanism is the number of input parameters (usually pair variables), which must be independently controlled in order to bring the device into a particular position." (Shigley and Uicker, 1995, p. 12)

If the degree of freedom is less or equal to zero, the system is regarded as a (rigid) structure, where a negative degree of freedom indicates that the structure is overconstrained. As coverage of the topic of degrees of freedom to its full extent would go far beyond the scope of this work, it was attempted to organize the general concepts by type of methodology, though boundaries often blur.

1.1.1 Counting Formulas

Probably the most straightforward and fastest approach is the determination of degrees of freedom by counting formulas that take into account only the most fundamental properties as the number of bodies and joints, type or degree of freedom of the respective joints and a parameter describing the "motion type" of the system. Gogu (2008) provides an exhaustive discussion of counting formulas and their deficiencies in determining the correct degree of freedom for general mechanisms, from which some key points will be reviewed hereafter.

Over 150 years ago, Chebyshev provided a formula for determining the degrees of freedom of a mechanism (Chebyshev, 1854). He specified the number of links and joints necessary to form planar mechanisms with one degree of freedom. Sylvester (1875)

modifies the equation such that it can be applied to planar linkages with one degree of freedom without a declared base frame and also mentions how multiple joints are to be counted. Grübler (1883) picks up on Sylvester's equation, which he later extends to the spatial case with helical joints, still regarding only systems with one degree of freedom (Grübler, 1917). To unite the calculation of degrees of freedom for planar and spatial mechanisms within one formula, Somov (1887) introduces a motion parameter indicating which of both is concerned. Kutzbach (1929) introduces a formula for the calculation of the degree of freedom for spatial and planar mechanisms benefitting from the motion parameter and furthermore taking into account joints with variable degrees of freedom, though the whole system has to be subject to the same motion type. The contributions of Chebyshev, Grübler, and Kutzbach are grouped into the well-known Chebyshev-Grübler-Kutzbach formula, published in a variety of versions, which in its original form sums up the degrees of freedom of all joints and subtracts the number of constraints introduced by the closure of the independent kinematic loops of a mechanism assuming one common motion type. Through extensions by Voinea and Atanasiu (1960) and Manolescu and Manafu (1963) also loops of different motion types can be mixed. Indeed, the most challenging part is to determine the correct motion parameter for the individual kinematic loops, for which a pure observation of the number and type of joints and links is not sufficient, as well as the number of dependent constraints within the assembled system. Though, if these are known, a universally valid formalism for the number of degrees of freedom of mechanisms can be stated:

> "[...] the number of independent coordinates (parameters) needed to define the configuration of a mechanism with closed loops is the difference between the number of independent motion parameters of the joints [...] before loop closures provide further constraints, and the number [...] of joint parameters that lose their independence after loop closures." (Gogu, 2008, p. 63)

In fact, the Chebyshev-Grübler-Kutzbach formula yields a lower bound for the degree of freedom such that the apparent degree of freedom (see sec. 2.4.2) is always greater than or equal to the thereby obtained degree of freedom. As a consequence, on the one hand, the ability to correctly determine the degree of freedom of a (sub-) system is required for the detection of rigid (sub-) systems. On the other hand, knowledge (and replacement) of overconstrained rigid subsystems within a mechanism reveals dependent constraints and therefore aids the correct determination of the overall degree of freedom.

1.1.2 Analysis of the Jacobian Matrix

In general, this problem can be solved mathematically by analysis of the rank of the Jacobian matrix derived from the constraint equations of the multibody system. A loss of rank indicates the redundancy of some of the constraint equations, increasing the degree of freedom. As pointed out by Gogu, Moroskine (1954) already referred to this relationship, and furthermore Angeles and Gosselin illustrated for several examples how "the degree of freedom of the chain can be uniquely computed as the dimension of the nullspace of the said matrix." (Angeles and Gosselin, 1988, p. 219). The analysis of the Jacobian and its condition number is often used in the context of parallel manipulators and reveals sensitivities of input to output velocities as well as insights on singular configurations for instance, in (Merlet, 2005a; Wang and Gosselin, 1998; Yang et al., 2008). For the detection of a rigid or overconstrained subsystem, as required in computer-aided design, the Jacobian can be determined for a specific realization called a witness and provides insights on redundantly placed constraints by a user (Foufou and Michelucci, 2012; Michelucci and Foufou, 2006). Though, the establishment of the set of constraint equations is cumbersome, especially for complex mechanisms. In addition, the numerical calculation of the rank of the Jacobian matrix presumes that numerical values for all dimensions are known, and then consequently only returns the correct degree of freedom for the given realization of the mechanism. Furthermore, in the proximity of a singular configuration, one has to be cautious regarding the interpretation of obtained numerical values. Gogu proclaims the symbolic rank determination by the use of available computer-algebra systems as a resort to these issues, though, this is a non-trivial task, and despite ongoing research, capabilities for the symbolical analysis of equations for these systems are still somewhat limited and time-consuming.

1.1.3 Approach Based on Lie Groups

An approach for the analysis of degrees of freedom of kinematic chains that does not depend on actual dimensions and numerical values is based on the concept of group theory and was first introduced by Hervé (1978). In general, any rigid body displacement can be understood as an affine transformation, and it can be shown that the set of rigid body displacements forms a group. Indeed, the set of all relative displacements between two bodies within a kinematic chain whose constrained relative motion is a subset of the rigid body displacements and under certain circumstances may form a subgroup

that leaves some geometric properties invariant. For instance, if two bodies connected by a revolute joint perform two subsequent rotations about the joint axis, the result is again a rotation about the same axis by an angle corresponding to the angle sum. By mathematical group composition and intersection, relationships about the relative degrees of freedom of bodies can be determined from the dimension of the corresponding displacement subgroup. By this means, the degrees of freedom of kinematic chains can be derived without the knowledge of actual dimensions, as described by Angeles (1988). Herve classified the chains for which this method is applicable into trivial, exceptional, and paradoxical chains, whereby the first two categories can be examined using the group approach, while for the latter one, geometric information needs to be involved. The concept is used for the mobility analysis of kinematic chains and was further developed by Fanghella and Galletti (1994) as well as Rico Martínez and Ravani (2003) and was also used by Thomas and Torras (1988) in the context of computer-aided design. This approach has been complemented with Lie algebra on screws, which transfers the analysis from finite to infinitesimal kinematics (Hervé, 1999; Müller and Maißer, 2003; Rico Martínez et al., 2003). Furthermore, Lee and Hervé (2002) applied this approach successfully to analyze discontinuous mobilities.

1.1.4 Approach Based on Assur Groups

Another concept used for structural analysis of mechanisms is based on Assur groups, commonly used in eastern Europe and Russia, which originates in the work of Assur (1913) but became especially popular after its adoption by Artobolevskii (1951). The term group here is not to be confused with the previously regarded mathematical definition but instead declares a set of planar kinematic chains with zero degrees of freedom when fixed at the terminal joints, with the additional property of being minimal in the sense that no simpler substructures may be yielded by the removal of one or more links (Pennock and Kamthe, 2006). The underlying idea is that these chains can be used for a sequential assembly of many technical mechanisms by subsequent addition, such that the kinematic equations can be derived in a hierarchical fashion. As a result, the complexity of mechanisms can be broken up into simpler modules, which leads to a variety of decomposition schemes. Fields of application are for instance the synthesis of mechanisms by adding Assur groups to a driving mechanism (Campos et al., 2008; Jinkui and Weiqing, 1998; Manolescu, 1979), position analysis in particular also including singular positions (Mitsi et al., 2003; Servatius et al., 2010b), or generation and analysis of Baranov trusses by attaching the terminal joints of an Assur group to a

single base frame (Rojas and Thomas, 2012). More recently, Servatius et al. (2010a,b) presented the analogies to rigidity theory and showed how existing combinatorial concepts could directly be merged with the theory of Assur groups (Nixon et al., 2014; Shai et al., 2013; Sljoka et al., 2011). Since being limited in its original form to planar mechanisms, efforts are undertaken to extend the theory also to the spatial case (Yang et al., 2015).

1.1.5 Representation as Frameworks

The analysis of frameworks with respect to rigidity and degrees of freedom such as bar-joint, body-bar, body-hinge, or even body-cad[1] frameworks, to which many kinds of technical kinematic chains can be mapped, is an active field of research, especially among mathematicians. This generalized treatment allows a graph representation, i. e., in bar-joint frameworks, joints and bars are expressed by vertices and edges respectively, together with a configuration assigning coordinates to the vertices. Constraints induced by the edges can be expressed in a rigidity matrix subject to further analysis. One can distinguish between the geometric aspect, taking into account a specific embedding in space, and a combinatorial aspect, concerning the topology, i. e., the number and distribution of edges. The analysis of these frameworks with respect to rigidity dates back to 1864 when Maxwell (1864) stated a general condition for a statically determined spatial joint-bar framework. In 1970 Laman proposed a relationship between the number of bars and joints in planar bar-joint frameworks for minimal rigidity that has to be fulfilled for each subsystem in order for the overall framework to be minimally rigid. In consequence, a variety of algorithms based on Laman's theorem were derived: Sugihara (1980) introduced the first polynomial-time algorithm, followed by further algorithms with improvements based on determining the network flow (Imai, 1985), matroid sums (Crapo, 1990; Gabow and Westermann, 1992), bipartite matching (Hendrickson, 1992) and a generalized "pebble game" (Jacobs and Hendrickson, 1997), by which not only rigid but also overconstrained subsystems could be identified. However, a generalization of Laman's theorem to three dimensions is not directly possible, since, for the spatial case, it only states a necessary though not sufficient criterion as the example in sec. 6.1 illustrates. Though for body-bar frameworks, Tay's characterization gives a combinatorial approach to treat rigidity in n-dimensional space (Tay, 1984). An algorithm that makes use of this description and recursively merges rigid subsystems reducing average run time is found, for instance, in (Moukarzel, 1996) and for body-bar frameworks

[1] These frameworks include constraints specifically present in computer aided design.

incorporating multiple joints by using a mixed constraint graph in (Shai and Müller, 2013). Franzblau (2000) introduced additional edges to model bond angles in (spatial) molecules to receive upper and lower bounds on the generic degree of freedom. The search for combinatorial criteria for the spatial case continues (Chubynsky and Thorpe, 2007; Connelly, 2005; Jackson and Jordán, 2005; Servatius and Servatius, 2010), just to name a few. Cheng et al. (2009) also emphasize the existence of non-trivial rigid subsystems with implied edges. Particularly body-cad frameworks attract recent attention for identification of redundant constraints (Farre et al., 2016; Haller et al., 2012; Jackson and Owen, 2016; Lee-St. John and Sidman, 2013).

1.1.6 Other Approaches

Some other mainly graph-based methods often use simplification and decomposition techniques. Agrawal and Rao (1987a), for instance, present a method using a path loop connectivity matrix for detecting fractionated degrees of freedom. An example of a loop-decreasing method for the detection of degenerate chains in planar closed-loop chains with revolute joints only is provided by Hwang and Hwang (1991), which though according to Sunkari and Schmidt (2005) does not properly detect all degenerate chains. Another method for rigid subchain detection that subsequently removes binary chains and as a result of this reduces complexity is proposed by Lee and Yoon (1992), which was later adopted by Sunkari (2006) for the structural analysis and synthesis of planar and spatial mechanisms that are compliant with the Chebyshev-Grübler-Kutzbach formula. Tuttle (1996) first generated rigid chains with seven or fewer links, and then through matching, identified these more complex systems. In the context of mechanism synthesis, a method for detecting degenerate chains within simple planar kinematic chains and chains containing multiple joints based on an independent set of kinematic loops was presented by Ding et al. (2008). Xia et al. (2012) proposed a loop-based development for planar, spherical, spatial as well as mixed systems for the detection of rigid and overconstrained subsystems analyzing the kinematic network. This approach has the advantage of complexity reduction by decomposition into individual smaller closed kinematic chains and was extended to spatial cases with isolated degrees of freedom by Simroth et al. (2015c).

1.2 Goal and Limitations

The goal of the present work is to identify whether a kinematic chain contains rigid or overconstrained subsystems at the possible presence of isolated degrees of freedom and, in this particular case, to localize the parts of which the rigid subsystem is composed. The idea starts from the premise that isolated degrees of freedom, i. e., degrees of freedom that leave a characteristic measurement of a kinematic chain unaltered (see sec. 5.2.1) have no effect on the transmission of motion within a kinematic chain and consequently, subsystems which only possess isolated degrees of freedom can be regarded as rigid. To that end, it is necessary to be able to (1) identify isolated degrees of freedom within kinematic chains and (2) to track these within kinematic networks, such that it is possible to detect structurally rigid subsystems despite a degree of freedom greater than zero.

When speaking of degrees of freedom, if not declared otherwise, finite or full-cycle (see sec. 2.4.3) mobility is of concern, denoting the number of possible independent finite displacements within a mechanism. It is assumed that the correct degree of freedom of the individual kinematic loops can be determined by the method based on isotropy groups described in sec. 3.3. For this reason, this work confines to ordinary multibody systems with rigid bodies and idealized joints. Implicated by the underlying symbolic representation of kinematic chains through elementary translations and rotations, certain geometric properties resulting from specific lengths and angles cannot be accounted for, thus excluding paradoxical and some exceptional kinematic chains. For the detection of isolated degrees of freedom, the involved joints are assumed to be representable by subgroups of rigid body displacements, which is valid for all lower pair joints and some even more complex constructs.

1.3 Overview of the Present Work

In ch. 2, some general concepts of degrees of freedom in multibody systems are introduced. For this reason, first, the essential elements and terms of multibody systems are reviewed, and a classification of a multibody system with respect to its topological structure is depicted. Afterward, awareness is raised for challenges encountered when using the general degree of freedom counting formulas in sec. 2.4.1. For better distinction, several general concepts of degrees of freedom are reviewed, which also reveals some ambiguities regarding the terminology used. In sec. 2.5 the concept of isolated

degrees of freedom as used throughout this work is introduced, and classification into three different types is proposed.

The kinematic foundation for the concept of kinematic networks is laid in ch. 3. This chapter shall provide both, the basic background on kinematics necessary to grasp the concept of a kinematic transformer, and an introduction to the group-theoretic perspective of rigid body displacements, which will be utilized for the detection of isolated degrees of freedom in ch. 5. To ease the understanding of displacement subgroups, a rather theoretic description of the single rigid body kinematics is chosen in sec. 3.1. In a similar manner, next, open kinematic chains are first regarded as group compositions of displacement subgroups, and afterward, the kinematics are derived by concatenation of elementary rotations and translations in sec. 3.3. At last, single-loop kinematic chains are analyzed and classified with respect to their displacement group properties, the derivation of closure conditions using isotropy groups is discussed, and finally, the results are incorporated within a building block of a kinematic transformer.

The mapping of multibody systems to graphs is addressed in ch. 4. For this purpose, at first basic graph-theoretic elements and terminology are illustrated in sec. 4.1. Since only closed kinematic chains come into consideration for rigidity detection, a topological analysis is conducted, and respective subsystems are extracted according to sec. 4.2. After that, the concept of kinematic networks is explained, to which end it is necessary to decompose the extracted subsystems into sets of independent loops as discussed in sec. 4.3.1. Based on this network, general dependencies between the loops and a favorable sequence in which the elements can be processed is derived. At last, the efficient implementation and derivation of general coupling conditions for multiple joints within the graph-theoretic context is covered. The chapter concludes with a method for the automated association of displacement subgroups to joints composed of concatenated elementary transformations, which is required both for the detection and treatment of multiple joints as well as for the identification of isolated degrees of freedom in the next chapter.

Afterward, ch. 5 elaborates on the identification of isolated degrees of freedom in sec. 5.1, utilizing the concept of group intersection for displacement subgroups. In sec. 5.2 a unique designation for isolated degrees of freedom is declared, which allows for tracking and classifying isolated degrees of freedom within kinematic networks. The detection of rigid subsystems is then first demonstrated in sec. 5.3 for systems without isolated degrees of freedom, thus exemplifying the dependencies within the kinematic network in the form of a loop connection graph. The method is then extended such

that isolated degrees of freedom can be accounted for, and insights on the reduction of search space are given. At last, a summary is provided, including all necessary steps.

The capabilities of the method are then demonstrated in ch. 6 for two non-trivial examples comprising isolated degrees of freedom. In particular, the first example is a well-known counterexample to the general Chebyshev-Grübler-Kutzbach formula, while the second example features the peculiarity of containing rigid subsystems which are mobile when detached. The significant results of this work are then summarized and reflected in ch. 7.

2 Mobility Determination in Multibody Systems

The use of computers for the design and analysis of mechanical systems greatly reduces development time, the need for prototypes, and physical tests. Of main interest are the described motions as well as the internal forces and moments which result from interaction with the external environment. One of the probably most fundamental properties and key elements of this work are the degrees of freedom (also termed *mobility*) of a mechanical system, which determine whether it is capable of accomplishing the intended tasks or if there exist rigid subsystems that can be reduced to a single entity. For this reason, a mathematical model of the physical-mechanical system is required whose general setup will be addressed in the next section, and afterward, different types and classifications of degrees of freedom will be covered.

2.1 Introduction to Multibody Systems

A mechanical system is characterized by its deformable components with physical properties as inertia, elasticity, viscosity, and distributed forces acting on their volumes and surfaces. When using the methodology of continuum mechanics, these systems can be described by partial differential equations which depend on time and location. Yet, analytical solutions are only available for special cases, such that numerical solutions for general cases can only be found by mathematical discretization. However, for mechanical systems, it is often favorable to start the discretization process already when deriving the mathematical model from the mechanical system. Typical examples of discretized models are finite-element systems or multibody systems (Woernle, 2016). At this, multibody systems are usually resolved in a much coarser fashion than finite-element systems, making them particularly suitable for the simulation of the dynamic behavior of complex mechanical systems and large motions.

2.2 Elements of Multibody Systems

A multibody system can be seen as an idealized model of a mechanical system, whose components are *rigid bodies* on which forces and moments are acting. The underlying idea of multibody systems is to mimic the physical properties of real mechanical systems as inertia, elasticity, viscosity, and force by discrete and idealized elements, as shown in fig. 2.1. This allows for the derivation of a computationally more efficient set of

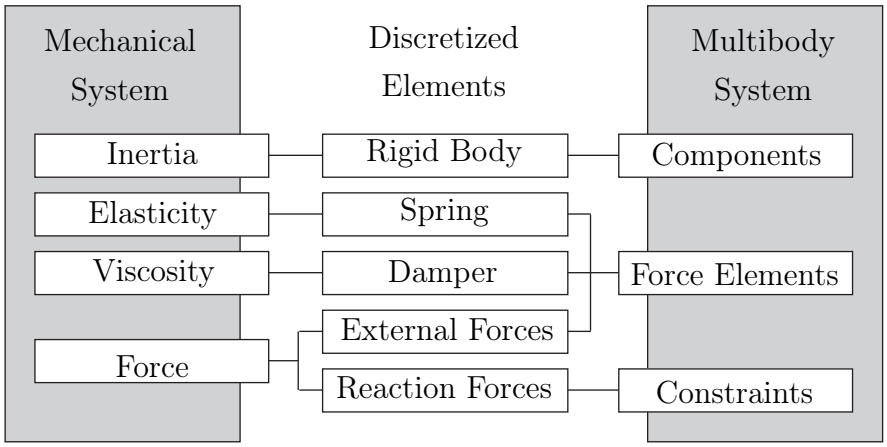

Figure 2.1: Ideal multibody system

equations compared to continuous models. The forces and moments of a multibody system can then be grouped into external and reaction forces and moments. External forces are applied in the form of massless *force elements* like springs, dampers, or actuators, as well as force fields like gravitation. Reaction forces, on the other hand, are the result of restricting relative motions of bodies by adding *constraints* to the model.

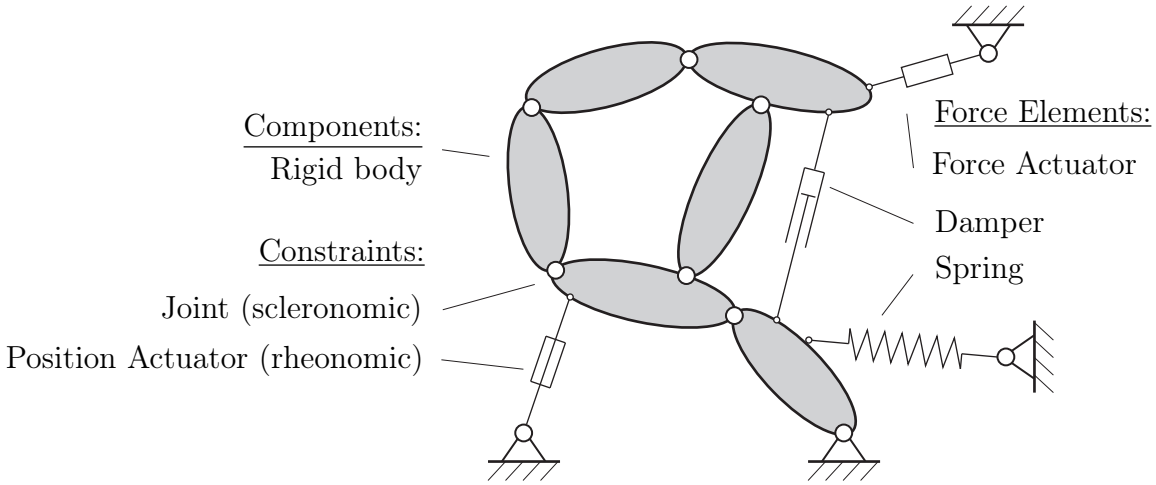

Figure 2.2: General multibody system (cf. Woernle, 2016, p. 2)

2.2.1 Mass Related Elements

Mass related elements of mechanical systems are usually idealized as point masses or rigid bodies in an ordinary multibody system or as deformable bodies in case of flexible

multibody systems. A rigid body is formed by a discrete or continuous set of material points for which, in contrast to deformable bodies, any two body-fixed reference points do not change their relative position (Samin and Fisette, 2003). Indeed, many mechanical systems are purposefully designed by appropriate choice of materials and material thicknesses to keep deformations negligibly small in comparison to the overall motion, thus justifying the assumption of rigid bodies for many technical applications. Each rigid body $\mathcal{B}_i$ with mass m_i and inertia tensor $\mathbf{\Theta}_i$ is characterized by a set of

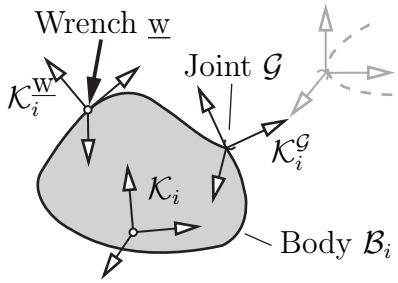

Figure 2.3: Kinematic skeleton of a rigid body

body-fixed frames which form a kinematic skeleton and usually refer to one body-fixed base frame. Depending on the formalism used to set up the system of equations, the origin of the base frame is often beneficially chosen at the center of mass and its axes oriented along the principal axes of the inertia tensor. Further frames $\mathcal{K}_i^{\mathcal{G}}$ and $\mathcal{K}_i^{\underline{\mathrm{w}}}$ mark attachment points of joints $\mathcal{G}$ as well as application points of external wrenches $\underline{\mathrm{w}}$, respectively. Once the kinematic skeleton with all its reference frames is known, the actual geometry and occupied volume of the rigid body are only of importance, e. g., for collision analysis, but can be discarded for the rigidity analysis of the system.

2.2.2 Constraints

The number of independent motions two bodies can perform with respect to one another can be reduced by adding constraints to the model. Constraints result in reaction forces and moments which are perpendicular to the allowed motions and thus prevent relative movement along the restricted direction. Examples of rheonomic constraints are kinematic actuators, while scleronomic constraints are introduced for instance, by rigid massless bars and ideal joints.

Joints are also referred to as *kinematic pairs* and can be categorized according to Reuleaux (1875) into two types by means of their contact type. The category of *higher*

pairs is formed by connections that can be described by line or point contacts, which, for instance, is the case for a cam and follower or a universal joint. The category of *lower pairs* on the other side features joints whose elements are in surface contact and is composed of six joints, namely revolute (R), prismatic (P), screw or helical (H), cylindrical (C), spherical (S), and planar (E) joints, as shown in tab. 2.1 (Shigley and Uicker, 1995).

Table 2.1: Lower kinematic pairs (cf. Kecskeméthy, 1993a, p. 21)

Type		$f_\mathcal{G}$	Symbol
Revolute	R	1	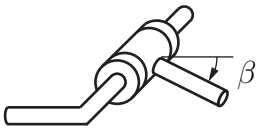
Prismatic	P	1	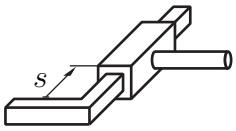
Helical	H	1	$s = h \cdot \beta$ 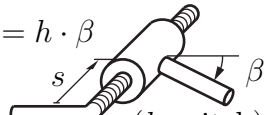 (h: pitch)
Cylindrical	C	2	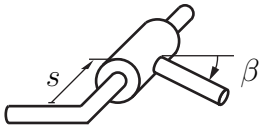
Spherical	S	3	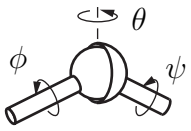
Planar	E	3	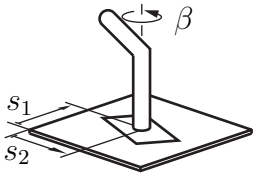

In particular, revolute and prismatic joints can also be seen as special cases of the screw joint with helix angles of 0° and 90° respectively while cylindrical, spherical, and planar joints, as well as the higher pair of a universal joint, can be created by combining revolute and prismatic joints in series. The relative motion, which is then allowed by a joint $\mathcal{G}$, can be parameterized by a set of joint variables $\underline{\beta}_\mathcal{G} = [\beta_1, \ldots, \beta_{f_\mathcal{G}}]^\mathrm{T}$ whose number is equal to the degrees of freedom $f_\mathcal{G}$ or *connectivity* of the joint.

2.2.3 Force Elements

In order to express elasticity, viscosity, and general forces of a mechanical system, active and passive massless force elements like springs, dampers, and actuators are attached at certain points of the multibody system. Force elements of ordinary multibody systems may be constant (e. g., gravitational force), depend on position (e. g., springs), velocity (e. g., dampers), or even on accelerations necessary for determining reaction forces (e. g., friction forces), while active force elements additionally depend on time (e. g., force actuators).

2.3 Topological Structures of Multibody Systems

The topological structure of multibody systems significantly contributes to the complexity of the resulting equations. Following the IFToMM terminology published by Ionescu (2003), bodies are also referred to as *links* whereby throughout this work, only rigid *links* are of concern. An assembly of links that are connected by joints is termed a *kinematic chain*. If one of these links is defined as a *fixed frame*, the kinematic chain forms a *mechanism*. There are two topological types of multibody systems that can be distinguished: Systems formed by *open kinematic chains* and by *closed kinematic chains*, as shown in tab. 2.2.

Table 2.2: Classification of kinematic chains (cf. Woernle, 2016, p. 280)

Open system			Closed system	
Open Kinematic Chain	Simple Open Kinematic Chain	Complex Kinematic Chain	Closed Kinematic Chain	Single-Loop Kinematic Chain
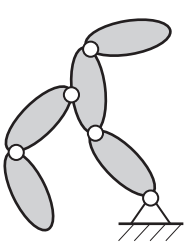	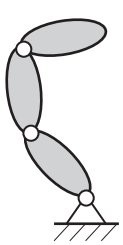	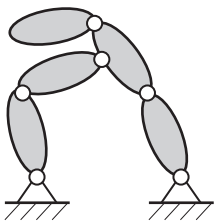	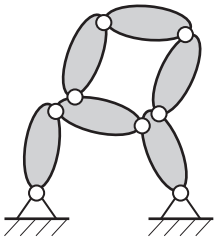	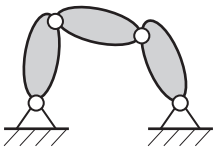

Open kinematic chains exhibit a topological tree structure, which implies that any cut

at a joint will separate the system into two parts. As a result, all joint variables are independent and thus form a set of minimal coordinates. The relative motion between two adjacent links is then defined by the intermediate joint's specific degree of freedom. Starting at a link declared as a base frame, a unique path to all other links can be found, and hereby assigning each link a single predecessor. As a consequence, the absolute motion of each link can be determined recursively by superimposing the relative motion defined by the intermediate joint on the absolute motion of the predecessor. A *simple open kinematic chain* fulfills the additional requirement that none of the links is connected to more than two other links. An example of this would be a serial manipulator.

In *closed kinematic chains*, each link is connected to at least two other links. This implies that closed kinematic chains cannot be separated by a single cut, such that there always exist two or more paths between any two links. Therefore, the joint variables have to fulfill additional conditions for the assembly and do not represent an independent set of minimal coordinates. Indeed, only a number of joint variables equal to the degree of freedom of the kinematic chain will serve as a set of minimal coordinates. Closed kinematic chains where each link is connected to exactly two other links will be referred to as *single-loop kinematic chains* or just as *loops*.

With *complex kinematic chains*, here combinations of open and closed subsystems are declared. Usually, complex kinematic chains can be dissected into their closed and open subchains for which the relevant methodologies can be applied and will be merged thereafter.

2.4 Degrees of Freedom of Multibody Systems

One structural key parameter for the analysis and design of multibody systems is the *degree of freedom*. In order to approach this topic with its often context-sensitive terminology, a short introduction to different definitions and formulas is given in this section.

For the description of the position and orientation, termed *pose*, of an unconstrained rigid body in space, there are six independent coordinates necessary, which will be elaborated in sec. 3.1.3. When it is connected to a fixed reference frame by a joint with $f_{\mathcal{G}_i}$ degrees of freedom defined according to the IFToMM[1] terminology as the "number of

[1]International Federation for the Theory of Mechanisms and Machines

independent coordinates needed to describe the relative positions of pairing elements" (Ionescu, 2003, p. 772), there are only $f_{\mathcal{G}_i}$ independent *joint variables* necessary. The joint variables are quantities that define the relative motion between the connected links. In other words, the joint imposes $r_{\mathcal{G}_i} = 6 - f_{\mathcal{G}_i}$ constraints, which the absolute coordinates of the link must obey, and therefore, $r_{\mathcal{G}_i}$ coordinates are dependent. Consequently, for an open kinematic chain, the poses of all links can be determined by the set of all joint variables, whereby the number of joint variables directly corresponds to the degree of freedom of the open kinematic chain.

Things are more sophisticated once closed kinematic chains are of concern, as some of the joint variables lose their independence through the introduction of closure conditions. In general, six joint variables lose their independence for the closure of a spatial single-loop kinematic chain. Yet, sometimes certain geometric conditions may exist, which for example, force all links of a single-loop kinematic chain to move within one plane, with the result that less than six joint variables lose their independence. For a single-loop kinematic chain, the number of joint variables that lose their independence corresponds to the *motion parameter* b as originally used by Somov (1887) for which a variety of terms exist, but throughout this work, *spatiality* will be used as introduced by Gogu (2005). In general, the spatiality of a planar or spherical mechanism is $b = 3$ and for a spatial mechanism $b = 6$.

According to Gogu (2008), any single-loop kinematic chain with a spatiality less than six can be considered *overconstrained*. The degree N by which a mechanism is overconstrained is given by the difference of the six generally introduced constraints per single-loop kinematic chain, and the actually introduced constraints b. Consequently, a planar four-bar mechanism only features one degree of freedom due to the parallelity of its revolute joints' axes. It is said to be overconstrained by degree $N = 6 - 3 = 3$. Obviously, an open kinematic chain will never be overconstrained.

In multi-loop closed kinematic chains, further joint variables lose their independence, as some of the joint variables are shared among several loops and therefore are subject to additional constraints. Due to this complexity, the correct determination of the abovementioned properties is not trivial. The next section then recalls some of the common formulas which will be used in this work to determine some of the necessary key parameters.

2.4.1 Formulas for the Generic Degree of Freedom

A lot of research has been done on determining the degrees of freedom of mechanisms from which a variety of formulas result. Gogu (2008) provides a thorough overview of different criteria and limitations from where the following formulas were picked and adapted in notation. These formulas will be referred to throughout this work for reference.

Chebyshev (1854) set up a formula for determining the number of independent variables necessary for the description of planar mechanisms with one degree of freedom. Grübler (1917) proposed a similar formula, which he later extended for the spatial case, yet still proceeding from mechanisms with one degree of freedom. The generalization of Kutzbach's version then detached from single degree of freedom mechanisms and yields the following formula in adapted notation (Kutzbach, 1929):

$$f = b \cdot (n_{\mathcal{B}} - 1) - \sum_{i=1}^{n_{\mathcal{G}}} b - f_{\mathcal{G}_i} \tag{2.1}$$

Here, b represents the previously mentioned spatiality, $n_{\mathcal{B}}$ the number of links, $n_{\mathcal{G}}$ the number of joints, and $f_{\mathcal{G}_i}$ the connectivity of joint $\mathcal{G}_i$. The first part of the equation yields the total degree of freedom of the unconstrained links, whereas the second part enumerates the constraints introduced by the connecting joints. Note that $n_{\mathcal{B}}$ also includes the predefined base frame, and diminishing $n_{\mathcal{B}}$ by one removes the six absolute degrees of freedom of the unbound system, thus effectively fixing it in space.

These contributions are commonly known as the Chebyshev-Grübler-Kutzbach formula for closed kinematic chains which in its original form reads (Gogu, 2008, p.59):

$$f = \sum_{i=1}^{n_{\mathcal{G}}} f_{\mathcal{G}_i} - n_L \cdot b \tag{2.2}$$

In particular, the number of degrees of freedom of the open kinematic chain expressed by the sum of joint degrees of freedom is reduced by the closure conditions of the n_L loops with spatiality b, assuming all loops to be of the same spatiality. The number of structurally independent loops is given by the graph-related Euler formula expressed in terms of bodies and joints

$$n_L = n_{\mathcal{G}} - n_{\mathcal{B}} + 1 \ , \tag{2.3}$$

whereby the choice of suitable loops will be further discussed in sec. 4.3.1. In order to account for systems with loops of different spatiality, i. e., systems with mixed planar

and spatial loops, the extended Chebyshev-Grübler-Kutzbach formula in the version of Voinea and Atanasiu (1960) can be formulated:

$$f = \sum_{i=1}^{n_\mathcal{G}} f_{\mathcal{G}_i} - \sum_{k=1}^{n_L} b_k \tag{2.4}$$

As the last modification to be listed here, the version for which according to Gogu (2008) contributions were proposed by (Gronowicz, 1981; Manolescu and Manafu, 1963) and (Agrawal and Rao, 1987b; Davies, 1983; Rico Martínez and Ravani, 2004) leads to

$$f = \sum_{i=1}^{n_L} f_{L_i} - \sum_{j=1}^{n_\mathcal{G}^c} f_{\mathcal{G}_j}^c \ , \tag{2.5}$$

where the second term represents the number of degrees of freedom $f_{\mathcal{G}_j}^c$ of the $n_\mathcal{G}^c$ joints shared between the n_L loops and is subtracted from the sum of degrees of freedom f_{L_i} of the n_L uncoupled loops.

The degree of freedom calculated by the formulas above is often referred to as *generic* (Müller, 2007, p. 463), or *general mobility* (Phillips, 1984, p. 11). Yet, as Phillips concludes

> "the general mobility criterion, although of great importance for strengthening the wisdom of the analyst and the designer by being properly and usefully applicable in all of the general circumstances, is not a one-shot formula for solution of all of the real Problems of practical machine design" (Phillips, 1984, p. 29),

as the following example will show.

2.4.2 The Apparent Degree of Freedom in Overconstrained Mechanisms

In order to demonstrate the shortcomings of the abovementioned degree of freedom counting formulas, the mechanism depicted in fig. 2.4 will be analyzed. The mechanism consists of $n_\mathcal{B} = 9$ links $n_\mathcal{G} = 12$ binary revolute joints indicated by angle symbols, where *multiple joints* (i. e., joints connecting more than two links) were decomposed into a respective number of binary joints. An efficient treatment of multiple joints will be discussed in sec. 4.4. For the $n_L = 12 - 9 + 1 = 4$ marked structurally independent planar loops $L_{1,\dots,4}$, 4 shared joints are encircled. Due to the decomposition of multiple

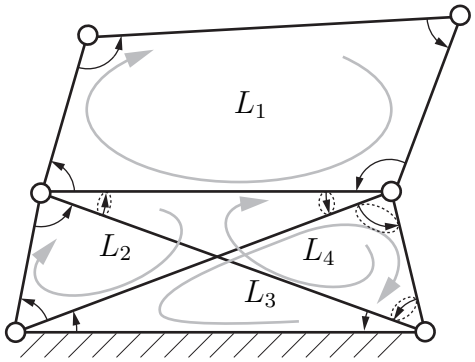

Number of bodies:	$n_\mathcal{B} = 9$
Number of joints:	$n_\mathcal{G} = 12$
Number of loops:	$n_L = 12 - 9 + 1 = 4$
Spatiality:	$b_{1,\dots,4} = 3$
Joint connectivities:	$f_{\mathcal{G}_{1,\dots,12}} = 1$
Loop mobilities:	$f_{L_{1,\dots,4}} = 4 - 3 = 1$

Figure 2.4: Two stacked four-bar linkages of which the lower one is rigid (cf. Simroth et al., 2016, p. 108)

joints, each loop features four joints with one degree of freedom each, such that each loop according to eq. 2.2 with the spatiality $b = 3$ has one degree of freedom.

Applying any of the equations in sec. 2.4.1 yields the erroneous result of zero degrees of freedom, even though the mechanism clearly has one degree of freedom corresponding to the relative motion of the upper loop L_1:

$$\text{eq. 2.1:} \quad f = b \cdot (n_\mathcal{B} - 1) - \sum_{i=1}^{n_\mathcal{G}} b - f_{\mathcal{G}_i} = 3 \cdot (9-1) - 12 \cdot (3-1) = 0$$

$$\text{eq. 2.2:} \quad f = \sum_{i=1}^{n_\mathcal{G}} f_{\mathcal{G}_i} - n_L \cdot b = 12 \cdot 1 - 4 \cdot 3 = 0$$

$$\text{eq. 2.4:} \quad f = \sum_{i=1}^{n_\mathcal{G}} f_{\mathcal{G}_i} - \sum_{k=1}^{n_L} b_k = 12 \cdot 1 - 4 \cdot 3 = 0$$

$$\text{eq. 2.5:} \quad f = \sum_{i=1}^{n_L} f_{L_i} - \sum_{j=1}^{n^c_\mathcal{G}} f^c_{\mathcal{G}_j} = 4 \cdot 1 - 4 \cdot 1 = 0$$

The reason behind is the second diagonal link within the lower structure, which introduces an additional distance constraint which has to comply with the existing dimensions, as an assembly would not be possible otherwise. This "redundant constraint" (Phillips, 1984, p. 10) leads to a negative degree of freedom for the lower structure and therefore "compensates" the real degree of freedom of the upper part, leading to an overall degree of freedom of zero. Gogu (2005) states a formula for the degree N by which a kinematic chain is overconstrained:

$$N = \sum_{i=1}^{n_\mathcal{G}} (6 - f_{\mathcal{G}_i}) - (6 \cdot (n_\mathcal{B} - 1) - f) \tag{2.6}$$

Following eq. 2.6 the mechanism is overconstrained by a degree of $N = 12 \cdot 5 - (6 \cdot (9 - 1) - 1) = 13$ of which a degree of 12 corresponds to all four planar loops being overconstrained by three, while the last one represents the redundant constraint introduced by the additional link. Note that eq. 2.6 requires the "correct" degree of freedom of the mechanism for which Gogu proposed a general formula which "is valid without exception" (Gogu, 2008, p. 63)

$$f = \sum_{i=1}^{n_{\mathcal{G}}} f_{\mathcal{G}_i} - r \ , \tag{2.7}$$

with r being the number of joint variables that become dependent after closing the loops. The degree of freedom determined by eq. 2.7 can be best described by the term *apparent mobility* as used by Phillips (1984), which can be understood as the observable mobility of a mechanical system. Yet, the crux of the matter remains, namely, the correct determination of dependencies among the constraint equations which effectively reveal the correct value or r. A discussion regarding this issue is given in the following section.

2.4.3 Finite and Instantaneous Degrees of Freedom

In an attempt not to go beyond the scope of this discussion, just a general description of finite and instantaneous degrees of freedom together with an example to raise awareness about related ambiguities shall be given.

First, it has to be understood that the number of apparent degrees of freedom is subject to change for a given *assembly mode*[2] of a kinematic chain. That is, the number r of constraints that lose their independence may vary for different *configurations*. By configuration here, a set of possible values for the joint variables which obey the constraints for the given kinematic chain is regarded.

The example shown in fig. 2.5 shall illustrate the variation in apparent degree of freedom, for which the generic degree of freedom by the Chebyshev-Grübler-Kutzbach formula eq. 2.2 yields $f = 7 \cdot 1 - 2 \cdot 3 = 1$. This obviously matches the apparent degree of freedom for the general configuration shown in a), but for the configuration in c) with axes of two revolute joints being coaxial. Instead, two apparent degrees of freedom can be observed. Both configurations allow for smooth motions which can be

[2]There may be different ways of assembling links and joints of a kinematic chain, such that there is no transition from a configuration in one assembly mode to a configuration in another mode without disassembling the kinematic chain.

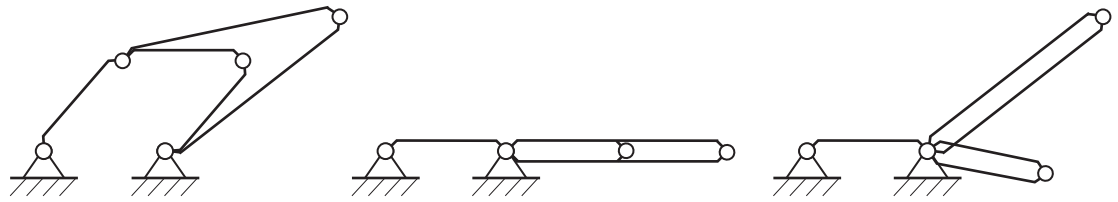

a) *Instantaneous:* $f = 1$ b) *Instantaneous:* $f = 3$ c) *Instantaneous:* $f = 2$

Figure 2.5: A mechanism with varying instantaneous and full-cycle degrees of freedom

viewed as distinct *operational modes* of the mechanism. The configuration shown in b), which Hunt (1978, p. 389) terms *uncertainty configuration*, resembles a bifurcation from which both modes can be entered.

In order to elucidate this behavior, one has to distinguish whether *finite* or *infinitesimal* displacements are of concern. In that sense, the finite mobility for a given configuration is determined by the minimum number of scalar variables that are required to define the pose of all links within a kinematic chain (Diez-Martínez et al., 2006, p. 456). On the other side, the instantaneous mobility describes the characteristics of a kinematic chain at a specific position and is related to the number of infinitesimal displacements within the joint variables required to define an infinitesimal displacement (Gogu, 2008, p. 79). One conclusion that can directly be drawn is that the instantaneous degree of freedom is always greater than or equal to the finite degree of freedom since the infinitesimal variations are always included within the finite variations.

For instantaneous degrees of freedom sometimes also the terms *transitory* (Phillips, 1984, p. 28) or *differential* (Müller, 2007, p. 461) are used, while for finite mobility also *full-cycle* (Hunt, 1978, p. 383), *permanent* (Lee and Hervé, 2002, p. 645), *local* (Müller, 2007, p. 461), and *global* (Gogu, 2008, p. 33) appear. Note that Müller defines a local degree of freedom for each mode corresponding to the respective finite degree of freedom and declares the largest local degree of freedom as the global degree of freedom. As such, the instantaneous degree of freedom in fig. 2.5 b) equals three while the finite degree of freedom equals two, corresponding to the highest finite degree of freedom present at that configuration. Gogu defines the smallest instantaneous degree of freedom as the global degree of freedom, though in general, both statements agree, if *kinematotropic* chains, i. e., kinematic chains with modes of the different finite degrees of freedom as the one in fig. 2.5, as well as kinematic chains, which are "paradoxical-in-the-small," as defined by Müller (2007, p. 461), are excluded. The latter of which, as for instance, the extended Watt linkage in (Müller, 2007, p. 461), features an instantaneous degree

of freedom larger than the finite degree of freedom throughout all configurations of one operation mode. As this work aims at the general detection of rigid structures, these particular cases of kinematotropic and paradoxical-in-the-small chains are excluded, to avoid resulting ambiguities.

Last, the method of how the number of joint variables that lose their independence when the loops of a kinematic chain are closed shall be inspected, on which depends whether finite or instantaneous degrees of freedom are determined. Indeed, according to Moroskine (1954), this number directly relates to the rank of the Jacobian matrix, which represents a linear mapping of the joint velocity space to the space of general velocities. In that sense, when only structural parameters and symbolic dimensions are concerned, usually, a general statement about a mechanism's *finite* degree of freedom is derived. On the other hand, if a specific configuration is concerned for which numerical values of dimensions and joint variables are known, the instantaneous degree of freedom is determined (Gogu, 2008, p. 66).

Though the numerical method theoretically provides the correct instantaneous degree of freedom, the procedure requires the full assembly of the kinematic constraint equations. Furthermore, the numerical calculation of the rank for multi-loop systems is error-prone due to rounding errors or, in close neighborhoods of singularities, due to values for the determinant close to zero, suggesting a loss of rank. Also, the idea of numerically deducing the finite degree of freedom by evaluating the instantaneous degree of freedom at a sufficient number of configurations has to be treated with caution due to the previously mentioned example.

A symbolical rank determination, as suggested by Gogu, would eliminate the drawbacks of the numerical approach, but the equation solving capabilities of recent computer algebra systems are still limited in the case of complex mechanical systems. As the method presented in this work relies on the correct determination of the finite degree of freedom and to circumvent the symbolic rank determination, a group theoretic approach applicable to many typical kinematic chains is suggested in sec. 3.4.2.

Throughout the remainder of this work, if not declared otherwise, the use of 'degree of freedom' is to be understood as a finite degree of freedom.

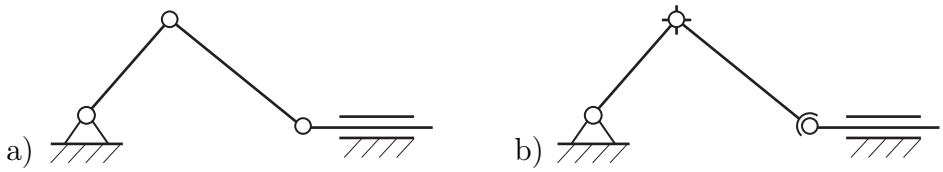

Figure 2.6: The revolute joints of the overconstrained slider-crank in a) are replaced by a universal and a spherical joint of which some degrees of freedom are locked in b)

2.4.4 Locked Degrees of Freedom

Locked degrees of freedom are often encountered in the context of overconstrained mechanisms – or rather in the attempt to avoid them. Kinematic chains with locked degrees of freedom "have either joints which remain immobile or joints with connectivity greater than one which function as lower pair joints with lower connectivity." (Waldron, 1973, p. 98). Other terms encountered in this context are *idle* (Gogu, 2008, p. 124), *inactive* (Hunt, 1978, p. 38), or *passive* (Waldron, 1973, p. 98), (Phillips, 1984, p. 32) degrees of freedom. Yet, one has to be cautious as the term passive degrees of freedom is also used for under-actuated manipulators (Shiriaev et al., 2010, p. 893), (Jain and Rodriguez, 1993, p. 411), to distinguish between actuated and non-actuated joints or chains in parallel manipulators (Liu et al., 2014, p. 250), or in the context of isolated degrees of freedom (Kramer, 1992, p. 106).

The illustration in fig. 2.6 a) shows a planar slider-crank mechanism which, by choice of its joints, is overconstrained according to eq. 2.6 by $N = 4 \cdot 5 - (6 \cdot 3 - 1) = 3$. If the revolute joints are now replaced by a universal and spherical joint, as shown in fig. 2.6 b) and applying the Chebyshev-Grübler-Kutzbach formula eq. 2.2, the mechanism retains its degree of freedom of 1, but due to increased joint connectivities $N = (5 + 4 + 3 + 5) - (6 \cdot 3 - 1) = 0$ is not overconstrained anymore. Apparently, the mechanism still performs a planar motion, and consequently, the effective connectivities of the universal and spherical joints are reduced to one. The joint variables corresponding to the "locked" degrees of freedom are now constants.

In fact, the reduction of the degree by which a mechanism is overconstrained through adequate replacement of joints plays an important role when the actual mechanical system is to be built. Due to finite precision in manufacturing, physical realizations of perfectly parallel axes or exact dimensions are impossible, such that one will always "end up with an 'almost overconstrained' mechanism" (Müller, 2007, p. 464) which may only be able to move due to flexure of bodies and joint clearances. Thus, in reality,

locked degrees of freedom are usually necessary to allow for misalignments, which in turn result in small motions along the locked degrees of freedom. An example of locked degrees of freedom introduced for manufacturing purposes is shown in fig. 4.1. The upper two spherical joints actually function as simple revolute joints but are able to compensate for errors in orientation. Especially in the context of this work, it is worth mentioning that a kinematic chain of which all degrees of freedom are locked can be regarded as a structure.

2.4.5 Redundant Degrees of Freedom

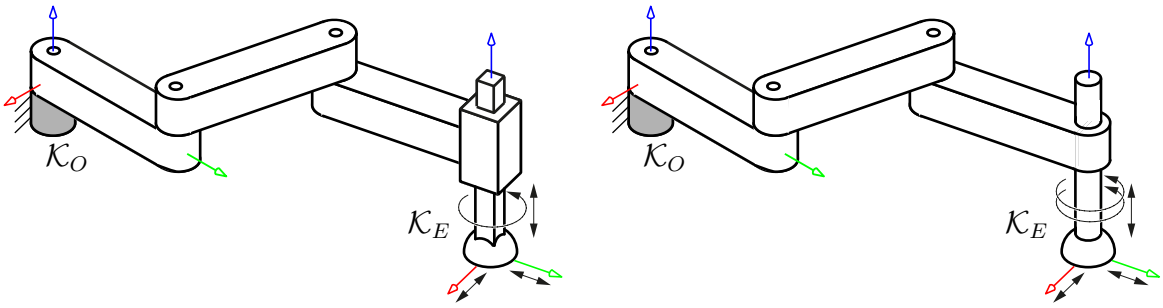

a) b)

Figure 2.7: a) Non-redundant and b) redundant SCARA-robot

According to IFToMM terminology, *redundant degrees of freedom* in the context of robotics can be defined as the "amount by which the degree of freedom of a robot exceeds the number of independent variables that are necessary to define the task to be performed." (Ionescu, 2003, p. 822). The SCARA[3]-manipulator shown in fig. 2.7 a) whose end-effector features four degrees of freedom is commonly used for pick and place operations. If in fig. 2.7 b) the prismatic joint is replaced by a cylindrical joint, its degree of freedom increases to five, yet the connectivity between the base frame $\mathcal{K}_0$ and the end effector $\mathcal{K}_E$, or in other words, the dimension of the operation space of the end-effector with respect to the fixed reference frame remains four. The additional rotation about the axis of the cylindrical joint therefore is a *redundant degree of freedom*.

2.5 Isolated Degrees of Freedom

In fig. 2.8 a spatial four-bar mechanism that features two degrees of freedom according to eq. 2.2 is depicted. Clearly, one of these degrees of freedom corresponds to the

[3]SCARA: Selective Compliance Assembly Robot Arm

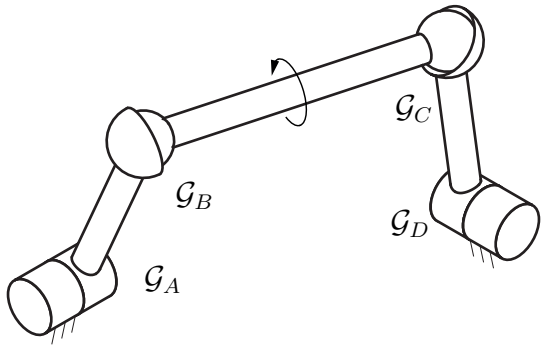

Figure 2.8: Joint variables in $\mathcal{G}_A$ and $\mathcal{G}_D$ are invariant to the indicated isolated bar spin

indicated bar spin between both spherical joints, while the other originates from the kinematic chain's internal motion. By inspection, it can be seen that the joint angles in $\mathcal{G}_A$ and $\mathcal{G}_D$ are independent of the rotation angle of the bar, which therefore appears to be an *isolated degree of freedom*. If, for some reason, it happens to be that all remaining degrees of freedom are locked as described in sec. 2.4.4, within this context, the kinematic chain can be seen as a *structure*. Therefore, the identification of these kinds of degrees of freedom will be essential, which requires more thorough consideration.

Up to this point, a wide variety of terms and definitions have been used for these kinds of degrees of freedom. Hunt (1978, p. 334) described the mobilities of a bar between two spherical joints as *superfluous spin-freedoms* and suggested their removal for the kinematic analysis. The terms *passive* and *idle*, which are also used for locked degrees of freedom, as indicated in sec. 2.4.4, can be found with definitions and properties from Kramer, Tsai, Angeles, and Sharma like:

> "A passive degrees of freedom is one which is unconstrained but which does not affect the transmission of motion in a mechanism." (Kramer, 1992, p. 106f.)

> "Passive degrees of freedom cannot be used to transmit motion or torque about an axis." (Tsai, 2001, p. 80)

> "[...] degrees of freedom that are 'idle' or 'passive,' i. e., degrees of freedom not affecting the transmission of motion from link 1 to link n." (Angeles, 1982, p. 178)

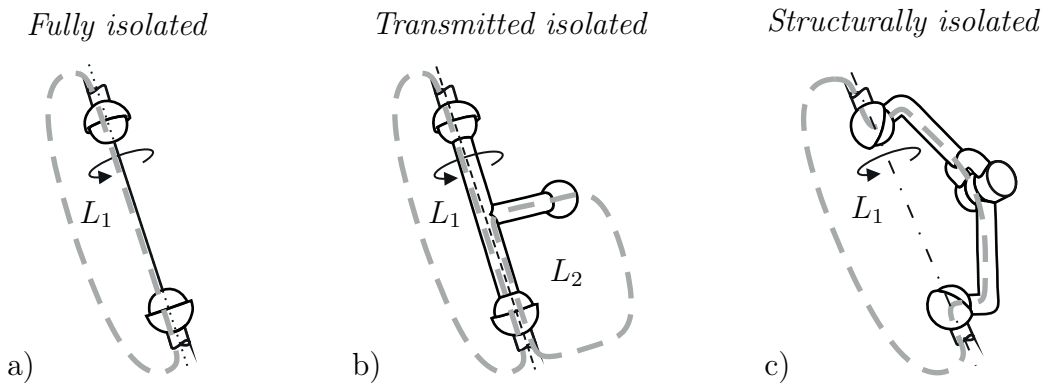

Figure 2.9: Different types of isolated degrees of freedom (Simroth et al., 2016, p. 111)

> "A mechanism may have a redundant degree of freedom, i. e., a link can be displaced without causing any displacement to other links."
> (Sharma and Purohit, 2006, p. 78)

or similar by Razmara et al. (2000, p. 2), Shigley and Uicker (1995, p. 362). Sometimes these motions are even referred to as parasitic, according to Hsu et al. (2004, p. 122) or Rolland (1999, p. 832)[4]. To elude confusion with ambiguous uses in different contexts, as well as to emphasize its character of being decoupled from other degrees of freedom, the term *isolated degrees of freedom* which has also been previously mentioned by Mazzone et al. (2003, p. 189) and Woernle (2016, p. 285) will be used throughout this work. For this purpose, the concept will be generalized to arbitrary subchains with more than one link:

If a minimal cut set of joints, which by removal would split a closed kinematic chain into two subchains C_I and C_{II}, allows a relative motion between C_I and C_{II}, that leaves all joint variables within C_I and C_{II} invariant, there exist isolated degrees of freedom corresponding to the number of independent parameters necessary to describe this relative motion.

In addition, isolated degrees of freedom will be categorized into *fully* or *structurally* isolated, depending on whether at least one of the subchains C_I and C_{II} contains only a single link or if both are comprised of several links, as well as into *transmitted* isolated

[4]Note that usually the term parasitic degrees of freedom or motions is used for undesired but inevitable dependent motion directions (Carretero et al., 2000, p. 17), (Isaksson et al., 2015, p. 4), (Merlet, 2005b, p. 1) or for motions due to flexible compliant joints (Togashi et al., 2014, p. 436)

for which the following descriptions will be recited from Simroth et al. (2016, p. 111):

a) *Fully isolated* degree of freedom:
These are immaterial motions which can be completely removed from the mechanism without any effect; this is the case for example of the isolated spin of an infinitesimally thin spherical-spherical bar about its longitudinal axis shown in fig. 2.9 a).

b) *Transmitted isolated* degree of freedom:
These are isolated degrees of freedom that have already been counted once as fully isolated in one loop so that they become transmitted in a neighboring loop; an example is shown in fig. 2.9b), where the spin of the rod has been counted as isolated in loop L_1 but becomes transmitted to loop L_2; this will be essential when regarding the transmission of isolated degrees of freedom at loop coupling conditions of spherical joints.

c) *Structurally isolated* degree of freedom:
These are isolated degrees of freedom that comprise whole subchains; they leave the internal motion of whole subchains within one loop invariant but operate on the absolute motion of the chain as proper degrees of freedom; an example is shown in fig. 2.9 c) where the isolated degree of freedom does not change the internal configuration of the revolute joint on the spun subchain, but the chain rotates as a whole about the implied spin axis connecting both spherical joints. Note that in this type of isolated degrees of freedom, the spin axis is not constant with respect to any body but changes with the internal motion of the involved subchain.

Isolated degrees of freedom can also be seen as redundant degrees of freedom according to sec. 2.4.5, but the opposite is not necessarily the case, as redundant degrees of freedom allow for relative motions within the subchains. A detailed description of how to isolated degrees of freedom can be detected will be given in sec. 5.1.

3 Kinematic Processing in Multibody Systems

Mechanics, in general, address the motion of bodies and their interaction with forces. The area of mechanics can be subdivided into *dynamics* and *kinematics* (see fig. 3.1)[1]. In dynamics, the results of forces acting upon the bodies are analyzed, whereby dynamics can be further categorized into *statics*, which focuses on the state of static equilibrium with all bodies at rest, while *kinetics* addresses the motion resulting from external forces. In kinematics, the pure motion of bodies in the absence of any forces is studied in terms of pose, velocity, acceleration, and time. In this chapter, the gen-

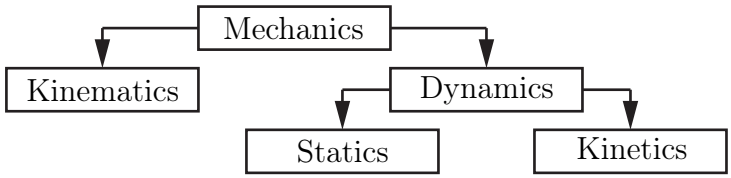

Figure 3.1: Fields of mechanics for rigid bodies classified by presence of forces

eral kinematics of both open-loop and closed-loop mechanical systems are elaborated. There are two principal tasks to be solved in kinematics:

Forward kinematics is concerned with the absolute motion, including position, orientation, velocities, and accelerations of all components of a multibody system for known relative joint motions. For serial manipulators, there is always a unique closed-form solution for this problem. For systems with closed kinematic chains, which occur, for example, in parallel manipulators, there may exist several solutions for the same set of given joint motions, and the determination of an analytical solution is rather complex if one can be found at all (Merlet, 2006).

The task of determining the relative joint variables for a given absolute position and orientation of an end effector is the aim of *inverse kinematics*. Thus, the joint variables have to fulfill constraints for which there may be several possible solutions, or in case the desired end-effector position and orientation cannot be attained due to structure and dimensions of the mechanical system, there even may be no solution at all.

To that end, *global kinematics* can be understood as a mapping of a set of independent generalized coordinates $\underline{q} = [q_1, \ldots, q_f]^{\mathrm{T}}$ and their time derivatives to the absolute

[1]Sometimes mechanics is also classified by time dependency: The time independent field of statics and the time dependent field of kinematics which is divided into dynamics and kinetics depending on whether forces are of concern or not (Shigley and Uicker, 1995, p. 4)

positions, orientations, velocities, and accelerations of all components of a multibody system with f degrees of freedom. Furthermore, this problem can be subdivided into *relative kinematics* and *absolute kinematics*, as shown in fig. 3.2.

Relative kinematics map the generalized coordinates to joint variables in accordance with closure conditions introduced by closed kinematic chains. Absolute kinematics then establish a link between the relative joint variables and the absolute motion of all components of the multibody system with respect to a fixed reference frame.

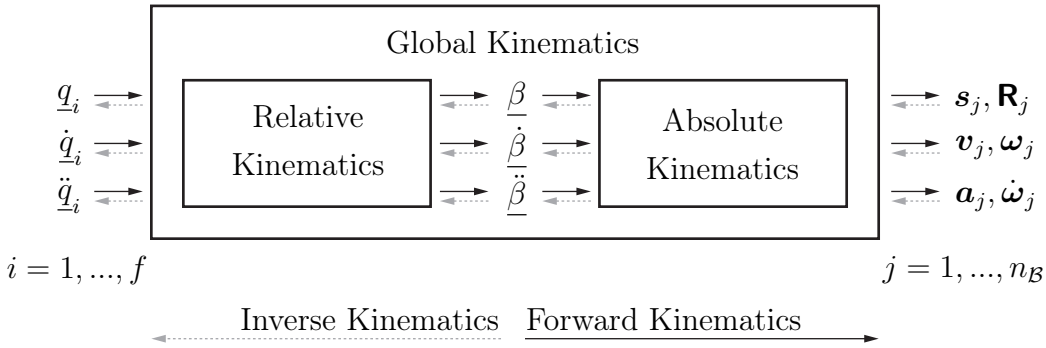

Figure 3.2: Division of global kinematics into relative and absolute kinematics (cf. Kecskeméthy, 1993a, p.24)

3.1 Rigid Body Kinematics

The continuous sequence of positions of all the material particles of a rigid body with respect to a fixed coordinate frame describes its absolute motion. When bodies are assumed rigid, the distances between particles are constant in time, and such is their position with respect to a body-fixed coordinate frame. Thus, it is sufficient to describe the general motion of a rigid body by the position and orientation as well as velocity and acceleration of one body-fixed reference frame with respect to a space fixed reference frame. In the following, the position of an exemplary particle position will be analyzed for further insides on the general motion. A comprehensive explanation is given by Bottema and Roth (1990) from which the basic theory of kinematics is reflected.

Considering one particle or point P of a rigid body, let a transformation $\mathbf{T}(P \rightarrow P')$ of Euclidean 3-space $\mathbb{R}^3$ be a bijective mapping of that point P to an image point P', such that its inverse $\mathbf{T}^{-1}$ is uniquely defined as the transformation $P' \rightarrow P$. For two transformations $\mathbf{T_1}(P \rightarrow P')$ and $\mathbf{T_2}(P \rightarrow P'')$ the product $\mathbf{T_2 T_1}$ results in the transformation $P' \rightarrow P''$ for which associativity is satisfied as the transformation

$(\mathbf{T_3T_2})\mathbf{T_1}$ is equal to $\mathbf{T_3}(\mathbf{T_2T_1})$. Last, an identity transformation $\mathbf{I}(P \to P)$ is defined, that retains P unaltered. Such a transformation fulfills four group axioms, namely closure, invertibility, associativity, as well as the identity, and therefore forms a group that is closed under $\mathbb{R}^3$. Examples of such transformations are scalings, shear mappings, translations, rotations, or reflections.

Yet, only transformations $\mathbf{T}(P \to P')$ which conserve the distances $\overline{\mathrm{PR}}$ of all point pairs (P, R) such that these equal the distances $\overline{P'R'}$ of their image point pairs $(P'R')$ apply to rigid body motion and are called isometries or Euclidean transformations (Berger, 2010). While isometries also imply that angles in original and image space are conserved, orientations are not. This gives rise to the categorization into indirect and direct isometries, the former one describing reflections. The latter then contain only Euclidean transformations, which also preserve orientations and form the special Euclidean group $SE(n)$. Indeed, transformations in $SE(3)$ describe the three-dimensional kinematics of rigid bodies. This group can be further broken down into a translational and a rotational subgroup with subgroups being subsets closed under the same group operation as the enclosing group.

For the description of translations and rotations, a three-dimensional fixed reference space with *origin* O is introduced, and the position vector $P = OP$ of an arbitrary point P of the undisplaced body-fixed space is defined. The position vector $P' = OP'$ then is associated with the displaced body-fixed space. A general displacement $\mathbf{D}(P \to P')$ is composed of a translation $\mathbf{S}$ and a rotation $\mathbf{R}$ as follows.

3.1.1 Translation

A translation $\mathbf{S}(P \to P')$ is a displacement by a vector of translation $\boldsymbol{r} = \overline{OO'}$ for which the image P' of P can be determined as

$$P' = P + \boldsymbol{r} \ . \tag{3.1}$$

The inverse of displacement $\mathbf{S^{-1}}(P' \to P)$ then can be written as

$$P = P' - \boldsymbol{r} \ . \tag{3.2}$$

For a rigid body subjected to a pure translation, all its points are moved in parallel. It can be shown that translations form a commutative subgroup of $SE(n)$, and accordingly, a sequence of translations can be performed in an arbitrary order without altering the final result. The number of parameters necessary to perform a translation corresponds to the dimension n of $\boldsymbol{r}$, which is three for the three-dimensional space.

3.1.2 Rotation

A rotation $\mathbf{R}(P \to P')$ is a displacement about a fixed point O for which

$$P' = \mathbf{R}P \ . \tag{3.3}$$

Hereby, $\mathbf{R}$ is an orthogonal matrix assembled of n linearly independent unit vectors and a determinant equal to $+1$ for proper rotations. The inverse results directly from the orthogonality property such that $\mathbf{R}^{-1} = \mathbf{R}^T$ and the inverse transformation $\mathbf{R^{-1}}(P' \to P)$ can be expressed as

$$P = \mathbf{R}^T P'. \tag{3.4}$$

Rotations then form the special orthogonal group $SO(n)$ of orthogonal matrices with matrix multiplication as the group operation. Since the matrix product is not commutative, the sequence of rotations is likewise not arbitrary. A rotation can be parametrized by $n(n-1)/n$ independent parameters, which is three in three-dimensional space, as the remaining parameters result from the orthogonality conditions and a norm equal to one for each vector.

3.1.3 General Displacement Expressed by Homogeneous Coordinates

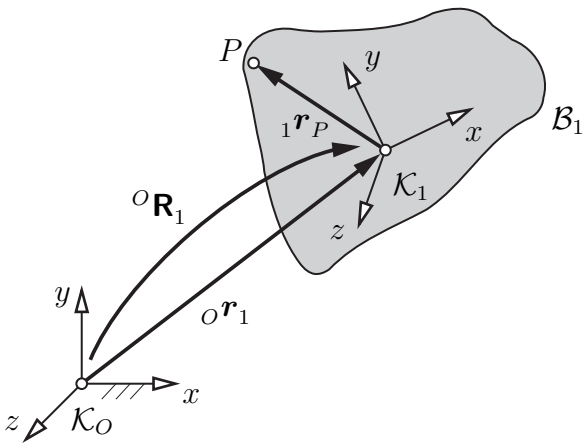

Figure 3.3: Pose of a rigid body $\mathcal{B}_1$ specified by its position and orientation with respect to a fixed reference frame $\mathcal{K}_O$

Composing a translation $\mathbf{S}$ and a rotation $\mathbf{R}$ yields the general displacement $\mathbf{D}(P \to P')$

$$P' = \boldsymbol{r} + \mathbf{R}P \ . \tag{3.5}$$

The displacement of all points of a rigid body defines its *pose* (Angeles, 1988) such that it is sufficient to define the origin by a position vector $\boldsymbol{r}$ and the orientation expressed by a rotation matrix $\mathbf{R}$ of an arbitrary body-fixed coordinate frame, as shown in fig. 3.3. For a rigid body, $\boldsymbol{r}$ and $\mathbf{R}$ are time-dependent functions for which the continuous sequence of poses represents its motion.

A convenient way for the notation of general displacements is the use of homogeneous coordinates, which allows a uniform representation of rotations and translations. More precisely, homogeneous coordinates enable the expression of rigid body transformations in eq. 3.5 from position P_i to P_j as linear mappings

$$P_j = {}^i\mathbf{A}_j P_i \tag{3.6}$$

with its inverse

$$P_i = {}^i\mathbf{A}_j^{-1} P'_j \tag{3.7}$$

by a single matrix ${}^i\mathbf{A}_j$. For this purpose, the transformation can be represented in four-dimensional space by introducing an additional parameter t, which naturally will be normalized to one. A point can be represented by

$$\overset{\text{H}}{P} = \begin{pmatrix} x \\ y \\ z \\ t \end{pmatrix} \quad , \quad P = \begin{pmatrix} x/t \\ y/t \\ z/t \end{pmatrix} \quad \text{and for } t = 1: \quad \overset{\text{H}}{P} = \begin{pmatrix} x \\ y \\ z \\ 1 \end{pmatrix} \quad , \quad P = \begin{pmatrix} x \\ y \\ z \end{pmatrix} \tag{3.8}$$

with $\overset{\text{H}}{P}$ denoting the point P in homogeneous coordinates. A property of homogeneous coordinates is the possibility to express points in infinity by setting $t = 0$ which also allows an origin-independent formulation of direction vectors

$$\overset{\text{H}}{\underline{e}}_1 = \begin{pmatrix} 1 \\ 0 \\ 0 \\ 0 \end{pmatrix} \qquad \overset{\text{H}}{\underline{e}}_2 = \begin{pmatrix} 0 \\ 1 \\ 0 \\ 0 \end{pmatrix} \qquad \overset{\text{H}}{\underline{e}}_3 = \begin{pmatrix} 0 \\ 0 \\ 1 \\ 0 \end{pmatrix} \quad . \tag{3.9}$$

In this manner, a general displacement and its inverse of one frame $\mathcal{K}_i$ to another frame $\mathcal{K}_j$ can be formulated by the 4×4 transformation matrix

$${}^i\mathbf{A}_j = \begin{pmatrix} {}^i\mathbf{R}_j & {}^i_i\boldsymbol{r}_j \\ 0 & 1 \end{pmatrix} \quad \text{and} \quad {}^j\mathbf{A}_i = ({}^i\mathbf{A}_j)^{-1} = \begin{pmatrix} {}^i\mathbf{R}_j^T & -{}^i\mathbf{R}_j^T {}^i_i\boldsymbol{r}_j \\ 0 & 1 \end{pmatrix} \tag{3.10}$$

composed of the rotation matrix $\mathbf{R}$, and the position vector $\boldsymbol{r}$ as defined before, where the notation ${}^1_2\boldsymbol{r}_3$ denotes a relative vector from frame $\mathcal{K}_2$ to frame $\mathcal{K}_3$ expressed in coordinates of frame $\mathcal{K}_1$.

This allows for a simple concatenation of several transformations, noted as the matrix product of homogeneous transformation matrices

$$ {}^{i}\mathbf{A}_{j} = {}^{i}\mathbf{A}_{k}\,{}^{k}\mathbf{A}_{j} \ . \tag{3.11} $$

3.1.4 Velocities

Starting with the position of a general point P of a rigid body which according to sec. 3.1.3 is given by

$$ {}^{0}_{0}\boldsymbol{r}_{P} = {}^{0}_{0}\boldsymbol{r}_{1} + {}^{0}\mathbf{R}_{1}\ {}^{1}_{1}\boldsymbol{r}_{P} \ , \tag{3.12} $$

its velocity can be expressed by the time derivative

$$ {}^{0}_{0}\dot{\boldsymbol{r}}_{P} = {}^{0}_{0}\dot{\boldsymbol{r}}_{1} + {}^{0}\dot{\mathbf{R}}_{1}\ {}^{1}_{1}\boldsymbol{r}_{P} + \underbrace{{}^{0}\mathbf{R}_{1}\ {}^{1}_{1}\dot{\boldsymbol{r}}_{P}}_{=0} \ . \tag{3.13} $$

Due to the rigidity condition, the body cannot be deformed such that ${}^{1}_{1}\dot{\boldsymbol{r}}_{P} = 0$. By expressing the vector ${}^{1}_{1}\boldsymbol{r}_{P}$ in coordinates of $\mathcal{K}_0$

$$ {}^{0}_{0}\dot{\boldsymbol{r}}_{P} = {}^{0}_{0}\dot{\boldsymbol{r}}_{1} + \underbrace{{}^{0}\dot{\mathbf{R}}_{1}\ ({}^{0}\mathbf{R}_{1})^{T}}_{={}^{0}_{0}\widetilde{\boldsymbol{\omega}}_{1}}\ {}^{0}_{1}\boldsymbol{r}_{P} \tag{3.14} $$

the Poisson equation is obtained

$$ {}_{0}\widetilde{\boldsymbol{\omega}}_{1} = {}^{0}\dot{\mathbf{R}}_{1}\ ({}^{0}\mathbf{R}_{1})^{T} \ . \tag{3.15} $$

Insights into the structure of $\widetilde{\boldsymbol{\omega}}$ can be gained through the time derivative of ${}^{0}\mathbf{R}_{1}$

$$ \mathbf{I} = {}^{0}\mathbf{R}_{1}\ ({}^{0}\mathbf{R}_{1})^{T} \tag{3.16} $$

$$ \mathbf{0} = \underbrace{{}^{0}\dot{\mathbf{R}}_{1}\ ({}^{0}\mathbf{R}_{1})^{T}}_{{}_{0}\widetilde{\boldsymbol{\omega}}_{1}} + \underbrace{{}^{0}\mathbf{R}_{1}\ ({}^{0}\dot{\mathbf{R}}_{1})^{T}}_{({}^{0}\dot{\mathbf{R}}_{1}\ ({}^{0}\mathbf{R}_{1})^{T})^{T} = ({}_{0}\widetilde{\boldsymbol{\omega}}_{1})^{T}} \tag{3.17} $$

$$ {}_{0}\widetilde{\boldsymbol{\omega}}_{1} = -({}_{0}\widetilde{\boldsymbol{\omega}}_{1})^{T} \ . \tag{3.18} $$

A square matrix is defined to be skew-symmetric if it is equal to the negative of its transpose. As shown in eq. 3.18, $\widetilde{\boldsymbol{\omega}}$ obviously is skew-symmetric:

$$ \widetilde{\boldsymbol{\omega}} = \begin{bmatrix} 0 & -\omega_z & \omega_y \\ \omega_z & 0 & -\omega_x \\ -\omega_y & \omega_x & 0 \end{bmatrix} \tag{3.19} $$

A comparison of vector product and scalar product of a skew-symmetric matrix

$$\underbrace{\begin{bmatrix} 0 & -\omega_z & \omega_y \\ \omega_z & 0 & -\omega_x \\ -\omega_y & \omega_x & 0 \end{bmatrix}}_{\begin{bmatrix} \omega_x \\ \omega_y \\ \omega_z \end{bmatrix} \times} \cdot \begin{bmatrix} r_x \\ r_y \\ r_z \end{bmatrix} = \begin{bmatrix} r_x \\ r_y \\ r_z \end{bmatrix} = \begin{bmatrix} \omega_y r_z - \omega_z r_y \\ \omega_z r_x - \omega_x r_z \\ \omega_x r_y - \omega_y r_x \end{bmatrix} \tag{3.20}$$

$$\tag{3.21}$$

leads to the conclusion that from $\widetilde{\boldsymbol{\omega}}$ a vector $\boldsymbol{\omega}$ can be extracted, which is the *angular velocity*. Inserting $\boldsymbol{\omega}$ into eq. 3.13 yields Euler's law of motion which is independent of the coordinate frame of decomposition

$$ {}_0\dot{\boldsymbol{r}}_P = {}_0\dot{\boldsymbol{r}}_1 + {}_0\boldsymbol{\omega}_1 \times {}_1\boldsymbol{r}_P \ . \tag{3.22}$$

The translational velocity ${}_0\boldsymbol{v}_1$ and angular velocity ${}_0\boldsymbol{\omega}_1$ then describe the velocity of a rigid body at a certain point in time.

3.1.5 Accelerations

In order to determine the acceleration for an arbitrary point P of a rigid body with respect to a fixed reference frame $\mathcal{K}_0$, the time derivative of the velocity eq. 3.13 yields

$$ {}^0_0\ddot{\boldsymbol{r}}_P = {}^0_0\ddot{\boldsymbol{r}}_1 + {}^0\ddot{\mathbf{R}}_1 \, {}^1_1\boldsymbol{r}_P + \underbrace{{}^0\dot{\mathbf{R}}_1 \, {}^1_1\dot{\boldsymbol{r}}_P}_{=0} \ . \tag{3.23}$$

Again, an equation independent of the frame of decomposition is determined by finding a suitable replacement for ${}^0\ddot{\mathbf{R}}_1$. Taking the derivative of eq. 3.15

$$ {}_0\dot{\widetilde{\boldsymbol{\omega}}}_1 = {}^0\ddot{\mathbf{R}}_1 \, ({}^0\mathbf{R}_1)^T + {}^0\dot{\mathbf{R}}_1 \, ({}^0\dot{\mathbf{R}}_1)^T \tag{3.24}$$

yields a relation between the *angular acceleration* ${}_0\dot{\boldsymbol{\omega}}_1$ and the elements of the rotation matrix ${}^0\mathbf{R}_1$. Solving eq. 3.24 for ${}^0\ddot{\mathbf{R}}_1$ by right-sided multiplication with ${}^0\mathbf{R}_1$ yields

$$ {}^0\ddot{\mathbf{R}}_1 = {}_0\dot{\widetilde{\boldsymbol{\omega}}}_1 \, {}^0\mathbf{R}_1 - {}^0\dot{\mathbf{R}}_1 ({}^0\dot{\mathbf{R}}_1)^T {}^0\mathbf{R}_1 \ . \tag{3.25}$$

Rearranging eq. 3.15 for ${}^0\dot{\mathbf{R}}_1$

$$ {}^0\dot{\mathbf{R}}_1 = {}_0\widetilde{\boldsymbol{\omega}}_1 \, {}^0\mathbf{R}_1 \tag{3.26}$$

and repeatedly inserting eq. 3.26 into eq. 3.25 making use of $\widetilde{\boldsymbol{\omega}}$'s skew-symmetric property yields

$$ {}^0\ddot{\mathbf{R}}_1 = {}_0\dot{\widetilde{\boldsymbol{\omega}}}_1 {}^0\mathbf{R}_1 - {}_0\widetilde{\boldsymbol{\omega}}_1 \underbrace{{}^0\mathbf{R}_1({}^0\dot{\mathbf{R}}_1)^T}_{= ({}_0\widetilde{\boldsymbol{\omega}}_1)^T = -{}_0\widetilde{\boldsymbol{\omega}}_1} {}^0\mathbf{R}_1 \ . \tag{3.27} $$

Reinsertion into eq. 3.23 yields Euler's equation on acceleration level

$$ {}^0_0\ddot{\boldsymbol{r}}_P = {}^0_0\ddot{\boldsymbol{r}}_1 + ({}^0_0\dot{\widetilde{\boldsymbol{\omega}}}_1 {}^0\mathbf{R}_1 + {}^0_0\widetilde{\boldsymbol{\omega}}_{10}{}^0\widetilde{\boldsymbol{\omega}}_1 {}^0\mathbf{R}_1)\ {}^1_1\boldsymbol{r}_P \tag{3.28} $$

$$ {}_0\ddot{\boldsymbol{r}}_P = {}_0\ddot{\boldsymbol{r}}_1 + {}_0\dot{\boldsymbol{\omega}}_1 \times {}_1\boldsymbol{r}_P + {}_0\boldsymbol{\omega}_1 \times ({}_0\boldsymbol{\omega}_1 \times {}_1\boldsymbol{r}_P) \ . \tag{3.29} $$

3.2 Open Kinematic Chains

A kinematic chain is said to be open if each link is not connected to more than two other links and a terminal link being connected to only one link. Connecting two links by a joint introduces constraints that effectively reduce the set of possible relative displacements between the connected links. The resulting subset of displacements may form a subgroup of the group of general displacements. This is indeed the case for all lower kinematic pairs. Hervé (1978) has thoroughly enumerated all ten subgroups of the group of general displacements D and classified them by their conjugation classes.

In terms of group theory, the conjugate group H^g to a subgroup $H \leq D$ of the group of displacements by an element $g \in D$ representing a specific displacement is defined as

$$ H^g = \{ghg^{-1} \mid h \in H\} \ . \tag{3.30} $$

The *orbit* of H^g, i. e., the conjugate groups of H by all elements $g \in D$, is called the *conjugacy class* of H (Kosmann-Schwarzbach, 2010). For instance, the subset of displacements permitted by a revolute joint about a certain axis $\boldsymbol{u}$ through a point O form a subgroup of D which will be denoted as $R_{\boldsymbol{u},O}$ and contains as elements the rotations $R_{\boldsymbol{u},O}(\varphi)$ with $\varphi \in \mathbb{R}$. It can be shown, that any two rotations of the same or opposite angle are conjugate by another rotation (Kosmann-Schwarzbach, 2010). Thus, the conjugacy class, which will be denoted by R, defines the motion type of rotational displacements and is composed of all subgroups of rotational displacements about any axis. In a similar manner, the motion types T for translational, H for helical, etc. can be defined according to tab. 3.1. The X type motion refers to spatial translation with an additional rotation about a certain direction, which is also called Schönfließ-motion and resembles the motion, for example, performed by a SCARA manipulator,

as shown in fig. 2.7. The Y type motion, sometimes referred to as *translating screw motion* (Fanghella, 1988), results from a translational planar motion for which there exists an additional screw motion perpendicular to the plane.

Table 3.1: Conjugation classes of the general displacement group D (adapted from Thomas and Torras (1988) and Hervé (1992))

Dim.	Symbol	Description	Associated lower pair
0	E	Identity transformation	
1	$T_{\boldsymbol{u}}{}^*$	Translations in the direction of $\boldsymbol{u}$	(P) Prismatic
	$R_{\boldsymbol{u},O}{}^*$	Rotations about an axis determined by the direction of $\boldsymbol{u}$ and point O	(R) Revolute
	$H_{\boldsymbol{u},O,p}{}^*$	Screw motions about an axis ($\boldsymbol{u}$, O) with pitch p	(H) Screw
2	$T_P{}^{2\mathrm{D}*}$	Translations parallel to plane P	
	$C_{\boldsymbol{u},O}{}^*$	Combined rotations and translations along an axis ($\boldsymbol{u}$, O)	(C) Cylindrical
3	$T^{3\mathrm{D}*}$	Spatial translations	
	$G_{\boldsymbol{P}}$	Planar movements parallel to plane P	(E) Planar
	S_O	Spherical rotations about point O	(S) Spherical
	$Y_{\boldsymbol{u},p}$	Screw translations allowing planar translations perpendicular to $\boldsymbol{u}$ and screw motions of pitch p along any axis parallel to $\boldsymbol{u}$	
4	$X_{\boldsymbol{u}}$	Translating hinge motions allowing spatial translations and rotations about any axis parallel to $\boldsymbol{u}$	
6	D	General rigid body motions	

* Abelian group

3.2.1 Kinematic Chains as Compositions of Displacement Subgroups

The concept of displacement groups may be used to determine some general properties of the permitted relative motions of links in a serial chain. For a serial chain of n links, there are $n(n-1)/2$ possible pairings of links which Hervé termed *liaisons* or *bonds*, whose relative motion can be analyzed by composing and intersecting bonds for which a short introduction is given following Hervé (1992).

A serial chain of three links connected by two kinematical pairs inhibits three bonds – two formed directly from the intermediate kinematical pairs and a bond between the first and the last link. Each bond represents a set of possible relative displacements between the involved links. Insights on the permitted relative displacements between the first and the last link can be attained by the composition product of the operators corresponding to the intermediate bonds. Respecting the closure axiom of a group, if

the bonds between the first and second as well as the second and third link are subsets of the same displacement subgroup, the result of their composition is again a subset of the common displacement subgroup or is the subgroup itself. By serially linking lower kinematic pairs, the displacement subgroups listed in tab. 3.1 can be generated by group composition. For instance, the bond between the end-effector and the fixed frame of the SCARA manipulator shown in fig. 3.4 is represented by subgroup $X_{\boldsymbol{u}}$ with $\boldsymbol{u}$ as the vertical axis. Here, the three revolute joints with parallel axes are a motion generator of the planar subgroup $G_{\boldsymbol{P}}$ with $\boldsymbol{u} \perp P$ and the prismatic joint is a generator of $T_{\boldsymbol{u}}$. The group composition $G_{\boldsymbol{P}} \cup T_{\boldsymbol{u}}$ then yields the displacement subgroup $X_{\boldsymbol{u}}$.

By this means, in many cases, conclusions about type and dimension of the relative motion can be drawn. In tab. 3.2 conditions for certain displacement subgroups to be included within other subgroups as well as their dimensions are given. It shall be noted that not all displacement subsets resulting from compositions have a group structure, which for instance, is the case for a universal joint created by two revolute joints with perpendicular axes.

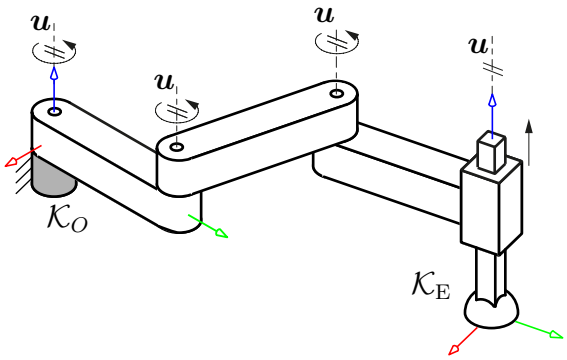

Figure 3.4: SCARA manipulator whose end effector performs an X type motion

3.2.2 Kinematics of Serial Chains

For open kinematic chains, the absolute kinematics can be derived in an explicit manner. As all joint variables $\underline{\beta}$ are independent and thus form a set of generalized coordinates $\underline{q}$, the only task remaining is the calculation of the absolute poses, velocities, and accelerations of all bodies with respect to the joint variables $\underline{\beta}$.

For a chain composed of n elementary kinematic pairs $\mathcal{G}_1 ... \mathcal{G}_n$, i. e., revolute and prismatic joints, pose, velocity, and acceleration of each link can be determined from the sequence of relative transformations. Each elementary joint $\mathcal{G}_i$ is described by its joint

Table 3.2: Subgroups and conditions for inclusion (adapted and extended from Hervé (1978))

Subgroups:	$T_{\boldsymbol{u}}$	$R_{\boldsymbol{u},\mathcal{O}}$	$H_{\boldsymbol{u},\mathcal{O},p}$	${T_P}^{\mathrm{2D}}$	$C_{\boldsymbol{u},\mathcal{O}}$	T^{3D}	$G_{\boldsymbol{P}}$	$S_{\mathcal{O}}$	$Y_{\boldsymbol{u},p}$	$X_{\boldsymbol{u}}$	D
Dimension:	1	1	1	2	2	3	3	3	3	4	6
$T_{\boldsymbol{u}'}$	$\boldsymbol{u} \parallel \boldsymbol{u}'$										
$R_{\boldsymbol{u}',\mathcal{O}'}$		$\boldsymbol{u} \parallel \boldsymbol{u}'$ $\boldsymbol{u} \parallel \boldsymbol{\mathcal{O}\mathcal{O}}'$									
$H_{\boldsymbol{u}',\mathcal{O}',p'}$			$\boldsymbol{u} \parallel \boldsymbol{u}'$ $\boldsymbol{u} \parallel \boldsymbol{\mathcal{O}\mathcal{O}}'$ $p = p'$								
${T_P}^{\mathrm{2D}}$	$\boldsymbol{u} \parallel P$			$P \parallel P'$							
$C_{\boldsymbol{u}',\mathcal{O}'}$	$\boldsymbol{u} \parallel \boldsymbol{u}'$	$\boldsymbol{u} \parallel \boldsymbol{u}'$ $\boldsymbol{u} \parallel \boldsymbol{\mathcal{O}\mathcal{O}}'$	$\boldsymbol{u} \parallel \boldsymbol{u}'$ $\boldsymbol{u} \parallel \boldsymbol{\mathcal{O}\mathcal{O}}'$		$\boldsymbol{u} \parallel \boldsymbol{u}'$ $\boldsymbol{u} \parallel \boldsymbol{\mathcal{O}\mathcal{O}}'$						
T^{3D}	yes			yes		yes					
$G_{\boldsymbol{P}'}$	$\boldsymbol{u} \parallel P'$	$\boldsymbol{u} \perp P'$		$P \parallel P'$			$P \parallel P'$				
$S_{\mathcal{O}'}$		$\boldsymbol{u} \parallel \boldsymbol{\mathcal{O}\mathcal{O}}'$						$\mathcal{O} = \mathcal{O}'$			
$Y_{\boldsymbol{u}',p'}$	$\boldsymbol{u} \perp \boldsymbol{u}'$		$\boldsymbol{u} \parallel \boldsymbol{u}'$ $p = p'$	$P \perp \boldsymbol{u}'$					$\boldsymbol{u} \parallel \boldsymbol{u}'$ $p = p'$		
$X_{\boldsymbol{u}'}$	yes	$\boldsymbol{u} \parallel \boldsymbol{u}'$	$\boldsymbol{u} \parallel \boldsymbol{u}'$	yes	$\boldsymbol{u} \parallel \boldsymbol{u}'$	yes	$P \perp \boldsymbol{u}'$		$\boldsymbol{u} \parallel \boldsymbol{u}'$	$\boldsymbol{u} \parallel \boldsymbol{u}'$	
D	yes	yes	yes	yes	yes	yes	yes	yes	yes	yes	yes

$p, p' \in \mathbb{R} \setminus 0$

axis u_i as well as a joint variable

$$\beta_i = \begin{cases} \theta_i \text{ if } \mathcal{G}_i \text{ is a revolute joint} \\ \boldsymbol{s}_i \text{ if } \mathcal{G}_i \text{ is a prismatic joint} \end{cases} \tag{3.31}$$

and its time derivative $\dot{\beta}_i$. For this reason, two symbolic operators `Trans` and `Rot` for translations and rotations respectively will be defined according to tab. 3.3, such that each transformation represents either a translation or rotation about a single coordinate axis and therefore represents an R or T type motion. In a sequence of transformations, each transformation applies to the transformed coordinate frame of the preceding transformation. Indeed, these six transformations are sufficient to achieve any general displacement by consecutive composition in any arbitrary order. A general transformation ${}^{i-1}\mathbf{A}_i$ with a translation along the vector $\{a, b, c\}^T$ and a rotation expressed by z-x-z Euler angles φ, θ, and ϕ can be composed as

$$\begin{aligned} {}^{i-1}\mathbf{A}_i = &\texttt{Trans}(x_{i-1}, a) \circ \texttt{Trans}(y_{i-1}, b) \circ \texttt{Trans}(z_{i-1}, c) \circ \\ &\texttt{Rot}(z_{i-1}, \varphi) \circ \texttt{Rot}(x'_{i-1}, \alpha_i) \circ \texttt{Rot}(z_i, \phi) \ . \end{aligned} \tag{3.32}$$

The inverse kinematics problem for a spatial kinematic chain consists of determining the joint variables $\underline{\beta}$ with respect to six parameters $\underline{\beta}_q$, which describe the desired

Table 3.3: Symbolic operators for elementary transformations

Axis	Translation	Rotation
$x:$	$\texttt{Trans}(x,s) = \begin{pmatrix} 1 & 0 & 0 & s \\ 0 & 1 & 0 & 0 \\ 0 & 0 & 1 & 0 \\ 0 & 0 & 0 & 1 \end{pmatrix}$	$\texttt{Rot}(x,\theta) = \begin{pmatrix} 1 & 0 & 0 & 0 \\ 0 & \cos(\theta) & -\sin(\theta) & 0 \\ 0 & \sin(\theta) & \cos(\theta) & 0 \\ 0 & 0 & 0 & 1 \end{pmatrix}$
$y:$	$\texttt{Trans}(y,s) = \begin{pmatrix} 1 & 0 & 0 & 0 \\ 0 & 1 & 0 & s \\ 0 & 0 & 1 & 0 \\ 0 & 0 & 0 & 1 \end{pmatrix}$	$\texttt{Rot}(y,\theta) = \begin{pmatrix} \cos(\theta) & 0 & \sin(\theta) & 0 \\ 0 & 1 & 0 & 0 \\ -\sin(\theta) & 0 & \cos(\theta) & 0 \\ 0 & 0 & 0 & 1 \end{pmatrix}$
$z:$	$\texttt{Trans}(z,s) = \begin{pmatrix} 1 & 0 & 0 & 0 \\ 0 & 1 & 0 & 0 \\ 0 & 0 & 1 & s \\ 0 & 0 & 0 & 1 \end{pmatrix}$	$\texttt{Rot}(z,\theta) = \begin{pmatrix} \cos(\theta) & -\sin(\theta) & 0 & 0 \\ \sin(\theta) & \cos(\theta) & 0 & 0 \\ 0 & 0 & 1 & 0 \\ 0 & 0 & 0 & 1 \end{pmatrix}$

end-effector pose in world coordinates. The problem then can be regarded as a closed kinematic loop which is dealt with in sec. 3.3 with the six parameters $\underline{\beta}_q$ as the input $\underline{q}$ and the joint variables $\underline{\beta}$ as the output.

3.2.3 Velocity and Acceleration Transmission

The angular velocity $\boldsymbol{\omega}_n$ and translational velocity $\boldsymbol{v}_n$ of the origin O_n of a coordinate frame $\mathcal{K}_n$ at the end of a sequence of elementary joints can be determined by the sum of the relative velocities. Introducing the operator

$$\sigma_i = \begin{cases} 0 \text{ if } \mathcal{G}_i \text{ is a revolute joint} \\ 1 \text{ if } \mathcal{G}_i \text{ is a prismatic joint} \end{cases} \tag{3.33}$$

and its complement $\overline{\sigma} = 1 - \sigma$, following the notation and derivation from Kecskeméthy (1993a) and Krupp (1999), a compact expression for the velocities and accelerations

can be deduced

$$\boldsymbol{\omega}_n = \sum_{i=1}^{n} \overline{\sigma}_i \boldsymbol{u}_i \dot{\beta}_i \ , \tag{3.34}$$

$$\boldsymbol{v}_n = \sum_{i=1}^{n} \sigma_i \boldsymbol{u}_i \dot{\beta}_i + \overline{\sigma}_i (\underbrace{\boldsymbol{u}_i \times {}_{i-1}\boldsymbol{r}_n}_{\boldsymbol{\chi}_i}) \dot{\beta}_i \ . \tag{3.35}$$

In matrix form eq. 3.34 and eq. 3.35 can be expressed as

$$\begin{pmatrix} \boldsymbol{\omega}_n \\ \boldsymbol{v}_n \end{pmatrix} = \begin{pmatrix} \overline{\sigma}_1 \boldsymbol{u}_1 & \cdots & \overline{\sigma}_n \boldsymbol{u}_n \\ \sigma_1 \boldsymbol{u}_1 + \overline{\sigma}_1(\boldsymbol{\chi}_1) & \cdots & \sigma_n \boldsymbol{u}_n + \overline{\sigma}_n(\boldsymbol{\chi}_n) \end{pmatrix} \begin{pmatrix} \dot{\beta}_1 \\ \vdots \\ \dot{\beta}_n \end{pmatrix} \tag{3.36}$$

with angular and translational velocity combined as the twist

$$\underline{\mathrm{t}}_i = \begin{pmatrix} \boldsymbol{\omega}_i \\ \boldsymbol{v}_i \end{pmatrix} \tag{3.37}$$

the vector of joint velocities

$$\underline{\dot{\beta}} = \begin{pmatrix} \dot{\beta}_1 \\ \vdots \\ \dot{\beta}_n \end{pmatrix} \tag{3.38}$$

and the Jacobian matrix

$$(\mathbf{J}_t)_n = \begin{pmatrix} \overline{\sigma}_1 \boldsymbol{u}_1 & \cdots & \overline{\sigma}_n \boldsymbol{u}_n \\ \overline{\sigma}_1(\boldsymbol{\chi}_1) + \sigma_1 \boldsymbol{u}_1 & \cdots & \overline{\sigma}_n(\boldsymbol{\chi}_n) + \sigma_n \boldsymbol{u}_n \end{pmatrix} \tag{3.39}$$

which maps the joint velocities to the angular and translational velocity of the tip frame $\mathcal{K}_n$.

The angular and translational accelerations $\dot{\boldsymbol{\omega}}$ and $\boldsymbol{a}$ are formed by the time derivative of $\underline{\mathrm{t}}$

$$\underline{\dot{\mathrm{t}}}_n = \mathbf{J}_n \underline{\ddot{\beta}} + \dot{\mathbf{J}}_n \underline{\dot{\beta}} \ . \tag{3.40}$$

The time derivative of the Jacobian then yields

$$(\dot{\mathbf{J}}_t)_n = \begin{pmatrix} \overline{\sigma}_1 \dot{\boldsymbol{u}}_1 & \cdots & \overline{\sigma}_n \dot{\boldsymbol{u}}_n \\ \sigma_1 \dot{\boldsymbol{u}}_1 + \overline{\sigma}_1 \dot{\boldsymbol{\chi}}_1 & \cdots & \sigma_n \dot{\boldsymbol{u}}_n + \overline{\sigma}_n \dot{\boldsymbol{\chi}}_n \end{pmatrix} \tag{3.41}$$

with the following terms for the derivatives of the joint axes $\dot{\boldsymbol{u}}_i$ and cross products $\dot{\boldsymbol{\chi}}_i$

$$\dot{\boldsymbol{u}}_i = \sum_{j=1}^{i-1} \overline{\sigma}_j \boldsymbol{u}_j \times \boldsymbol{u}_i \dot{\beta}_j \tag{3.42}$$

$$\dot{\boldsymbol{\chi}}_i = \sum_{j=1}^{i} \overline{\sigma}_j \boldsymbol{u}_j \times \boldsymbol{\chi}_i \dot{\beta}_j + \overline{\sigma}_i \boldsymbol{u}_i \times \sum_{j=i+1}^{n} (\overline{\sigma}_j \boldsymbol{\chi}_j + \sigma_j \boldsymbol{u}_j) \dot{\beta}_j \ . \tag{3.43}$$

The performance of the Jacobian matrix in terms of computational time depends on the coordinate frame of decomposition for which, the root coordinate frame $\mathcal{K}_0$ (Waldron, 1982), an intermediate frame $\mathcal{K}_l$ (Renaud, 1981) or the tip frame $\mathcal{K}_n$ (Orin and Schrader, 1984) are possible choices. Further material on this topic can be found in (Stelzle et al., 1995).

3.3 Single-Loop Kinematic Chains

A single-loop kinematic chain is formed if each link in a kinematic chain is connected to exactly two other links. It can be represented as a sequence of n relative homogeneous transformations denoted by ${}^{i-1}\mathbf{A}_i$ between successive coordinate frames $\mathcal{K}_{i-1}$ and $\mathcal{K}_i$ such that the terminal reference frame $\mathcal{K}_n$ coincides with the initial reference frame $\mathcal{K}_1$. As a result, a general closure condition can be stated as

$$ {}^{1}\mathbf{A}_2 {}^{2}\mathbf{A}_3 \cdots {}^{n-1}\mathbf{A}_n = \mathbf{I}_4 \tag{3.44} $$

with $\mathbf{I}_4$ as the 4×4 identity matrix. From these twelve implied conditions, of which three arise from the position and nine from the orientation, a maximum of six independent constraint equations can be extracted as only three orientation equations are independent for reasons discussed in sec. 3.1.2. The actual number of independent constraint equations corresponds to the spatiality b of the loop as introduced in sec. 2.4. Picking these b independent constraint equations is not trivial, which in general are of the form

$$ g_i(\underline{\beta}^{out}, \underline{q}) = 0, \quad i = 1, \ ..., \ b \tag{3.45} $$

where the $n_{\mathcal{G}}$ joint variables $\underline{\beta}$ are divided into $\underline{\beta}^{out} = [\beta_1^{out}, \ldots, \beta_b^{out}]^{\mathrm{T}}$ output variables which depend on the remaining $\underline{q} = [q_1, \ldots, q_f]^{\mathrm{T}}$ input variables for a loop with f degrees of freedom. These are non-linear equations for the closure at position level in terms of the joint coordinates and linear equations for velocity and acceleration level in terms of the first- and second-order derivatives of the joint variables.

The reason for a spatiality of less than six relies on special geometric conditions, such that some of the equations become redundant. In general, these dependencies can be detected by numerical or symbolic rank analysis of the Jacobian matrix with deficiencies mentioned in sec. 2.4.3. In the next section, group-theoretic concepts are elaborated based on the previously introduced displacement subgroups, which allow conclusions on spatiality and degree of freedom a priori and without the knowledge of exact geometrical dimensions.

3.3.1 Kinematic Loops as Intersections of Displacement Subgroups

When declaring one link as the base and another as the tip, a closed chain can also be viewed as two parallel, serial chains connecting the base and tip link. The set of allowed displacements corresponding to the bond between the base and the tip link is then represented by the intersection of the displacement subsets established by the two individual serial chains. The possible cases are shortly reworked from Hervé (1992).

If each of the two bonds created by the parallel, serial chains can be represented by a displacement subgroup, the result of the intersection again forms a group. In that case, the intersection bond lies either within one of the two bonds or is a subgroup contained in both bonds. The first case would occur, for instance, for an intersection of the subgroup of spatial translations T^{3D} and a general displacement D. The resulting intersection is again within the T^{3D} subgroup. As an example of the latter case, two chains, which are motion generators of $X_{\boldsymbol{u_1}}$ and $X_{\boldsymbol{u_2}}$ with $\boldsymbol{u_1} \nparallel \boldsymbol{u_2}$, are assumed. The intersection due to the non-parallel rotation axes corresponds to a spatial translation:

$$X_{\boldsymbol{u_1}} \cap X_{\boldsymbol{u_2}} = T^{3D} \tag{3.46}$$

If neither subgroup is included within the other, nor a common subgroup exists, the intersection equals the identity displacement E and the closed kinematic chain can be viewed as rigid. The conditions necessary for the inclusion of one subgroup in another was already given in tab. 3.2. The pairwise intersections of all subgroups whose resulting common subgroups are not equal to the identity displacement are given in tab. 3.4.

The group representation of kinematic chains then gives rise to the following three classifications: A kinematic chain in which any possible bond between two links can be represented by a subset of a certain displacement subgroup is said to be *trivial*. It will directly obey the Chebyshev-Grübler-Kutzbach formula eq. 2.2 with a spatiality b equal to the dimension of the subgroup associated with the kinematic chain.

Kinematic chains which cannot be associated with a distinct displacement subgroup, but whose type of motion can be derived by the previously established methods of composition and intersection of bonds, form an exception to the general CGK formula and are termed *exceptional chains*. The third type cannot be analyzed by these methods and applies to so-called *paradoxical chains*, "which depend on specific geometric conditions that imply relations between bar lengths and angle trigonometric functions" (Hervé, 1999, p. 728).

In order to apply these insights to single-loop kinematic chains, which are expressed as sequences of elementary transformations introduced in sec. 3.2.2, it is necessary to associate these sequences to displacement subgroups as shown in the following section.

Table 3.4: Intersections of group compositions which are different from identity displacement and corresponding regular representation (adapted from Hervé (1992))

Group composition	Conditions	Intersection	Regular representation
${T_P}^{\mathrm{2D}} \cdot {T_{P'}}^{\mathrm{2D}}$		$T_{\boldsymbol{u}} \quad \boldsymbol{u} \parallel P \cap P'$	T^{3D}
${T_P}^{\mathrm{2D}} \cdot G_{\boldsymbol{P'}}$		$T_{\boldsymbol{u}} \quad \boldsymbol{u} \parallel P \cap P'$	$X_{\boldsymbol{v}} \quad \boldsymbol{v} \perp P'$
$G_{\boldsymbol{P}} \cdot G_{\boldsymbol{P'}}$		$T_{\boldsymbol{u}} \quad \boldsymbol{u} \parallel P \cap P'$	$R_{\boldsymbol{v},O} \cdot T^{\mathrm{3D}} \cdot R_{\boldsymbol{v'},O'} \quad \boldsymbol{v} \perp P, \boldsymbol{v'} \perp P'$
$Y_{\boldsymbol{u},p} \cdot {T_P}^{\mathrm{2D}}$	$\boldsymbol{u} \not\perp P$	$T_{\boldsymbol{v}} \quad \boldsymbol{v} \parallel P, \boldsymbol{v} \perp \boldsymbol{u}$	$X_{\boldsymbol{u}}$
$Y_{\boldsymbol{u},p} \cdot G_{\boldsymbol{P}}$	$\boldsymbol{u} \not\perp P$	$T_{\boldsymbol{v}} \quad \boldsymbol{v} \parallel P, \boldsymbol{v} \perp \boldsymbol{u}$	$X_{\boldsymbol{u}} \cdot R_{\boldsymbol{w},O} \quad \boldsymbol{w} \perp P$
$Y_{\boldsymbol{u},p} \cdot Y_{\boldsymbol{u'},p'}$	$\boldsymbol{u} \not\parallel \boldsymbol{u'}$	$T_{\boldsymbol{v}} \quad \boldsymbol{v} \perp \boldsymbol{u}, \boldsymbol{v} \perp \boldsymbol{u'}$	$R_{\boldsymbol{w},O} \cdot T^{\mathrm{3D}} \cdot R_{\boldsymbol{w'},O'} \quad \boldsymbol{w} \parallel \boldsymbol{u}, \boldsymbol{w'} \parallel \boldsymbol{u'}$
$Y_{\boldsymbol{u},p} \cdot C_{\boldsymbol{u'},O}$	$\boldsymbol{u} \perp \boldsymbol{u'}$	$T_{\boldsymbol{u'}}$	$Y_{\boldsymbol{u},p} \cdot R_{\boldsymbol{u'},O}$
$C_{\boldsymbol{u},O} \cdot C_{\boldsymbol{u'},O'}$	$\boldsymbol{u} \parallel \boldsymbol{u'}$	$T_{\boldsymbol{u}}$	$C_{\boldsymbol{u},O} \cdot R_{\boldsymbol{u'},O'}$
${T_P}^{\mathrm{2D}} \cdot C_{\boldsymbol{u},O}$	$\boldsymbol{u} \parallel P$	$T_{\boldsymbol{u}}$	${T_P}^{\mathrm{2D}} \cdot R_{\boldsymbol{u},O}$
$T^{\mathrm{3D}} \cdot C_{\boldsymbol{u},O}$		$T_{\boldsymbol{u}}$	$X_{\boldsymbol{u}}$
$G_{\boldsymbol{P}} \cdot C_{\boldsymbol{u},O}$	$\boldsymbol{u} \parallel P$	$T_{\boldsymbol{u}}$	$G_{\boldsymbol{P}} \cdot R_{\boldsymbol{u},O}$
$X_{\boldsymbol{u}} \cdot C_{\boldsymbol{u'},O}$	$\boldsymbol{u} \not\parallel \boldsymbol{u'}$	$T_{\boldsymbol{u'}}$	$X_{\boldsymbol{u}} \cdot R_{\boldsymbol{u'},O}$
$Y_{\boldsymbol{u},p} \cdot C_{\boldsymbol{u'},O}$	$\boldsymbol{u} \parallel \boldsymbol{u'}$	$H_{\boldsymbol{u},O,p}$	$X_{\boldsymbol{u}}$
$G_{\boldsymbol{P}} \cdot C_{\boldsymbol{u},O}$	$\boldsymbol{u} \perp P$	$R_{\boldsymbol{u},O}$	$X_{\boldsymbol{v}} \quad \boldsymbol{v} \perp P$
$S_O \cdot C_{\boldsymbol{u},O'}$	$OO' \parallel \boldsymbol{u}$	$R_{\boldsymbol{u},O}$	$S_O \cdot T_{\boldsymbol{u}}$
$S_O \cdot G_{\boldsymbol{P}}$		$R_{\boldsymbol{u},O} \quad \boldsymbol{u} \perp P$	$S_O \cdot {T_P}^{\mathrm{2D}}$
$S_O \cdot X_{\boldsymbol{u}}$		$R_{\boldsymbol{u},O}$	D
$S_O \cdot S_{O'}$		$R_{\boldsymbol{u},O} \quad \boldsymbol{u} = OO'/\lvert OO' \rvert$	$S_O \cdot R_{\boldsymbol{v},O'} \cdot R_{\boldsymbol{v'},O'}$
$Y_{\boldsymbol{u},p} \cdot Y_{\boldsymbol{u'},p'}$	$\boldsymbol{u} \parallel \boldsymbol{u'}$	${T_P}^{\mathrm{2D}} \quad P \perp \boldsymbol{u}$	$X_{\boldsymbol{u}}$
$Y_{\boldsymbol{u},p} \cdot X_{\boldsymbol{u'}}$	$\boldsymbol{u} \not\parallel \boldsymbol{u'}$	${T_P}^{\mathrm{2D}} \quad P \perp \boldsymbol{u}$	$X_{\boldsymbol{u}} \cdot R_{\boldsymbol{u'},O}$
$G_{\boldsymbol{P}} \cdot Y_{\boldsymbol{u},p}$	$\boldsymbol{u} \perp P$	${T_P}^{\mathrm{2D}}$	$X_{\boldsymbol{u}}$
$G_{\boldsymbol{P}} \cdot X_{\boldsymbol{u}}$	$\boldsymbol{u} \not\perp P$	${T_P}^{\mathrm{2D}}$	$R_{\boldsymbol{v},O} \cdot T^{\mathrm{3D}} \cdot R_{\boldsymbol{v'},O'} \quad \boldsymbol{v} \perp P, \boldsymbol{v'} \parallel \boldsymbol{u}$
$G_{\boldsymbol{P}} \cdot T^{\mathrm{3D}}$		${T_P}^{\mathrm{2D}}$	$X_{\boldsymbol{u}} \quad \boldsymbol{u} \perp P$
$Y_{\boldsymbol{u},p} \cdot T^{\mathrm{3D}}$		${T_P}^{\mathrm{2D}}$	$X_{\boldsymbol{u}}$
$X_{\boldsymbol{u}} \cdot X_{\boldsymbol{u'}}$	$\boldsymbol{u} \not\parallel \boldsymbol{u'}$	T^{3D}	$R_{\boldsymbol{u},O} \cdot T^{\mathrm{3D}} \cdot R_{\boldsymbol{u'},O'}$

3.4 Computational Processing of Displacement Groups

The concept of the displacement subgroups as presented by Hervé provides a powerful and intuitive approach to understanding some peculiarities of certain kinematic chains and deriving some key parameters such as the spatiality. Though, it is not very handy

when it comes down to automating this analysis by means of computer programs.

Quite straightforward to automate on the other side is an approach based on isotropy groups introduced by Kecskeméthy and Hiller (1992) and later extended by Liu et al. (2017) that was originally developed to find efficient closure conditions for single-loop kinematic chains. It turns out that both concepts are closely related, allowing access to computational processing of the approach from Hervé. For a more intuitive illustration of the general ideas and the functionality, this work mainly utilizes the displacement subgroups of Hervé. It is easily conceivable though, that additional benefits regarding automation capabilities could be gained by using the isotropy groups which constitutes a possible entry point for prospective development. Some close analogies of both concepts will be worked out hereafter and are demonstrated for the derivation of the degree of freedom for several single-loop kinematic chains in sec. 3.4.1. After some background information on isotropy groups is given, the *invariance properties matrix* (IPM) will be introduced according to Kecskeméthy and Hiller (1992) for further analysis.

Points, lines, and planes represent subsets of $\mathbb{R}^3$ and ξ shall represent one of these subsets. An *isotropy group* $\hat{\mathbf{A}}^{\mathrm{iso}(\xi)}$ with respect to one of these subsets ξ is then defined as

$$\hat{\mathbf{A}}^{\mathrm{iso}(\xi)} = \{\mathbf{A} \in D \mid \mathbf{A}\ \xi = \xi\} \tag{3.47}$$

such that $\hat{\mathbf{A}}^{\mathrm{iso}(\xi)}$ includes any displacement $\mathbf{A}$ within the group of general displacements D, which leaves the subset ξ invariant and furthermore forms a group again (Hilgert and Neeb, 2012, p. 361). By this means, the following isotropy groups can be identified (Meng et al., 2007, p.104):

$$\hat{\mathbf{A}}^{\mathrm{iso}(\xi)} = \begin{cases} S_O & \text{if } \xi \text{ is a point} \\ C_{\boldsymbol{u},O} & \text{if } \xi \text{ is a line} \\ G_{\boldsymbol{u}} & \text{if } \xi \text{ is a plane} \\ X_{\boldsymbol{u}} & \text{if } \xi \text{ is a point at infinity} \end{cases}$$

When considering only kinematic chains that consist of sequences of elementary transformations as introduced in sec. 3.2.2, the invariant elements are easy to track. A point will be denoted as O, a line as $\mathcal{L}_i$, a plane as Π_i, and a point at infinity in accordance with eq. 3.9 as $\underline{\overset{\mathrm{H}}{e}}_i$ with $i \in \{x, y, z\}$ representing the coordinate axes about which the elementary transformation is performed. In tab. 3.5 the respective invariant elements for each of the six elementary transformations are shown and marked by a 1, within the invariance properties matrix (IPM).

Table 3.5: Invariance properties matrix (IPM) for elementary transformations

		$\mathtt{Trans}(x,a)$	$\mathtt{Trans}(y,b)$	$\mathtt{Trans}(z,c)$	$\mathtt{Rot}(x,\alpha)$	$\mathtt{Rot}(y,\beta)$	$\mathtt{Rot}(z,\gamma)$
$X:$	$\overset{\mathrm{H}}{\underline{e}}_x$	1	1	1	1		
	$\overset{\mathrm{H}}{\underline{e}}_y$	1	1	1		1	
	$\overset{\mathrm{H}}{\underline{e}}_z$	1	1	1			1
	Π_x		1	1	1		
$G:$	Π_y	1		1		1	
	Π_z	1	1				1
	$\mathcal{L}_x$	1			1		
$C:$	$\mathcal{L}_y$		1			1	
	$\mathcal{L}_z$			1			1
$S:$	O				1	1	1

If a sequence of transformations is found that leaves one of the elements point, line, plane, or point at infinity invariant, the transformation sequence can be associated with the corresponding isotropy group. Transformations which are functions of joint variables will be termed *joint transformations* and are motion generators of the respective displacement subgroup. The constant transformations originating from the kinematic chain's geometry are referred to as *link transformations* and resemble only a single element of a displacement subgroup. Therefore, depending on the number and type of transformations, a transformation sequence that leaves one element ξ invariant, is either a generator of the corresponding isotropy group or represents only a subset. Hence, the dimension of the respective isotropy group forms an upper bound for the dimension of motion generated by the underlying transformation sequence.

If a transformation sequence leaves several elements invariant, the displacement subgroup in which the sequence operates is the result of the intersection of isotropy groups associated with the invariant elements. For example the transformation sequence of three subsequent rotations about the same axis

$$\mathbf{A} = \mathtt{Rot}(x,\alpha) \circ \mathtt{Rot}(x,\beta) \circ \mathtt{Rot}(x,\gamma) \tag{3.48}$$

leaves the origin O, plane Π_x, line $\mathcal{L}_x$, and a point at infinity $\overset{\mathrm{H}}{\underline{e}}_x$ invariant. Thus, the sequence describes a displacement, which is a subset of a subgroup common to

all respective isotropy groups S_O, $G_{\boldsymbol{x}}$, $C_{\boldsymbol{x},O}$, and $X_{\boldsymbol{x}}$. This common subgroup can be determined by intersecting the respective isotropy groups according to tab. 3.4 and tab. 3.2, as described in sec. 3.3.1

$$\mathbf{A}^{(\mathrm{G})} = \underbrace{X_{\boldsymbol{x}} \cap G_{\boldsymbol{x}}}_{G_{\boldsymbol{x}}} \cap \underbrace{C_{\boldsymbol{x},O} \cap S_O}_{R_{\boldsymbol{x},O}} = R_{\boldsymbol{x},O} \ . \tag{3.49}$$

As expected, this common subgroup is the group of all rotations about the x-axis.

3.4.1 Determining the Degree of Freedom of a Kinematic Loop

The Chebyshev-Grübler-Kutzbach formula eq. 2.2 can be further simplified for a single-loop kinematic chain which is composed of elementary transformations and joints as the connectivity of each joint $f_{\mathcal{G}_i}$ equals one

$$f = \sum_{i=1}^{n_{\mathcal{G}}} f_{\mathcal{G}_i} - n_L \cdot b = n_{\mathcal{G}} - b \ . \tag{3.50}$$

Therefore, only the spatiality is left to be determined. For a better understanding of the spatiality, the loop can be split at one link, thus forming a simple open kinematic chain whose terminal links are formed by the two parts of the split link. The number of independent relative motions between these two parts represents the spatiality of the corresponding closed loop. It is worth mentioning that the spatiality "does not vary with the choice of split up links" (Gogu, 2008, p. 100).

For an automated detection of the spatiality b without the necessity to establish the loop closure conditions, by means of the previously introduced IPM, invariant properties can be tracked and likewise an upper bound for the spatiality b and vice versa a lower bound for the degree of freedom can be derived by according group operations as exemplified for two closed kinematic chains in the following section.

Trivial Chains

At first, the invariant elements of the loop are detected and gathered in the invariance properties matrix similar to tab. 3.5 whereby the columns correspond to the elementary transformations in order of the given kinematic chain. For a single-loop kinematic chain, the IPM is cyclic, i. e., the last column also borders the first one.

If a sequence of transformations can be found, which contains all joint transformations of the loop and leaves one or more elements invariant, the spatiality of the loop is

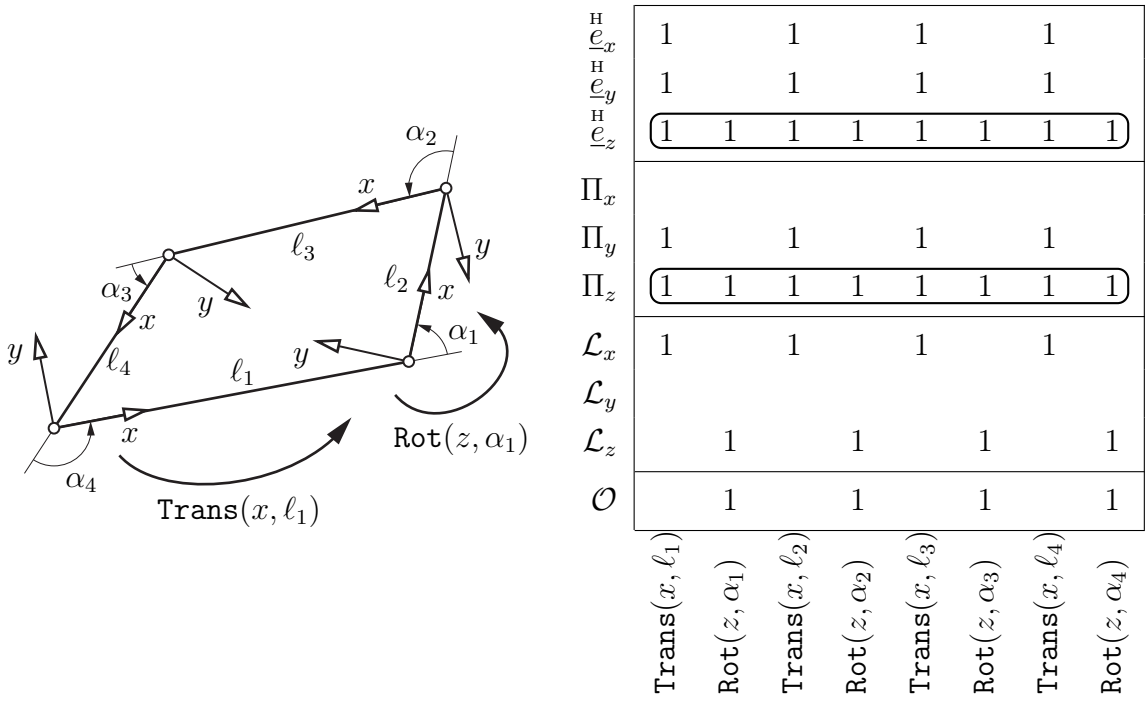

Figure 3.5: Planar four-bar mechanism and corresponding IPM

smaller or equal to the dimension of the associated isotropy group. The degree of freedom can then be calculated by eq. 3.50. Note that the sequence may be bordered by further constant transformations, and in some cases, it might be necessary to commute some of the elementary transformations in order to extend a particular sequence effectively. This is possible for successive transformations that form an Abelian group, as highlighted in tab. 3.1, i. e., subgroups which are commutative such that transformations can be performed in any order. Accordingly, any two translations, rotations about the same axis, or a translation and a rotation about the same axis may be swapped.

In this manner, for the simple four-bar mechanism shown in fig. 3.5 the highlighted sequence is found, which leaves the elements $\overset{\mathrm{H}}{\underline{e}}_z$ and Π_z invariant and contains all joint transformations. Thus, the motion of the kinematic chain is detected to be within the planar group

$$\mathbf{A}^{(\mathrm{G})} = X_{\boldsymbol{z}} \cap G_{\boldsymbol{z}} = G_{\boldsymbol{z}} \tag{3.51}$$

for which the spatiality is equal to $b = \mathtt{dim}(G_{\boldsymbol{z}}) = 3$. Therefore, the mechanism features

$$f = n_{\mathcal{G}} - b = 4 - 3 = 1 \tag{3.52}$$

degree of freedom and three independent closure conditions can be derived.

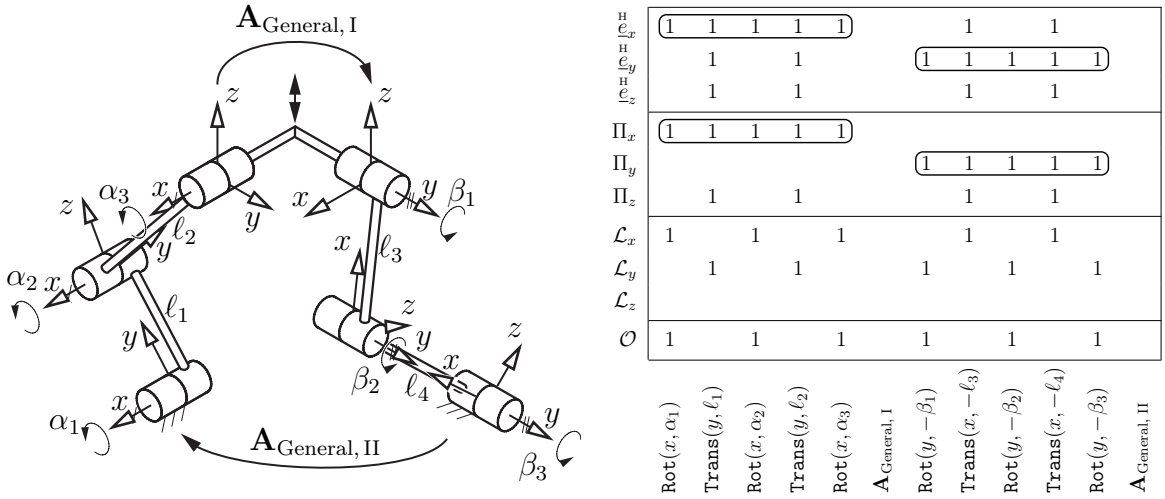

Figure 3.6: Exceptional kinematic chain of a Sarrus mechanism

Alternatively, the same result can be directly extracted from the IPM, as the plane Π_z is invariant with respect to all joint transformations and consequently, the mechanism is identified to be planar with a spatiality of 3.

Exceptional Chains

In some cases, two distinct transformation sequences $\mathbf{A}_I$ and $\mathbf{A}_{II}$ may be found, which together contain all joint variables and are disconnected either by intermediate constant transformations or by the fact that there are two different invariant elements associated. As a result, the spatiality of the loop cannot be expressed by a single associated displacement subgroup. Yet, when the open chain achieved by concatenating $\mathbf{A}_I$ and $\mathbf{A}_{II}$ is regarded, b directly follows from the dimension of the group composition:

$$b = \mathtt{dim}(\mathbf{A}_I{}^{(\mathrm{G})}) + \mathtt{dim}(\mathbf{A}_{II}{}^{(\mathrm{G})}) - \mathtt{dim}(\mathbf{A}_I{}^{(\mathrm{G})} \cap \ \mathbf{A}_{II}{}^{(\mathrm{G})}) \ . \tag{3.53}$$

Necessary to that end is that the dimension of any common subgroup is only counted once, from which the subtraction of $\mathtt{dim}(\mathbf{A}_I^{(G)} \cap \ \mathbf{A}_{II}^{(G)})$ follows.

This concept shall now be applied to the well-known overconstrained Sarrus mechanism (Sarrus, 1853) shown in fig. 3.6. The mechanism is composed of six elementary kinematic pairs and links, including the base frame. After the transformation sequence is established, a corresponding IPM which marks the invariant elements is created, as shown in fig. 3.6 with $\mathbf{A}_{\text{General, I}}$ and $\mathbf{A}_{\text{General, II}}$ representing general displacements between the respective rigidly connected frames.

Within the IPM, subchain $\mathbf{A}_I$ is identified as the longest sequence leaving $\overset{\text{H}}{e}_x$ and Π_x

invariant and a second subchain $\mathbf{A}_{II}$ was detected within the remaining columns of the IPM leaving $\overset{\text{H}}{\underline{e}}_y$ and Π_y invariant. Both subchains together contain all joint variables and are associated with the groups $X_{\boldsymbol{x}}$ and $G_{\boldsymbol{x}}$, as well as $X_{\boldsymbol{y}}$ and $G_{\boldsymbol{y}}$, respectively. The spatiality is then determined

$$b = \mathtt{dim}(\underbrace{X_{\boldsymbol{x}} \cap G_{\boldsymbol{x}}}_{G_{\boldsymbol{x}}}) + \mathtt{dim}(\underbrace{X_{\boldsymbol{y}} \cap G_{\boldsymbol{y}}}_{G_{\boldsymbol{y}}}) - \mathtt{dim}(\underbrace{(X_{\boldsymbol{x}} \cap G_{\boldsymbol{x}}) \cap (X_{\boldsymbol{y}} \cap G_{\boldsymbol{y}})}_{T_{\boldsymbol{z}}}) = 3 + 3 - 1 = 5 \tag{3.54}$$

such that the degree of freedom follows by eq. 3.50

$$f = 6 - 5 = 1 \ . \tag{3.55}$$

Clearly, there is no distinct displacement subgroup that can be associated with the kinematic chain, and even though the chain performs a spatial motion, its spatiality is only 5.

The same conclusion can be drawn by inspection of the IPM: All joint transformations are contained within subchains $\mathbf{A}_I$ and $\mathbf{A}_{II}$ leaving the respective planes invariant. Any measure between those planes, such as the intermediate angle, therefore is invariant with respect to all joint variables and the corresponding constraint does not impose any condition on the mobility of the kinematic chain. The number of possible independent constraints therefore reduces from 6 to 5.

Overdetermined Single-Loop Kinematic Chains

Previously, the term overconstrained was introduced, which for a single-loop kinematic chain eq. 2.6 can be further simplified with $n_{\mathcal{B}} = n_{\mathcal{G}}$ and $f = n_{\mathcal{G}} - b$ from which follows

$$N = 6 - b \ . \tag{3.56}$$

Similar to a system with more equations than variables to be solved for, here, the term *overdetermined* will be used for a loop that has been assigned more inputs q than encompassed degrees of freedom f. The degree d by which a loop is overdetermined will be defined as

$$d = q - f \tag{3.57}$$

where $d < 0$ indicates an underdetermined loop with an insufficient number of input joint variables. On the contrary, for $d > 0$, the underlying system of equations is

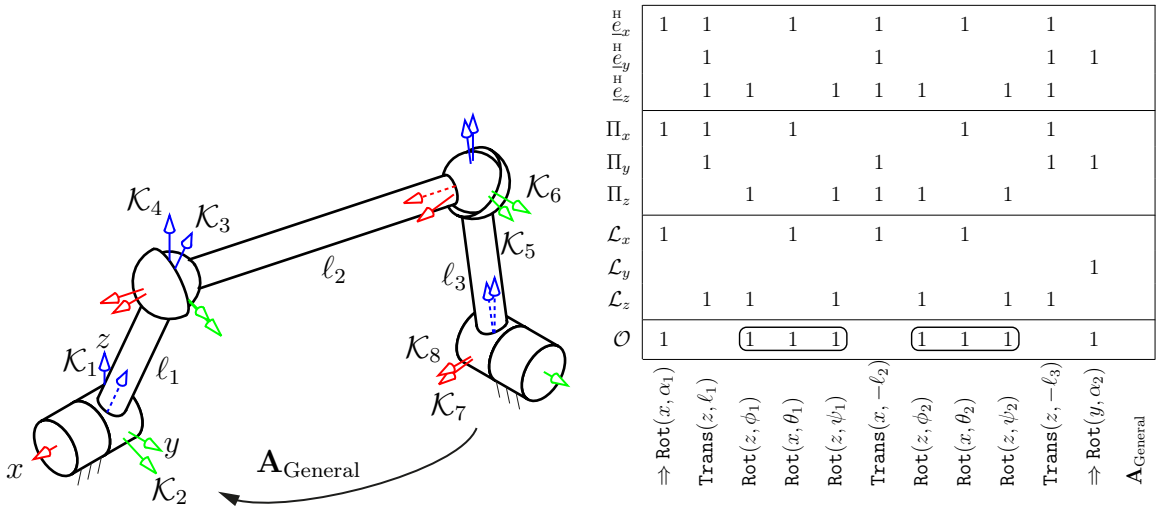

Figure 3.7: Four-bar mechanism with isolated degrees of freedom

overdetermined, and therefore, only an approximation for the given inputs can be determined. Yet, even if $q = f$ variables are assigned as inputs, in some cases, this set of input joint variables may not be independent, and therefore, additional joint variables are required as inputs.

This is, for instance, the case if the remaining joint variables to be solved for feature redundant degrees of freedom according to sec. 2.4.5. A lower bound for the number of additionally required inputs can be assessed by analyzing the spatiality of the kinematic chain, with all input joint variables regarded fixed. If the spatiality appears to be less than the number of remaining unfixed joint variables, a corresponding amount of additional inputs need to be provided.

As an example, a four-bar mechanism and its IPM with one isolated degree of freedom are shown in fig. 3.7 with a spatiality of $b = 6$ and $n_{\mathcal{G}} = 8$ elementary joints resulting from the decomposition of the spherical joints. In correspondence to the two degrees of freedom of this kinematic chain, both revolute joint angles $\underline{q} = [\alpha_1, \alpha_2]$ are defined as inputs. The spatiality can then be analyzed by treating the inputs as rigid link transformations for the IPM. Within the chain of the remaining $n'_{\mathcal{G}} = 6$ joint variables, the two highlighted sequences containing all joint variables are identified with a resulting spatiality of

$$b' = \mathtt{dim}(S_{O_4}) + \mathtt{dim}(S_{O_5}) - \mathtt{dim}(\underbrace{S_{O_4} \cap S_{O_5}}_{R_{\boldsymbol{x},O_5}}) = 3 + 3 - 1 = 5 \; . \tag{3.58}$$

Thus, the remaining chain features one redundant degree of freedom resulting from the isolated spin, which has to be provided as an input. With the additional input,

the loop is then overdetermined by $d = 3 - 2 = 1$. If initially a different set of input variables such as α_1 and ϕ_1 was chosen, no additional inputs would be necessary.

3.4.2 Kinematics of Single-Loop Kinematic Chains

Depending on the spatiality b of a single-loop kinematic chain, up to $b \leq 6$ independent constraint equations can be extracted from the general closure condition stated in eq. 3.45. Some common approaches for the formulation of geometric closure conditions from a "physical" perspective are according to Hiller and Woernle (1988):

- **Split the loop at one body:**
  As the body is considered to be rigid, both parts of the body must coincide in their pose for reassembly, from which b general constraint equations can be derived. The advantage of this method is its generality as it is independent of the embedded joints and geometric dimensions. Yet, if aiming for an explicit solution, complex algebraic eliminations are necessary for the b carefully chosen independent constraint equations.
- **Split the loop at one joint:**
  A cut at joint $\mathcal{G}$ removes $f_{\mathcal{G}}$ joint variables without any additional algebraic transformations. Thus, a system of $b - f_{\mathcal{G}}$ equations results, which is independent of the joint variables of the cut joint.
- **Split at a characteristic pair of joints:**
  By a cut at two joints $\mathcal{G}_1$ and $\mathcal{G}_2$, the two open kinematic chains are independent of the $f_{\mathcal{G}_1} + f_{\mathcal{G}_2}$ immanent joint variables. Therefore, only an implicit system of $h = b - (f_{\mathcal{G}_1} + f_{\mathcal{G}_2})$ joint variables for the two open chains has to be solved:

  $$g_{1\ldots h}^{\mathrm{char}}(\beta_{1\ldots h}^{out}; \underline{q}) = 0 \tag{3.59}$$

  The complementary joint variables included in the characteristic pair of joints then can always be determined explicitly, as the relative positions within both kinematic chains are known from the solution of the implicit system:

  $$g_{h\ldots b}^{\mathrm{comp}}(\beta_{1\ldots h}^{out}; \beta_{h\ldots b}^{out}; \underline{q}) = 0 \tag{3.60}$$

In the latter case, if the characteristic pair of joints in total contains $b-1$ joint variables, there is only one equation $g_1^{\mathrm{char}}(\beta_1^{out}; \underline{q})$ with one unknown dependent joint variable left, which can be solved explicitly. In that case, a sequence of b recursively solvable

functions g_i plus additional input equations

$$\underbrace{\begin{bmatrix} \beta_1^{in} \\ \vdots \\ \beta_f^{in} \\ g_1(\beta_1^{out}; \underline{\beta}^{in}) \\ \vdots \\ g_b(\beta_b^{out}; \beta_{b-1}^{out}, ..., \beta_1^{out}, \underline{\beta}^{in}) \end{bmatrix}}_{\underline{g}(\underline{\beta})} = \underbrace{\begin{bmatrix} 1 & & \\ & \ddots & \\ & & 1 \\ 0 & & \\ & \ddots & \\ & & 0 \end{bmatrix}}_{\underline{V}} \cdot \underbrace{\begin{bmatrix} q_1 \\ \vdots \\ q_f \end{bmatrix}}_{\underline{q}} \tag{3.61}$$

can be derived with each function containing exactly one unknown variable β_i more than the previous functions and $\underline{V}$ as a distribution matrix, which maps inputs to joint variables. If in addition, the dependent variables appear at most in second order within the functions $g_{1,...,b}$ (or $\tan(\beta_i/2)$ for revolute joints), the loop is explicitly solvable.

Closed-Form Solution

Due to its efficiency, it is worth searching for a recursive set of functions for which a method was developed by Kecskeméthy and Hiller (1992). The method is based on the previously introduced isotropy groups for finding geometric elements that stay invariant for specific transformation sequences. For the sake of completeness, the main idea of this approach that was recently extended by Liu et al. (2017) will be quickly reviewed.

If a scalar measure between two invariant elements $\underline{\xi}_A$ and $\underline{\xi}_B$ of a transformation sequence

$$\underbrace{\hat{\mathbf{A}}^{\mathrm{iso}(\underline{\xi}_A)}}_{\hat{\mathbf{A}}_A} \mathbf{A} \underbrace{\hat{\mathbf{A}}^{\mathrm{iso}(\underline{\xi}_B)}}_{\hat{\mathbf{A}}_B} \tag{3.62}$$

is determined, the measure is independent of the transformations included in $\hat{\mathbf{A}}_A$ and $\hat{\mathbf{A}}_B$ and consequently is only defined by the transformation $\mathbf{A}$. Possible measures or *projections* $g_{(...)} : \mathbb{R}^4 \times \mathbb{R}^4 \to \mathbb{R}$ as depicted by Hiller and Kecskeméthy (1989) for the elements plane Π_i[2], line $\mathcal{L}_i$, and point P of the origin between an initial frame $\mathcal{K}$ and

[2]The same measure applies to planes and "points at infinity"

the displaced frame $\mathcal{K}'$ are:

1. Squared distance between two points

$$g_{PP}(\mathbf{A}) = ||\mathtt{Trans}[\,\mathbf{A}\,]|| \tag{3.63}$$

2. Distance between a plane and a point

$$g_{EP}(\mathbf{A}, \overset{\mathrm{H}}{\underline{e}}_i) = (\overset{\mathrm{H}}{\underline{e}}_i)^T \mathbf{A}\ \overset{\mathrm{H}}{\underline{o}} \tag{3.64}$$

3. Cosine of the angle between two planes

$$g_{EE}(\mathbf{A}, \overset{\mathrm{H}}{\underline{e}}_i, \overset{\mathrm{H}'}{\underline{e}}_j) = (\overset{\mathrm{H}}{\underline{e}}_i)^T \mathbf{A}\ \overset{\mathrm{H}'}{\underline{e}}_j \tag{3.65}$$

4. Distance of two lines corresponding to the length of the common normal

$$g_{LL}(\mathbf{A}, \overset{\mathrm{H}}{\underline{e}}_i, \overset{\mathrm{H}'}{\underline{e}}_j) = (\overset{\mathrm{H}}{\underline{e}}_i)^T [\mathtt{Rot}[\,\mathbf{A}\,]\ \overset{\mathrm{H}'}{\underline{e}}_j \times \mathtt{Trans}[\,\mathbf{A}\,]] \tag{3.66}$$

5. Squared distance between a line and a point

$$g_{LP}(\mathbf{A}, \overset{\mathrm{H}}{\underline{e}}_i) = ||\mathtt{Trans}[\,\mathbf{A}\,]||^2 - (\overset{\mathrm{H}^T}{\underline{e}}_i\ \mathbf{A}\ \overset{\mathrm{H}}{\underline{o}})^2 \tag{3.67}$$

with $i, j \in \{x, y, z\}$, $\overset{\mathrm{H}}{\underline{o}} = [0, 0, 0, 1]^T$, and the operators $\mathtt{Trans}[\,\mathbf{A}\,] = \mathbf{A}\ \overset{\mathrm{H}}{\underline{o}} \equiv {}_{O_\mathcal{K}}\boldsymbol{r}_{O_{\mathcal{K}'}}$ and $\mathtt{Rot}[\,\mathbf{A}\,] \equiv {}^{\mathcal{K}}\mathbf{R}_{\mathcal{K}'}$ which extract the translational and rotational part of $\mathbf{A}$, respectively. For these purposes, a projection operator $\pi\,(\,\underline{\xi}_L, \underline{\xi}_R, \mathbf{A}\,)$ is introduced, which derives the scalar measurements from eq. 3.63 to eq. 3.67 with respect to the "left" and "right" coordinate frame of a transformation sequence $\mathbf{A}$. Possible combinations are shown in tab. 3.6 and the derivation of projection equations is given in (Krupp, 1999).

Table 3.6: Projections defined by $\pi\,(\,\underline{\xi}_L, \underline{\xi}_R, \mathbf{A}\,)$ (Kecskeméthy and Hiller, 1992, p. 394)

		$\underline{\xi}_R$		
		$\underline{o}$	Π_j	$\mathcal{L}_j$
$\underline{\xi}_L$	$\underline{o}$	$g_{PP}(\mathbf{A})$	$g_{EP}(\mathbf{A}^{-1};\ \overset{\mathrm{H}}{\underline{e}}\, j)$	$g_{LP}(\mathbf{A}^{-1};\ \overset{\mathrm{H}}{\underline{e}}\, j)$
	Π_i	$g_{EP}(\mathbf{A};\ \overset{\mathrm{H}}{\underline{e}}\, i)$	$g_{EE}(\mathbf{A};\ \overset{\mathrm{H}}{\underline{e}}\, i,\ \overset{\mathrm{H}}{\underline{e}}\, j)$	none
	$\mathcal{L}_i$	$g_{LP}(\mathbf{A};\ \overset{\mathrm{H}}{\underline{e}}\, i)$	none	$g_{LL}(\mathbf{A};\ \overset{\mathrm{H}}{\underline{e}}\, i,\ \boldsymbol{e}_j)$

Afterward, for a single-loop kinematic chain represented by a sequence of transformations

$$^1\mathbf{A}_2\,^2\mathbf{A}_3 \ldots ^{n-1}\mathbf{A}_n = \mathbf{I}_4 \tag{3.68}$$

the longest sequence in terms of joint variables leaving element $\underline{\xi}_A$ invariant is declared as $\hat{\mathbf{A}}_A$. Similarly, within the remaining transformations, the longest sequence $\hat{\mathbf{A}}_B$ that leaves an element $\underline{\xi}_B$ invariant can be labeled. With the intermediate sequences $\mathbf{A}_I$

and $\mathbf{A}_{II}$ the chain can be written as

$$\mathbf{A}_I \hat{\mathbf{A}}_B \mathbf{A}_{II} \hat{\mathbf{A}}_A = \mathbf{I}_4 \tag{3.69}$$

and is then resorted such that

$$\hat{\mathbf{A}}_B \mathbf{A}_{II} \hat{\mathbf{A}}_A = \mathbf{A}_I^{-1} \ . \tag{3.70}$$

Applying the projection operator to both sides of eq. 3.70

$$\underbrace{\pi\,(\,\underline{\xi}_B, \underline{\xi}_A; \hat{\mathbf{A}}_B \mathbf{A}_{II} \hat{\mathbf{A}}_A\,)}_{=\,\pi\,(\,\underline{\xi}_B, \underline{\xi}_A; \mathbf{A}_{II}\,)} = \pi\,(\,\underline{\xi}_B, \underline{\xi}_A; \mathbf{A}_I^{-1}\,) \tag{3.71}$$

yields a scalar equation, which only depends on the transformations included in the transformation sequences $\mathbf{A}_I$ and $\mathbf{A}_{II}$. If both sequences $\hat{\mathbf{A}}_A$ and $\hat{\mathbf{A}}_B$ contain together $b-1$ dependent joint variables β^{out}, eq. 3.71 yields a scalar equation containing only the remaining dependent joint variable and can be solved explicitly.

For instance, if $\hat{\mathbf{A}}_A$ and $\hat{\mathbf{A}}_B$ represent a spherical and a universal joint in a spatial loop, the measures $g_{PP}(\mathbf{A}_I)$ and $g_{PP}(\mathbf{A}_{II})$ between the center of the spherical joint and the intersection of the universal joint axes are independent of the five complementary joint variables. The corresponding closure condition $g_1(\beta_1^{out}; \underline{q}) = g_{PP}(\mathbf{A}_{II}) - g_{PP}(\mathbf{A}_I^{-1}) = 0$ can be solved for the dependent joint variable β_1^{out} as a function of the q inputs. Then the remaining complementary joint variables can always be determined explicitly, as described by Hiller and Woernle (1988, p.848) since the relative motions of the subchains $\mathbf{A}_I$ and $\mathbf{A}_{II}$ are known. An algorithm for the automatic derivation of the set of closure conditions is given by Kecskeméthy and Hiller (1992). If no explicit solution can be found, standard implicit methods need to be applied.

3.4.3 Closure Conditions on Velocity and Acceleration Level

Formally, the velocity relationships can be established by differentiating the constraint equations with respect to the joint variables and partitioning the joint variables into input $\underline{\beta}^{in}$ and output $\underline{\beta}^{out}$ variables unveils the following structure:

$$\dot{\boldsymbol{g}} = \frac{\partial \boldsymbol{g}}{\partial \underline{\beta}} \dot{\underline{\beta}} = \left(\underbrace{\begin{array}{ccc} 1 & & \\ & \ddots & \\ & & 1 \\ \mathrm{x} & \ldots & \mathrm{x} \\ \mathrm{x} & \ldots & \mathrm{x} \\ \mathrm{x} & \ldots & \mathrm{x} \\ \mathrm{x} & \ldots & \mathrm{x} \\ \mathrm{x} & \ldots & \mathrm{x} \\ \mathrm{x} & \ldots & \mathrm{x} \end{array}}_{\mathbf{J}_\beta^{in}} \underbrace{\begin{array}{cccccc} & & & & & \\ & & & & & \\ & & & & & \\ \mathrm{x} & \mathrm{x} & \mathrm{x} & \mathrm{x} & & \\ \mathrm{x} & \mathrm{x} & \mathrm{x} & \mathrm{x} & & \\ \mathrm{x} & \mathrm{x} & \mathrm{x} & \mathrm{x} & & \\ \mathrm{x} & \mathrm{x} & \mathrm{x} & \mathrm{x} & & \\ \mathrm{x} & \mathrm{x} & \mathrm{x} & \mathrm{x} & \mathrm{x} & \\ \mathrm{x} & \mathrm{x} & \mathrm{x} & \mathrm{x} & \mathrm{x} & \mathrm{x} \end{array}}_{\mathbf{J}_\beta^{out}} \right) \begin{bmatrix} \dot{\underline{\beta}}^{in} \\ \dot{\underline{\beta}}^{out} \end{bmatrix} = \mathbf{J}_\beta^{in} \dot{\underline{\beta}}^{in} + \mathbf{J}_\beta^{out} \dot{\underline{\beta}}^{out} = 0$$

Here, for the case of direct ordering of inputs, the dotted section is of diagonal form with f rows. The dashed and solid sections correspond to the implicit characteristic system $g_{1 \ldots h}^{\mathrm{char}}$ and explicit complementary system $g_{h \ldots b}^{\mathrm{comp}}$, respectively. For the case of $h = 1$, $\mathbf{J}_\beta^{out}$ is of triangular form, otherwise, for a loop composed of a sequence of elementary joints, there will be at least two complementary joint variables as depicted above. By rearrangement, the output velocities $\dot{\underline{\beta}}^{out}$ can be formulated as

$$\dot{\underline{\beta}}^{out} = \underbrace{-(\mathbf{J}_\beta^{out})^{-1} \mathbf{J}_\beta^{in}}_{\mathbf{J}_q} \dot{\underline{\beta}}^{in} \ . \tag{3.72}$$

A more elegant approach for the derivation of the Jacobian matrix is described by Krupp (1999, p. 71). Similar to the previous derivation of the position constraint equations, the closed kinematic chain can be partitioned into two open chains P_I and P_{II} with the same initial reference frame $\mathcal{K}_A$ and terminal frame $\mathcal{K}_B$. The twist ${}_A\underline{\mathrm{t}}_B = [{}_A\boldsymbol{\omega}_B, {}_A\boldsymbol{v}_B]^T$ for both chains has to be equal

$${}_A\underline{\mathrm{t}}_B = \mathbf{J}_I \dot{\underline{\beta}}_I = \mathbf{J}_{II} \dot{\underline{\beta}}_{II} \tag{3.73}$$

for which the Jacobians can be derived according to eq. 3.39 and which are functions of the joint velocities $\dot{\underline{\beta}}_I$ and $\dot{\underline{\beta}}_{II}$ contained in P_I and P_{II}, respectively. These again can be solved using the projection method, as shown by Krupp (1999, p. 72) and Woernle (1988).

Differentiating eq. 3.72 gives rise to the acceleration equation

$$\ddot{\underline{\beta}}^{out} = \dot{\mathbf{J}}_q \dot{\underline{\beta}}^{in} + \mathbf{J}_q \ddot{\underline{\beta}}^{in} \ . \tag{3.74}$$

Summarizing the previous equations, and associating $\underline{\beta}^{in}$ with f_L inputs $\mathbf{q}$ the following

equations are gained

$$\underline{\beta}^{out} = \underline{\beta}^{out}(\mathbf{q}) \ , \tag{3.75}$$

$$\dot{\underline{\beta}}^{out} = \mathbf{J}_q \dot{q} \ , \tag{3.76}$$

$$\ddot{\underline{\beta}}^{out} = \dot{\mathbf{J}}_q \dot{q} + \mathbf{J}_q \ddot{q} \ . \tag{3.77}$$

Hence, a building block termed *kinematical transformer* is introduced in fig. 3.8, which comprises the above equations. Once derived, the structural and geometric properties are already incorporated in the equations and therefore can be discarded. If there is no explicit solution possible or for the overdetermined case $d > 0$, an iterative solution scheme has to be applied.

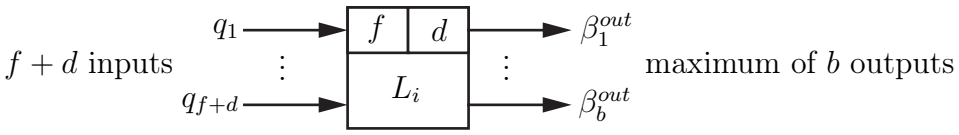

Figure 3.8: Symbolic representation of the kinematics of a closed kinematic chain

4 Graph-Theoretic Mapping of Multibody Systems

The application of graph theory to multibody systems brings along a wide variety of tools and algorithms which can be used for systematic analysis and efficient computation. After a short introduction to graph theoretic concepts, the main effort is put on the complex type of closed kinematic chains. These will be broken down into single closed kinematic chains for which, in many technical cases, efficient closed-form solutions may be found.

4.1 Introduction to Graph Theory Illustrated by the TriMule Hybrid Robot

For illustration, the five degree of freedom hybrid robot called *TriMule* from Dong et al. (2018) is regarded, which is composed of a two degree of freedom wrist mounted on a three degree of freedom parallel mechanism. The joints are indicated by R, P, U, S, as shown in fig. 4.1 corresponding to revolute, prismatic, universal, and spherical joints, respectively, while the underlined prismatic joints are actuated. In this section, a graph representation of the TriMule robot is established for which a short introduction to graph theory is given following the notation of Deo (1974) and additions of Berge (1976) as well as Gondran and Minoux (1984).

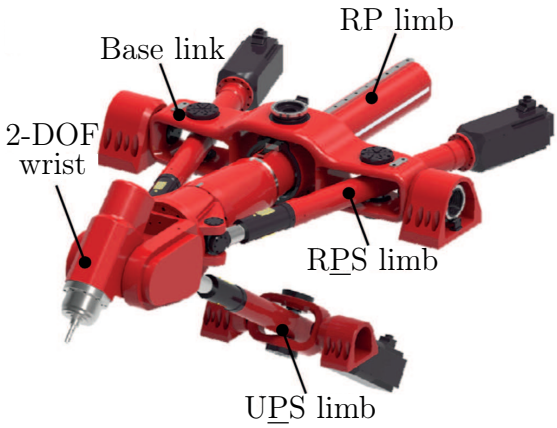

Figure 4.1: TriMule hybrid robot with five degrees of freedom (cf. Dong et al., 2018, p. 81)[1]

[1]Pictorial material in fig. 4.1, fig. 4.2, and fig. 4.10 by kind permission of Prof. Dr. Haitao Liu

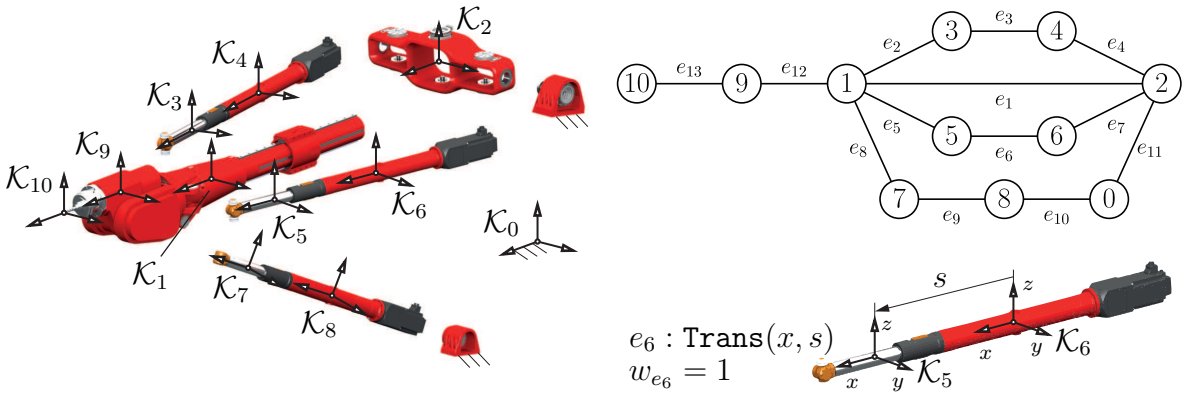

Figure 4.2: Topological graph of the TriMule robot

4.1.1 Basic Elements

A *graph* G = (V, E) can be understood as a set of n_v *vertices* V = $\{v_1, v_2, ...\}$ representing entities of any kind and a set of n_e *edges* E = $\{e_1, e_2, ...\}$ expressing the relations between these entities. An *undirected* edge $e_k = (v_i, v_j)$ is associated with an unordered pair of vertices, which are its *end vertices*. If an orientation is assigned to an edge defining one initial and one terminal end vertex, edges are termed *arcs* or *directed edges*, and the resulting graph forms a *directed graph* or *digraph*. Furthermore, any edge e_i may be associated with a *weight* w_{e_i}. An edge with identical initial and terminal end vertex is called a *self-loop*. Two end vertices of an edge or two nonparallel edges sharing a common vertex are *adjacent* to another, while an end vertex of an edge is *incident* to the edge and vice versa. The *degree* of a vertex is defined as the number of incident edges and can be further specified as *in-* and *out-degree* for directed edges terminating and originating at a vertex, respectively. A vertex v_i with no incident edges is termed *isolated vertex*, and a vertex with only one incident edge is referred to as *pendant vertex*. A graph with at least one pair of vertices sharing multiple incident edges is called a *multigraph* while a graph with edges connecting more than two vertices, forming so-called *hyperedges*, is termed *hypergraph*. A graph without parallel edges, hyperedges, or self-loops is considered a *simple graph*. As in general, hyperedges can be decomposed into binary edges connected to an additional vertex, in the following only graphs with binary edges are of concern if not stated otherwise. If it is possible to separate all vertices V of a graph G into two groups V_1 and V_2, such that no edges of G are incident to two vertices of the same group, G is called *bipartite*.

In fig. 4.2 coordinate systems $\mathcal{K}_1, ..., \mathcal{K}_{10}$ are assigned to the links of the TriMule robot, and $\mathcal{K}_0$ is designated as the fixed base. The relative poses of two bodies connected by

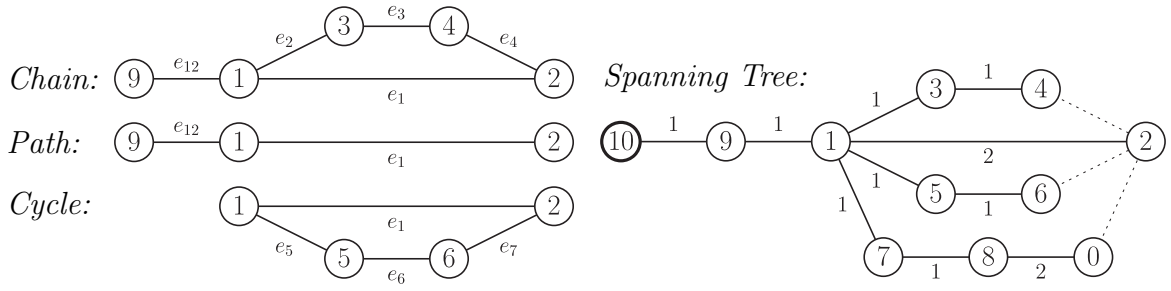

Figure 4.3: Examples of a chain, path, cycle and a spanning tree rooted at v_{10} with indicated dotted chords and weighted edges

a joint can be described by a sequence of elementary transformations as depicted in sec. 3.2.2. If the coordinate systems are then mapped to vertices $v_0, ..., v_{10}$, and their connections are represented by edges $e_1, ..., e_{13}$ a graph representation is established. The depicted example of the edge e_6 represents a directed edge from v_6 to v_5 in accordance with the defined transformation. Yet, as the inverse for each transformation sequence can be derived, orientations within the graph were not depicted. If necessary, an arbitrary number of additional coordinate systems can be introduced to characterize, for instance, articulation points of joints or external forces. For some of the following tasks, edges will also be weighted by the number of implied joint variables within the corresponding transformation sequence.

4.1.2 Structural Properties

If $\mathrm{V}' \subset \mathrm{V}$ and $\mathrm{E}' \subset \mathrm{E}$, $\mathrm{G}' = (\mathrm{V}', \mathrm{E}')$ is called a *subgraph* of $\mathrm{G} = (\mathrm{V}, \mathrm{E})$. The alternating sequence of vertices and edges being passed when traversing a graph between two vertices is called *chain*, with edges being incident to the preceding and succeeding vertex and not passing any edge twice. A *path* is a chain that fulfills the additional criteria that no vertex is passed twice[2]. A path that starts and terminates at the same vertex forms an *elementary cycle*. If not stated otherwise, herein by the term cycle, elementary cycles are concerned. In fig. 4.3 examples of a chain, path, and cycle are given.

If there is no path between a pair of vertices in a graph, the graph is *disconnected*, and both vertices belong to different *components* of the graph. A component is defined

[2]Note that Berge (1976) and Gondran and Minoux (1984) use the term *elementary chain* for paths and instead associate *path* to chains with edges directed in the same way. Here, this case will be indicated by the term *directed* in accordance to Deo (1974)

as a set of vertices for which paths between all pairs of vertices exist. Furthermore, a graph is *k-edge connected* if a minimum removal of k edges increases the number of components. A *bridge* is an edge whose removal increases the number of connected components. In that sense, the graph in fig. 4.2 is 1-edge connected, as the removal of the bridge e_{12} splits the graph into two components. An *acyclic graph*, i. e., a graph without cycles, is termed *tree* if it is connected and a *forest* in the other case. If one of the vertices is distinguished from the others, it is called *root*, and the corresponding tree will be considered a *rooted tree*. If a subgraph T of a connected graph G contains all vertices of G and is acyclic, it is called a *spanning tree* of G. All edges within a tree T are called *branches* while the remaining edges are termed *chords* of T and form the *cotree*. In fig. 4.3 a spanning tree rooted at v_{10} of the TriMule graph is indicated by solid edges. The dotted edges are the corresponding chords which together form the cotree. If the edges of a graph are associated with a weight, the spanning tree with the lowest sum of weights of its branches is called the *minimum spanning tree*.

4.1.3 Mathematical Representation

It can be shown that an undirected graph G can be associated with a vector space over the Galois field modulo 2 (see Deo, 1974) such that algebraic methods can be applied. The Galois field is defined as the set {0,1} with two operations *addition* and *multiplication* under modulo 2 arithmetic. In that sense, edge e_1 can be represented by the unit vector

$$(\underset{e_1}{1}, \underset{e_2}{0}, \underset{e_3}{0}, \underset{e_4}{0}, \underset{e_5}{0}, \underset{e_6}{0}, \underset{e_7}{0}, \underset{e_8}{0}, \underset{e_9}{0}, \underset{e_{10}}{0}, \underset{e_{11}}{0}, \underset{e_{12}}{0}, \underset{e_{13}}{0}) \tag{4.1}$$

and the path in fig. 4.3 can be derived from the vector sum of vectors corresponding to the set of edges $\{e_1, e_{12}\}$

$$(\underset{e_1}{1}, \underset{e_2}{0}, \underset{e_3}{0}, \underset{e_4}{0}, \underset{e_5}{0}, \underset{e_6}{0}, \underset{e_7}{0}, \underset{e_8}{0}, \underset{e_9}{0}, \underset{e_{10}}{0}, \underset{e_{11}}{0}, \underset{e_{12}}{1}, \underset{e_{13}}{0}) \, . \tag{4.2}$$

Obviously, any vector of the vector space associated with G can be obtained by a linear combination of the n_e linearly independent unit vectors associated with the individual edges, which thus form a *natural basis*. In the given context, a set of vectors $\boldsymbol{x}_1, \boldsymbol{x}_2, ..., \boldsymbol{x}_k$ is linearly independent if the expression

$$c_1\boldsymbol{x}_1 + c_2\boldsymbol{x}_2 + ... + c_k\boldsymbol{x}_k = 0 \tag{4.3}$$

with scalars $c_1, c_2, ..., c_k \in \{0, 1\}$ only holds for the trivial solution $c_1, c_2, ..., c_k = 0$ under modulo 2 arithmetic. As the dimension of a vector space is equal to the minimum number of linearly independent vectors necessary to span the vector space, the dimension must be equal to the number of edges n_e.

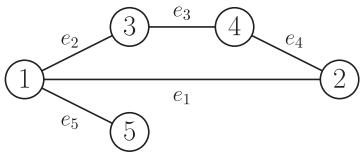

$$S = \begin{array}{c} \\ v_1 \\ v_2 \\ v_3 \\ v_4 \\ v_5 \end{array} \begin{array}{c} \begin{array}{ccccc} e_1 & e_2 & e_3 & e_4 & e_5 \end{array} \\ \begin{bmatrix} 1 & 1 & 0 & 0 & 1 \\ 1 & 0 & 0 & 1 & 0 \\ 0 & 1 & 1 & 0 & 0 \\ 0 & 0 & 1 & 1 & 0 \\ 0 & 0 & 0 & 0 & 1 \end{bmatrix} \end{array} \quad \overline{S}_{v_5} = \begin{array}{c} \\ v_1 \\ v_2 \\ v_3 \\ v_4 \end{array} \begin{array}{c} \begin{array}{ccccc} e_1 & e_2 & e_3 & e_4 & e_5 \end{array} \\ \begin{bmatrix} 1 & 1 & 0 & 0 & 1 \\ 1 & 0 & 0 & 1 & 0 \\ 0 & 1 & 1 & 0 & 0 \\ 0 & 0 & 1 & 1 & 0 \end{bmatrix} \end{array}$$

Figure 4.4: Subgraph of the TriMule with incidence matrix S and reduced incidence matrix $\overline{S}_{v_5}$

For computer processing and analysis, it is suitable to express graphs by matrices for which one common representation is an *incidence matrix*. The incidence matrix S is defined as an n_v by n_e matrix with rows corresponding to vertices and columns to edges. The entries are defined as

$$S_{i,j} = \begin{cases} 1 \text{ if edge } e_j \text{ is incident to vertex } v_i \text{ and} \\ 0 \text{ otherwise.} \end{cases} \tag{4.4}$$

The rank of the incidence matrix is $n_v - k$ where k is the number of connected components. For a disconnected graph, by proper swapping of rows and columns, the incidence matrix can be written in block diagonal form, such that each connected component is represented by a sub-matrix. Furthermore, if for a connected component, one vertex v_{ref} is declared as a *reference vertex*, the corresponding row of the associated incidence matrix can be removed, yielding the *reduced incidence matrix* $\overline{S}_{v_{\text{ref}}}$. As binary edges always have two entries per column, the removed row can be reconstructed without loss of information. For a tree graph with its $n_e = n_v - 1$ edges, the reduced incidence matrix is a non-singular square matrix. Examples of the incidence matrix of a subgraph of the previously established TriMule graph are shown in fig. 4.4.

The above concepts also apply with some changes to directed graphs. In particular, the non-negative entries of the incidence matrix have to account for the direction of the edges. Thus, $+1$ and -1 describe an edge out and into a vertex, respectively. In this sense, vector spaces associated with directed graphs are over the field of real numbers using ordinary arithmetic.

4.2 Topological Analysis and Decomposition

Once a graph-based representation of a multibody system has been established, the connected components can be identified easily from the incidence matrix. For each connected component, the absolute kinematics can be derived independently, for instance, using a systematic approach presented by Wittenburg (2008). In particular,

an open kinematic chain of $n_{\mathcal{B}}$ links, with one link declared as the base frame, can be represented by a rooted tree with respect to v_0. Utilizing the corresponding reduced square incidence matrix $\overline{S}_{v_0}$, a path matrix T can be derived from the inverse of the reduced incidence matrix

$$T = \overline{S}_{v_0}^{-1} \tag{4.5}$$

where the entries of T are defined as

$$T_{i,j} = \begin{cases} +1 \text{ if edge } e_i \text{ is on the path from } v_j \text{ to } v_0, \text{ directed towards } v_0, \\ -1 \text{ if edge } e_i \text{ is on the path from } v_j \text{ to } v_0, \text{ directed towards } v_j, \\ \quad 0 \text{ otherwise.} \end{cases} \tag{4.6}$$

The index $i = 1, ..., (n_{\mathcal{B}} - 1)$ corresponds to the vertices excluding v_0 and $j = 1, ..., n_{\mathcal{G}}$ to the edges. As the path of any vertex to the reference vertex is unique in a tree, each column contains all edges being passed. If displacement transformations between the links are stored in a second matrix in an adequate manner, the absolute kinematics for each body can be established by simple matrix multiplication. The same idea can then be transferred to the spanning tree of a closed kinematic chain. For a closed kinematic chain, the resulting equations are then supplemented by algebraic closure conditions introduced by the cut joints represented by the chords. The overall system of equations then needs to be solved iteratively in order to satisfy the closure conditions.

However, no advantage is taken of subsystems for which efficient closed-form solutions may exist. Complex kinematic chains, as shown in tab. 2.2 are characterized by the existence of at least one subsystem which forms a closed kinematic chain or subsystems of closed kinematic chains connected by serial chains. In the latter case, the relative kinematics of subsystems corresponding to the closed kinematic chains can be solved independently, which may be of particular interest if closed-form solutions exist for some of the subsystems. Furthermore, rigid or overconstrained subsystems may only exist within closed kinematic chains, such that only closed subsystems are of interest in this aspect. Therefore, subsystems representing open kinematic chains will be discarded, and only closed-loop kinematic chains are further analyzed. The decomposition can be achieved by identification and removal of bridges within the graph, such that the remaining connected components form closed kinematic chains whose relative kinematics can be solved independently. Tarjan is considered the first who introduced linear-time algorithms to accomplish these tasks Tarjan (1972, 1974). For the decomposition, a simple algorithm introduced by Schmidt (2013) is utilized which conducts the following steps:

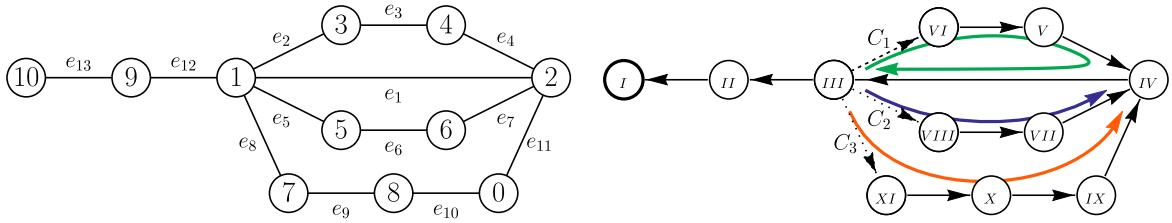

Figure 4.5: Depth-first search tree rooted at vertex 10 with roman numbering in order of visit, edge orientations indicating directed paths to root vertex 10, and dotted backedges

1. Create a depth-first search tree
   Starting at a root vertex, traverse the graph depth-first and label all vertices in order of visit. All tree edges will be oriented towards the root vertex, and all chords termed *backedges* will be oriented away from the root vertex.
2. Perform chain decomposition
   Mark vertices as unvisited and iterate through all vertices in the previously established order. For each backedge starting at the current vertex, follow the directed cycle spanned by the backedge and stop at the first visited vertex. All passed vertices are associated with a chain C_i and are marked visited.
3. Identify bridges
   All edges not listed in any chain are bridges. After the removal, each connected component forms a closed kinematic chain, which can be analyzed according to the next sections.

The steps are illustrated in fig. 4.5, where the roman numberings correspond to the order in which the vertices were visited during the depth-first search according to step 1. In step 2, the first and only vertex encountered which possesses backedges is v_{III}. Successively traversing the three backedges results in the following three chains

$$
\begin{aligned}
C_1 &= \{e_2, e_3, e_4, e_1\} \\
C_2 &= \{e_5, e_6, e_7\} \\
C_3 &= \{e_8, e_9, e_{10}, e_{11}\} \ .
\end{aligned}
$$

In step 3, edges e_{12} and e_{13} are identified as bridges as these are not included in any of the chains. After the removal of the bridges, only one component remains, representing the closed kinematic chain of the TriMule manipulator without the 2-DOF wrist.

4.3 Closed Kinematic Chains as Systems of Kinematic Transformers

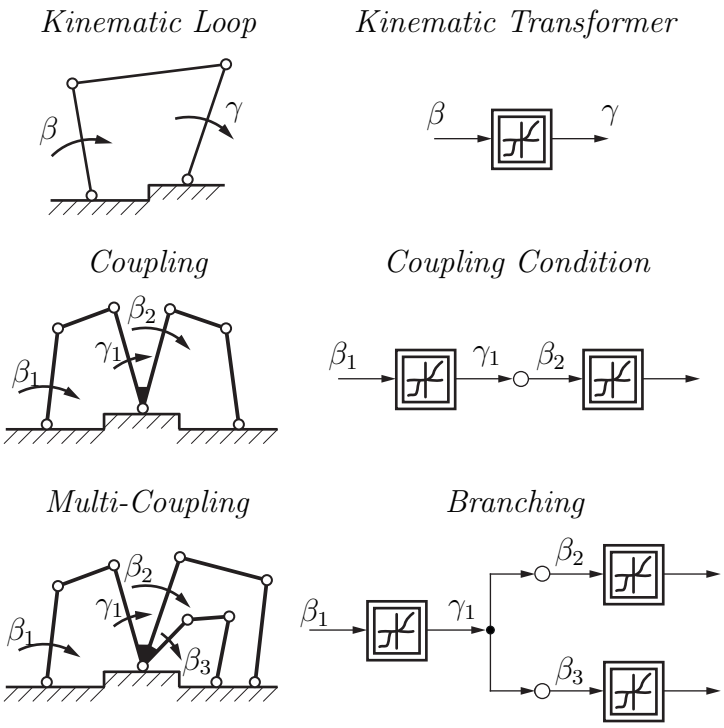

Figure 4.6: Elements of a kinematic network (cf. Kecskeméthy, 1993a, p. 49)

In sec. 3.3 an approach for an efficient solution of the relative kinematics of a single-loop kinematic chain was reviewed and condensed in the concept of a *kinematic transformer*. Following the idea of Hiller, Kecskeméthy, and Wörnle in Hiller et al. (1986), closed kinematic chains can be decomposed into a set of interconnected kinematic transformers termed *kinematic network*. Through the kinematic network, a hierarchical structure of equations can be derived, thus determining the order in which the kinematic loops have to be solved, possibly yielding a closed-form solution. Aside from efficient kinematics, the kinematic network will lay the foundation for the detection of rigid subsystems described in sec. 5.3. Therefore, its basic elements will be introduced in correspondence to Kecskeméthy (1993a).

In general, the kinematic network can be characterized by three building blocks: Kinematic transformers representing a single-loop kinematic chain each, *couplings* arising at well-defined joints, and *branchings* at joints shared among several loops. The resulting network then visualizes relations between the loops, from which the order of processing can be derived by an adequate orientation of edges. The building blocks are illustrated in fig. 4.6 based on a planar four-bar mechanism.

1. **Kinematic Transformers**
   The building block of a kinematic transformer comprises a non-linear set of equations, as shown in sec. 3.4.2, which are necessary to determine dependent relative joint variables from a set of independent input joint variables. In the present case, the output lever angle γ is defined through the transmission function $\gamma(\beta)$, which depends on the input angle β. Each kinematic transformer renders an individual module enclosing all geometric information of the kinematic loop.
2. **Couplings**
   In a multi-loop closed kinematic chain, individual kinematic transformers are not independent. As a result, certain coupling conditions have to be fulfilled. The number of couplings n_C that arise at a joint connecting $n_\mathcal{B}$ links is determined by the number of incident loops n_L:

   $$n_C = n_L - n_\mathcal{B} + 1 \tag{4.7}$$

   In the simple case of the two connected four-bar mechanisms in fig. 4.6 the input angle β_2 of the second kinematic transformer results from the sum of the output angle γ_1 and a constant angle α where sign and value correspond to lever geometry and measurement direction:

   $$\beta_2 = \pm\gamma_1 + \alpha \tag{4.8}$$

3. **Branchings**
   The case of an output joint variable, which gives rise to several couplings, is modeled by a *branching*. This is, for example, the case if the output lever of the first kinematic transformer also constitutes the input levers of the other two kinematic transformers, from which the following branching conditions arise:

   $$\beta_i = \pm\gamma_1 + \alpha_i \ , \quad i = 2, ... \tag{4.9}$$

By analysis of the block diagram of the kinematic network, some properties can directly be extracted. For instance, in correspondence to the modified Chebyshev-Grübler-Kutzbach formula in eq. 2.5, the sum of degrees of freedom of all kinematic transformers within a kinematic network reduced by the number of coupling conditions represents the degree of freedom of the system. Furthermore, after directing the edges of the kinematic network, which will be elaborated in sec. 4.3.2, the order in which the underlying set of equations has to be solved is visualized. In the case of an acyclic kinematic network without overdetermined kinematic transformers, a recursive solution for the system can be derived.

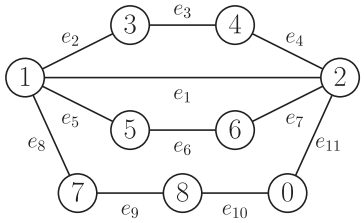

$$C = \begin{array}{c} \\ c_1 \\ c_2 \\ c_3 \\ c_4 \\ c_5 \\ c_6 \end{array} \begin{array}{c} \begin{array}{ccccccccccc} e_1 & e_2 & e_3 & e_4 & e_5 & e_6 & e_7 & e_8 & e_9 & e_{10} & e_{11} \end{array} \\ \left[\begin{array}{ccccccccccc} 1 & 1 & 1 & 1 & 0 & 0 & 0 & 0 & 0 & 0 & 0 \\ 1 & 0 & 0 & 0 & 1 & 1 & 1 & 0 & 0 & 0 & 0 \\ 0 & 1 & 1 & 1 & 1 & 1 & 1 & 0 & 0 & 0 & 0 \\ 1 & 0 & 0 & 0 & 0 & 0 & 0 & 1 & 1 & 1 & 1 \\ 0 & 1 & 1 & 1 & 0 & 0 & 0 & 1 & 1 & 1 & 1 \\ 0 & 0 & 0 & 0 & 1 & 1 & 1 & 1 & 1 & 1 & 1 \end{array} \right] \end{array}$$

Figure 4.7: Closed kinematic chain of the TriMule manipulator and corresponding cycle matrix C

4.3.1 Determination of Independent Single-Loop Kinematic Chains

When setting up a kinematic network, the question for a suitable set of independent loops within the closed kinematic chain arises, for which again some insights from graph theory can be used.

A cycle within a given graph can be represented by a vector, as mentioned in sec. 4.1.3. If all cycles of a graph are gathered in a matrix, such that each row represents the vector of exactly one cycle, a *cycle matrix* is attained with elements defined as

$$C_{i,j} = \begin{cases} 1 \text{ if edge } e_j \text{ is within the i}^{th} \text{ cycle} \\ 0 \text{ otherwise.} \end{cases} \tag{4.10}$$

The resulting cycle matrix for the closed kinematic chain of the TriMule manipulator is shown in fig. 4.7, which contains six cycles in total. Yet, not all of these cycles are independent, as for instance, the addition of cycles c_1 and c_2 under modulo 2 arithmetic yields the cycle c_3 as demonstrated in fig. 4.8. In fact, similar to a plane forming a subspace of the three-dimensional space, cycles form a *cycle subspace* of a graph, which in this case, contains six cycles. The dimension of the subspace and thus the number of independent cycles n_c necessary to generate all other cycles corresponds to the rank of the cycle matrix, which equals the *cyclomatic number*

$$n_c = n_e - n_v + k \tag{4.11}$$

where k is the number of connected components. The minimum set of cycles necessary to span the cycle subspace forms the cycle basis B. Note that eq. 2.3 from sec. 2.4.1 is the direct result of eq. 4.11. The equation can be easily understood for a tree with $n_e = n_v - 1$ edges for which any additional edge closes another cycle. While the number of independent cycles is fixed, the choice of the cycle basis is not unique. From a kinematic point of view, it appears reasonable, that a set of kinematic loops with only a few couplings is more likely to render an efficient closed-form solution than a

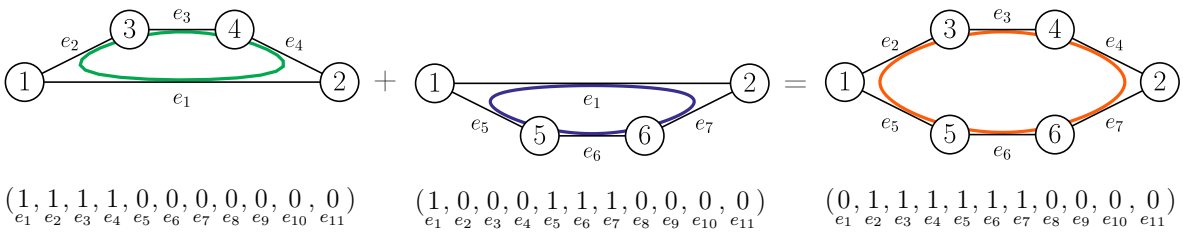

Figure 4.8: Addition of cycles

system of highly dependent kinematic loops. Since couplings arise at joints shared among several loops, shorter cycles in terms of joint variables in general lead to fewer couplings. If each edge of a graph is weighted by the number of joint variables necessary to describe the underlying joint displacements, the weight of each cycle w_c is the result of the sum of weights of its edges w_e. While no final conclusion on the optimal set of cycles could be drawn, it seems appropriate to favor a cycle basis with an overall weight of its cycles

$$w_B = \sum_{c \in B} w_c \tag{4.12}$$

which is the minimum of all cycle bases.

There exist a variety of different more or less restrictive classes of cycle bases, which are characterized by Kavitha et al. (2009). At first sight, a *fundamental cycle basis* B_f seems suitable, as the independence of cycles is directly ensured by its construction. Based on a minimum spanning tree, which can be derived resorting to the algorithms of Prim (1957) or Kruskal (1956), each chord closes a cycle consisting of the chord and a path connecting the chord's end vertices within the spanning tree. As there are exactly $n_e - n_v + 1$ chords for a connected component and each chord is contained in exactly one cycle, a sufficient number of independent cycles is attained. For the TriMule manipulator, a fundamental cycle basis is shown in fig. 4.9 with a total weight of $w_{B_f} = 10 + 7 + 12 = 29$.

Yet, the problem of finding a minimum fundamental cycle basis is NP-complete according to Deo et al. (1982), thus implying that it can only be inefficiently solved by testing all possible solutions. Fortunately, for the given problem, the cycle basis does not necessarily have to be fundamental, such that any minimum cycle basis is sufficient. For this reason, a simple greedy algorithm can be used, which successively adds independent cycles in order of non-decreasing weight. Independence of the partial set of cycles is easily checked by Gaussian elimination under modulo 2 arithmetic, after which rows of zeros indicate dependent cycles. However, the maximum number of

Figure 4.9: a) Fundamental cycle basis with highlighted chords of an underlying minimum spanning tree and b) the corresponding minimum cycle basis

possible cycles can become large with up to

$$2^{n_e - n_v + 1} - 1 \tag{4.13}$$

cycles, which directly follows from the number of linear combinations of cycles within the cycle basis, excluding the empty set. A first polynomial-time algorithm was presented by Horton (1987), who reduced the candidate set of cycles to $n_v \cdot n_e$. Ever since, many improvements have been achieved, as for example in (Amaldi et al., 2009; Hariharan et al., 2006; Kaveh and Roosta, 1994; Kavitha et al., 2004). An example of a minimum cycle basis for the TriMule manipulator is given in fig. 4.9b) with an overall weight of $w_{B_{\min}} = 7 + 7 + 9 = 23$ which is indeed less than the weight of the fundamental cycle basis.

Each cycle forms a kinematic transformer with kinematics derived in sec. 3.4.2 and all three cycles share e_1, which represents the combined prismatic rotational joint connecting $\mathcal{K}_1$ and $\mathcal{K}_2$, such that according to eq. 4.7 two couplings C_1 and C_2 arise. These are the elements of the kinematic network for which a solution is derived in the next section. Note that L_1 and L_2 are examples of exceptional chains with a spatiality $b = 5$ each, which can be derived analogously to the Sarrus linkage example in sec. 3.4.1.

4.3.2 Finding a Closed-Form Solution

After a minimum cycle basis is found, a kinematic network can be established by regarding kinematic transformers and couplings as vertices whose relations are represented by edges. A particularly beneficial solution for the kinematics of a multibody system exists, if the elements of the kinematic network can successively be solved in a sequence, such that any kinematic transformer or coupling is solved in terms of previously determined and externally provided joint variables which in quantity correspond

to the degree of freedom of the respective element. If all elements yield an explicit solution for the given set of inputs and the overall number of external inputs equals the degree of freedom of the multibody system, the kinematics can be solved recursively in closed form. Clearly, such recursively solvable systems with at least one global input, are non-rigid and do not need to be considered for further rigidity analysis.

For the detection of a suitable solution sequence, a sequence of elements can be regarded as a *topological order* of the kinematic network. Orientations of the edges are then defined in a way such that the terminal end vertex of a directed edge is a successor of the initial end vertex with respect to the topological order, forming a directed acyclic graph. For the TriMule robot, a recursively solvable ordering ($L_1 \rightarrow C_1 \rightarrow C_2 \rightarrow L_2 \rightarrow L_3$) is visualized in fig. 4.10. Here, the branching can be seen as a hyperedge with only one input. On the other hand, for some multibody systems or a certain choice of global

Figure 4.10: Kinematic network for TriMule robot with a recursive solution flow

inputs, such a recursively solvable sequence does not exist, and the kinematic network needs to be solved iteratively. In that case, when trying to solve the system sequentially, some of the inputs must be guessed at first, forming so-called *pseudo inputs*, with the result that the sum of external inputs exceeds the global degree of freedom of the system. The pseudo inputs then lead to additional implicit constraint equations at a succeeding element and the subsequence needs to be solved iteratively until the pseudo inputs are determined. The number of implicit constraints is marked within the kinematic network and is determined by the number of inputs exceeding the local degrees of freedom of an element. In order to keep subsystems with iterative solutions small and reduce the search space for rigidity analysis, a solution sequence with a minimum number of pseudo inputs is sought. In close relation to the *sink method* presented by Hiller and Anantharaman (1989), a simple greedy algorithm is applied, which builds up a topological order starting at the last element and successively prepending the element that yields the least number of implicit constraints. Afterward, underdeter-

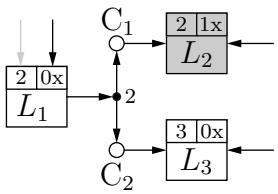

Figure 4.11: Non-recursive solution flow due to predefined inputs at the translational actuators entailing one indicated pseudo input

mined elements, i. e., elements with a higher degree of freedom than assigned inputs, are supplemented with a corresponding number of external inputs. Depending on the actual implementation, additional rules for prioritization may be applied, for instance, regarding whether implicit constraint equations are formed in couplings or loops. If for the resulting set of inputs, the number of inputs at each element corresponds to its degree of freedom and allows for an explicit solution, a recursive solution sequence has been found. The external inputs then form a set of independent *global inputs* for the system.

4.4 Multiple Joints

In this section, some attention shall be put on *multiple joints*, i. e., joints which connect more than two bodies, and arising coupling conditions. A thorough treatment of linear joint couplings is given by Kecskeméthy (1993a) based on linear transformations. Here the concept is extended to non-linear coupling conditions arising, for instance, at multiple spherical joints using the previously introduced tools of graph theory.

In analogy to a *binary* joint $\mathcal{G}$ that defines the set of allowed relative displacements between two links, a multiple joint $\hat{\mathcal{G}}$ defines the allowed relative displacements between any of the $n_{\mathcal{B}}$ connected links. In order to relate all of the $n_{\mathcal{B}}(n_{\mathcal{B}}-1)/2$ bonds, the bonds must belong to the same displacement subgroup $\hat{\mathcal{G}}^{(G)}$, which is associated with the multiple joint. From the displacement subgroups listed in tab. 3.1, here, only those subgroups are regarded, which can be generated by sequences of elementary transformations (i. e., all subgroups except H and Y). If one link is assumed as a reference and relative poses of the $n_{\mathcal{B}}-1$ remaining links with respect to the reference link are known, also the relative poses between any two of the links are defined. Thus, the number of independent joint variables necessary to define all relative poses is equal

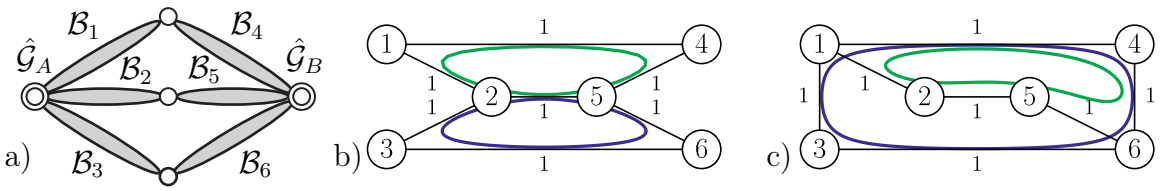

Figure 4.12: A kinematic chain a) and its topological graph with two different decompositions b) and c) of multiple joints $\hat{\mathcal{G}}_A$ and $\hat{\mathcal{G}}_B$

to the degree of freedom $f_{\hat{\mathcal{G}}}$ of the multiple joint

$$f_{\hat{\mathcal{G}}} = b \cdot (n_{\mathcal{B}} - 1) \tag{4.14}$$

where $b = \mathtt{dim}(\hat{\mathcal{G}}^{(G)})$. Consequently, any excess of joint variables used to describe the relations among the links leads to an equal number of coupling conditions that have to be fulfilled to ensure the multiple joint's integrity.

4.4.1 Modeling Strategy for Multiple Joints

In general, multiple joints can be circumvented by decomposition into $n_{\mathcal{B}} - 1$ independent binary joints. Indeed, this is a common practice for modeling multibody systems in commercial multibody software packages such as ADAMS[3], though the decomposition is not unique. In fact, the number of possible decompositions equals the number of spanning trees of a complete graph with $n_{\mathcal{B}}$ vertices, which can be enumerated by Cayley's formula (Cayley, 1889) and yields $n_{\mathcal{B}}^{n_{\mathcal{B}}-2}$ possible decompositions.

In addition, the choice of decomposition may affect the complexity of the corresponding kinematic network as the example of a kinematic chain with six links $\mathcal{B}_1, ..., \mathcal{B}_6$ connected by revolute joints in fig. 4.12 a) illustrates, where $\hat{\mathcal{G}}_A$ and $\hat{\mathcal{G}}_B$ can be regarded as multiple joints. If the multiple joints $\hat{\mathcal{G}}_A$ and $\hat{\mathcal{G}}_B$ connecting links $\mathcal{B}_{1,...,3}$ and $\mathcal{B}_{4,...,6}$ respectively, are decomposed into binary joints, as shown in b), a minimum cycle basis B with a total weight of $w_B = 8$ is derived. On the other hand, the decomposition in c) gives rise to a minimum cycle basis B' with a larger weight of $w_{B'} = 9$ and an additional coupling due to a second shared edge. Therefore, the direct replacement of multiple joints by binary joints not only obliviates some topological information but also has an impact on the resulting kinematic network.

In that sense, it seems advisable to treat multiple joints as a whole within the topological graph of a kinematic chain for setting up the kinematic network. Formally, a

[3] ADAMS: Automatic Dynamic Analysis of Mechanical Systems

multiple joint can be thought of as a hyperedge that connects all incident links in the topological graph of a kinematic chain with a weight corresponding to the dimension of the displacement subgroup associated with the multiple joint. Two intuitive approaches come to mind for modeling this behavior, as illustrated in fig. 4.13:

a) Insert binary edges for all possible pairs of connected links
b) Insert an artificial vertex adjacent to all connected links

Figure 4.13: Decomposition of multiple joints by complete graphs a) and by artificial vertices b)

Both approaches are successfully applied in literature, as by Yan and Hsu (1988) and Ding et al. (2013). Yet, in the first case, a complete graph with $n_{\mathcal{B}}(n_{\mathcal{B}}-1)/2$ edges is inserted for each multiple joint which not only increases the run time for detection of the minimum cycle basis but also introduces additional cycles.

In the second case, one vertex and only $n_{\mathcal{B}}$ edges are temporarily added for each multiple joint. To differentiate the artificial vertices within the topological graph, these will be marked, leading to a *bicolored* graph. However, the $n_{\mathcal{B}}$ links of a multiple joint are now connected by paths of two edges. In order to compensate for the extra edge when determining the weight of the minimum cycle basis, the edge weights are divided by two. Afterward, a minimum cycle basis without extra cycles and of the same weight as for directly connected links can be found.

For the reasons above, the second approach will be implemented for the establishment of the topological graph. After a minimum cycle basis has been detected, the artificial multiple joint vertices have to be resolved into equivalent binary edges and couplings for setting up the kinematic network.

4.4.2 Coupling Conditions at Multiple Joints

For the derivation of coupling conditions, a multiple joint $\hat{\mathcal{G}}$ is assumed connecting $n_{\mathcal{B}}$ links $\mathcal{B}_{1,\dots,n_{\mathcal{B}}}$ shared among n_L loops. Each loop L_k defines the relative pose of two links $\mathcal{B}_i$, $\mathcal{B}_j$, for which a set of $\mathtt{dim}(\hat{\mathcal{G}}^{(G)})$ joint variables $\underline{\beta}_k$ is necessary. The relative poses

can then be described by standard sequences of elementary transformations which are functions of these joint variables. Each sequence acts as a motion generator of the respective group $\hat{\mathcal{G}}^{(G)}$.

A multiple joint is then expressed as a graph with vertices $v_{1,\dots,n_\mathcal{B}}$ corresponding to the connected links $\mathcal{B}_{1,\dots,n_\mathcal{B}}$ and edges $e_{1,\dots,n_L}$ with a weight $w_{e_k} = \mathtt{dim}(\hat{\mathcal{G}}^{(G)})$ incident to the vertices v_i, v_j representing the links connected by loop L_k. Clearly, a cycle within the graph forms a single-loop kinematic chain giving rise to $b = \mathtt{dim}(\hat{\mathcal{G}}^{(G)})$ closure conditions. In this context, the cycle forms a *coupling* between the involved loops and the implied closure equations form *coupling conditions* on the respective joint variables. Therefore, the number of couplings directly corresponds to the cyclomatic number in eq. 4.11 with the number of connected components $k = 1$ as in closed kinematic chains, all links are part of at least one loop. Therefore, the number of couplings at a multiple joint $\hat{\mathcal{G}}$ is equal to

$$n_C = n_L - n_\mathcal{B} + 1 \tag{4.15}$$

which is in direct agreement with Kecskeméthy (1993a, p. 53). As each coupling introduces b equations, the total number of coupling conditions consequently reads $b \cdot (n_L - n_\mathcal{B} + 1)$.

Since the transformation sequences corresponding to each edge define displacements within the same displacement subgroup, all single-loop kinematic chains resembling the couplings must be trivial as in sec. 3.4.1. A general procedure for deriving the resulting closure conditions has already been provided in sec. 3.4.2. Although the coupling conditions, in general, are non-linear, a considerable amount of technically implemented joints correspond to the commutative groups indicated in tab. 3.1. For these, the transformation sequences can be rearranged and partitioned into elementary transformations of the same kind, which can be solved independently yielding linear coupling conditions. The coupling of a cylindrical joint for instance, can be partitioned into a sequence of translations and rotations leading to two decoupled linear equations.

For illustration, an example of a multiple spherical joint connecting five links is shown in fig. 4.14 a). In fig. 4.14 b) it is assumed that a minimum cycle basis within the topological graph was found, in which six loops were recognized to include the multiple joint. Each loop then defines the relative position between two links of the multiple joint, expressed by an edge within the corresponding multiple joint graph in fig. 4.14 c). Edge e_1 for instance defines the relative pose of $\mathcal{B}_2$ with respect to $\mathcal{B}_1$ by a transformation sequence such as $\mathtt{Rot}(z, \beta_{1a}) \circ \mathtt{Rot}(x, \beta_{1b}) \circ \mathtt{Rot}(z, \beta_{1c})$. The three joint variables

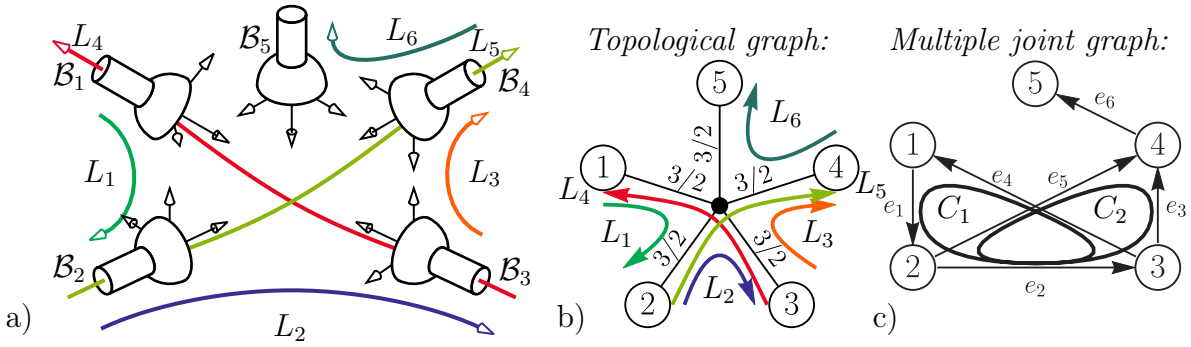

Figure 4.14: a) Multiple spherical joint, b) its representation by a bicolored topological graph, and c) couplings resulting from its decomposition

yield the weight of $w_{e_1} = 3$.

According to eq. 4.15 two couplings arise whose coupling conditions arise from the closure of the two cycles shown in fig. 4.14 c). When concatenating the transformation sequences of the coupling cycles, edge directivity must be acknowledged. If the orientation of an edge is in opposition to the direction of the corresponding coupling cycle, its inverse transformation is incorporated. Note that the edge introduced by L_6 forms a bridge and is not included in any couplings. Thus, the relative pose of $\mathcal{B}_5$ is solely determined by L_6 and is not subject to any coupling conditions. Furthermore, the edge introduced by L_2 is part of two couplings and consequently forms a branching. The resulting kinematic network is depicted in fig. 4.15. The number next to the couplings indicates the number of introduced coupling conditions.

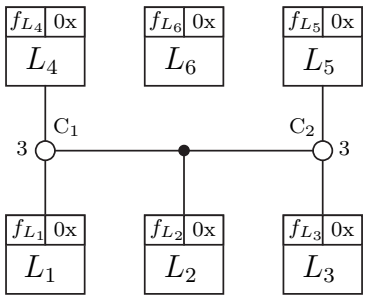

Figure 4.15: Kinematic network of the multiple spherical joint

4.4.3 Detection of Decomposed Multiple Joints

If a multibody system was modeled without explicitly indicating multiple joints, the following approach is proposed to detect multiple joints as such to take advantage of the

aforementioned benefits. For this reason, the topological graph is prepared such that additional coordinate frames are introduced at the attachment points of joints, and each joint is modeled as a sequence of consecutive elementary joint transformations between two of these attachment points. In that manner, the edges of the topological graph can be partitioned into joint and link edges, containing only joint and link transformations, respectively. If all link edges are removed, a disconnected subgraph containing only joint edges is obtained. Each connected component contains either one joint edge in case of a binary joint or several joint edges in case of a potential multiple joint.

As stated before, all bonds between the connected links of a multiple joint must belong to the same displacement subgroup. Therefore, for the component of a potential multiple joint, all edges or just a connected subset of edges must form motion generators of the same displacement subgroup. In the latter case, only the denoted subset of edges forms a multiple joint.

Whether a set of edges has a mutual displacement subgroup can be tested easily using the IPM. For each edge, an IPM for the respective transformation sequence is established – for all edges, the elements found to be invariant must be the same. In addition, each edge must also be a motion generator of the corresponding subgroup as elaborated in sec. 4.5. If a set of joint edges has been identified to form a multiple joint, it can be replaced within the topological graph by a multiple joint vertex connected to the vertices incident to the former joint edges. Afterward, the search for a minimum cycle basis and derivation of couplings is carried out as previously described.

4.5 Associating Joint Transformations to Displacement Subgroups

By concatenation of elementary joint transformations or analogously by group composition of the respective displacement subgroups, joints and subgroups of a higher degree of freedom and dimension can be generated. In the foresight of detecting isolated degrees of freedom in ch. 5, the following method is introduced to find a potential displacement subgroup of which a transformation sequence might be a generator.

In order to associate a given joint transformation sequence $\mathbf{A}_{1,...,n} = \mathbf{A}_1 \mathbf{A}_2 ... \mathbf{A}_n$ to its representative displacement subgroup ${\mathbf{A}_{1,...,n}}^{(\mathrm{G})}$, provided it can be represented by a displacement subgroup, an IPM according to tab. 3.5 is constructed, where $\mathbf{A}_i$ with $i \in \{1, ..., n\}$ represents elementary joint transformations. For the analysis, two operations

Table 4.1: Composition of displacement subgroups based on isotropy groups

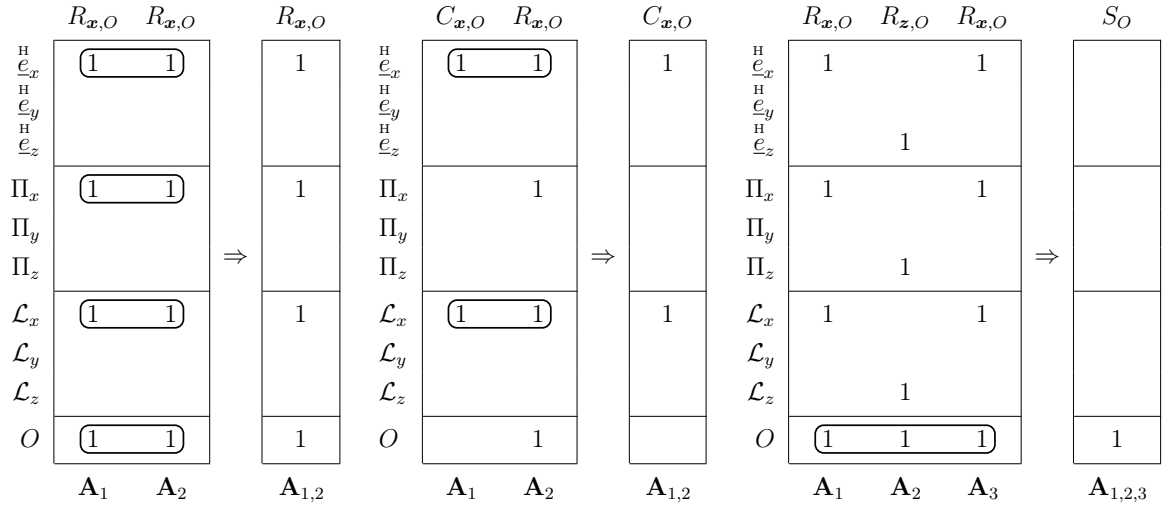

a) Same subgroup b) Included subgroup c) Common superior group

will be of particular interest: First, each column is associated with the displacement group derived by the group intersection of the isotropy groups correlated to its invariant elements. Second, a sequence of columns is associated with the displacement group corresponding to the group composition of the groups previously associated with the respective columns.

For this purpose, it shall be determined whether a sequence of neighboring columns is a generator of another displacement subgroup by searching for common invariant elements. For instance, a sequence $\mathbf{A}_1\mathbf{A}_2\mathbf{A}_3 = \mathtt{Rot}(z,\varphi) \circ \mathtt{Rot}(x,\theta) \circ \mathtt{Rot}(z,\psi)$ leaves the element O invariant and can directly be associated with the spherical group S_O[4]. Thus, the three columns can be merged into a single column $\mathbf{A}_{123}$ associated with S_O with only one invariant element O. Yet, if the number of motion generators is less than the dimension of the subgroup associated with the common invariant elements, the sequence of transformations only forms a subset of that group. This may also be true for a sufficient number of motion generators, of which some are redundant. For instance, a z-z-x sequence of rotations featuring the same number and type of motion generators as the previous example only specifies a subset of S_O, corresponding to a universal joint as one of the first two rotations is redundant.

Therefore, it is necessary to merge redundant transformations first. Under the following conditions, neighboring columns can be merged repeatedly into one column, again

[4]Due to singularities, the rotation sequence does not fully represent the spherical group S_O. Yet, for the general case, it is sufficient to assume non-parallel axes.

representing a displacement subgroup:

a) **Neighboring columns representing the same subgroup:**
If consecutive columns share all their invariant elements, each column is a generator of the same group such that the sequence can be reduced to a single column retaining all invariant elements, as shown in tab. 4.1 a).

b) **Columns representing subgroups of a neighboring column:**
If a column i shares all its invariant elements with a neighboring column which features additional invariant elements, the neighboring column represents a subgroup of column i and can be merged, retaining only the common invariant elements as depicted in tab. 4.1 b).

c) **Neighboring columns forming a generator of a superior group:**
If several columns have one or more invariant elements in common and cannot be reduced by the previous two rules, the columns represent independent subgroups of the group associated with the common invariant elements. The sequence of columns forms a generator of the superior group, provided that the sum of dimensions of the subgroups is greater or equal to the dimension of the superior group. The columns can then be replaced by a single column retaining only the common invariant elements, as illustrated in tab. 4.1 c).

If, after recursive application of these rules, only one column is left, the joint transformation sequence can be associated with the displacement subgroup of the remaining column. The dimension of that displacement subgroup then represents the connectivity of the joint, while the number of joint variables exceeding the dimension equals the redundant degrees of freedom as depicted in sec. 2.4.5.

5 Detection of Rigid Subsystems with Isolated Degrees of Freedom

Certain kinematic chains may not be able to exhibit any relative motions, i. e., feature zero degrees of freedom and are called *structures* (Sharma and Purohit, 2006, p. 73). In other words, all degrees of freedom are locked, implying that all joint variables are independent of time, and instead solely depend on the constraint equations introduced by the structure itself. Once the joint variables have been determined, the structure and its underlying set of equations can be replaced by a single entity, leading to a reduced kinematic chain. If the structure was additionally overconstrained, inconsistencies regarding the Chebyshev-Grübler-Kutzbach formula could subsequently be eliminated.

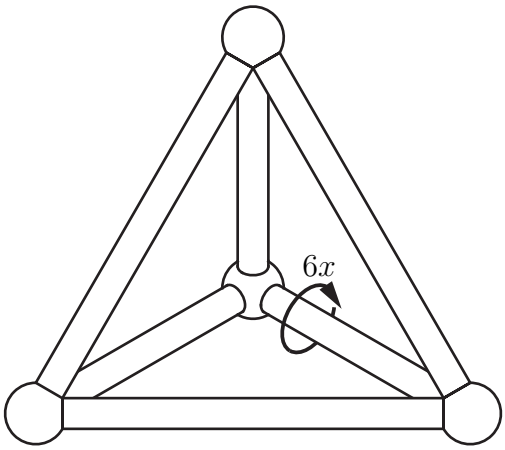

$$n_{\mathcal{B}} = 6$$
$$n_{\mathcal{G}} = 8$$
$$f = 6 \cdot (6 - 1) - 8 \cdot 3 = 6$$

Figure 5.1: Example of a structure featuring isolated degrees of freedom.

The same idea can be applied to kinematic chains that possess isolated degrees of freedom according to sec. 2.5, but besides show no relative motion of its links. The Chebyshev-Grübler-Kutzbach formula regards these isolated degrees of freedom as proper degrees of freedom, which obscure the "rigid character" of a structure as well as potentially overconstrained subsystems. For illustration, in fig. 5.1 a tetrahedron is shown, which is composed of six bars and four multiple spherical joints that can equivalently be counted as eight binary spherical joints. Consequently, the system implicates six degrees of freedom corresponding to the six isolated bar spins. If this structure were embedded into another kinematic chain at its tips, clearly, the bar spins had no impact on the surrounding system, and the tetrahedron could just as well be replaced by a single rigid body. Therefore, here a kinematic chain of which all degrees of freedom are either locked or isolated is regarded as a structure as well. This chapter addresses

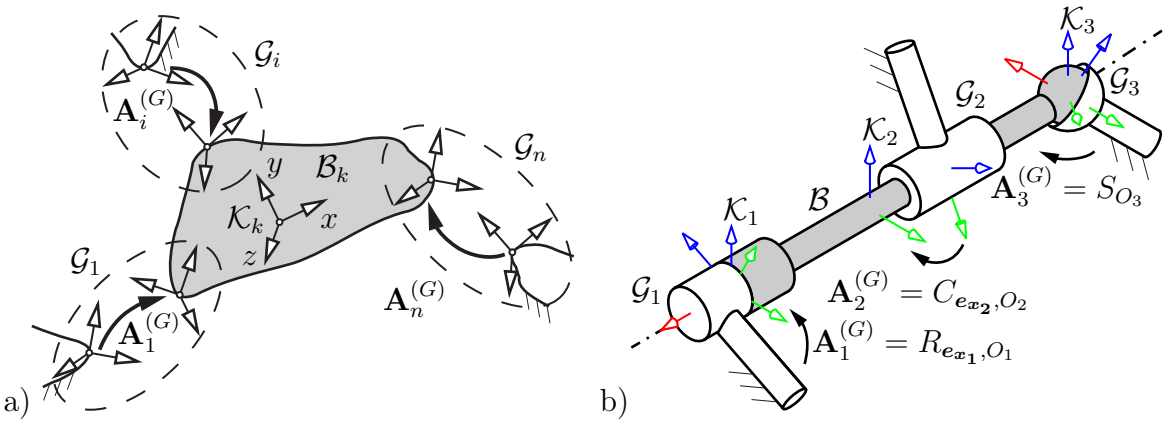

Figure 5.2: a) A general link $\mathcal{B}_k$ with attached joints $\mathcal{G}_1$ to $\mathcal{G}_n$ and an example in b) which features a fully isolated degree of freedom

the detection of such structures by means of identifying and tracking isolated degrees of freedom.

5.1 Classification of Isolated Degrees of Freedom by Groups

5.1.1 Fully Isolated Degrees of Freedom

The concept of *fully isolated* degrees of freedom was introduced for immaterial motions, which can be "removed from the mechanism without any effect." (Simroth et al., 2016, p. 111). This description shall be further accounted for, resorting to the previously presented concept of displacement subgroups.

In a closed kinematic chain, each link is connected to at least $n \geq 2$ other links by joints $\mathcal{G}_1$, ..., $\mathcal{G}_n$, as shown in fig. 5.2 a). If a link $\mathcal{B}_k$ is able to perform a particular type of motion (1) without violating the constraints imposed by the attached joints, and (2) leaves the poses of all connected bodies invariant, the respective degree of freedom of that motion is regarded fully isolated.

In order to determine whether a link $\mathcal{B}_k$ features isolated degrees of freedom, first, all directly connected links are assumed fixed in space. The set of displacements that $\mathcal{B}_k$ can undergo is the result of the intersections of the n bonds with its immediate neighbors defined by the joints $\mathcal{G}_1, ..., \mathcal{G}_n$. If all joints can be represented by displacement subgroups ${\mathcal{G}_1}^{(\mathrm{G})}, ..., {\mathcal{G}_n}^{(\mathrm{G})}$, whose intersection

$$f^{\mathrm{iso(G)}} = {\mathcal{G}_1}^{(\mathrm{G})} \cap ... \cap {\mathcal{G}_i}^{(\mathrm{G})} \cap ... \cap {\mathcal{G}_n}^{(\mathrm{G})} \tag{5.1}$$

is derived according to sec. 3.3.1 and yields a displacement subgroup $f^{\mathrm{iso(G)}}$ apart from the identity displacement, link $\mathcal{B}_k$ features isolated degrees of freedom. The number of isolated degrees of freedom f^{iso} directly relates to the dimension of the corresponding displacement subgroup $\mathtt{dim}(f^{\mathrm{iso(G)}})$.

For instance, link $\mathcal{B}$ shown in fig. 5.2 b) is connected to three other links by a revolute joint $\mathcal{G}_1$, a cylindrical joint $\mathcal{G}_2$, and a spherical joint $\mathcal{G}_3$. Each of these joints can be associated with a respective displacement subgroup, with all groups sharing a common characteristic axis. Obviously, $\mathcal{B}$ is able to spin about its own axis without altering the relative poses of the connected links. The isolated degree of freedom can be determined according to eq. 5.1

$$f^{\mathrm{iso(G)}} = {\mathcal{G}_1}^{(\mathrm{G})} \cap {\mathcal{G}_2}^{(\mathrm{G})} \cap {\mathcal{G}_3}^{(\mathrm{G})} = \underbrace{R_{\boldsymbol{e_{x_1}},O_1} \cap C_{\boldsymbol{e_{x_2}},O_2}}_{R_{\boldsymbol{e_{x_1}},O_1}} \cap S_{O_3} = R_{\boldsymbol{e_{x_1}},O_1} \ , \tag{5.2}$$

where the x-axis $\boldsymbol{e_{x_i}}$ and origin O_i correspond to the body-fixed frame $\mathcal{K}_i$, respectively. Therefore, $\mathcal{B}$ features a single isolated degree of freedom associated with the dimension of the rotational displacement subgroup $R_{\boldsymbol{e_{x_1}},O_1}$. For this analysis, the displacement subgroups ${\mathbf{A}_1}^{(\mathrm{G})}$, ${\mathbf{A}_2}^{(\mathrm{G})}$, and ${\mathbf{A}_3}^{(\mathrm{G})}$ associated with the joint transformations $\mathbf{A}_1$, $\mathbf{A}_2$, and $\mathbf{A}_3$ are obtained following the method proposed in sec. 4.5. The group intersections are then evaluated by means of tab. 3.4 such that common subgroups are identified.

5.1.2 Structurally Isolated Degrees of Freedom

The concept of fully isolated degrees of freedom can be extended to whole subchains for which a subset of displacements obeying the constraints of connected joints exists, which leave both, the poses of the links outside the subchain as well as the relative poses within the subchain invariant. In this case, the term *structurally* isolated degree of freedom will be used.

For this reason, a closed kinematic chain is regarded, which shall be partitioned into two distinct components by cutting a minimum set of n joints $\mathcal{G}_1, ..., \mathcal{G}_n$, such that each component in itself is connected as indicated in fig. 5.3 a). Assuming that each of these joints can be associated with a displacement subgroup, the kinematic chain features a structurally isolated degree of freedom in analogy to eq. 5.1, if the group intersection of the displacement subgroups associated with the cut joints is different from the identity displacement.

While a structurally isolated degree of freedom acts on the absolute motion of a kine-

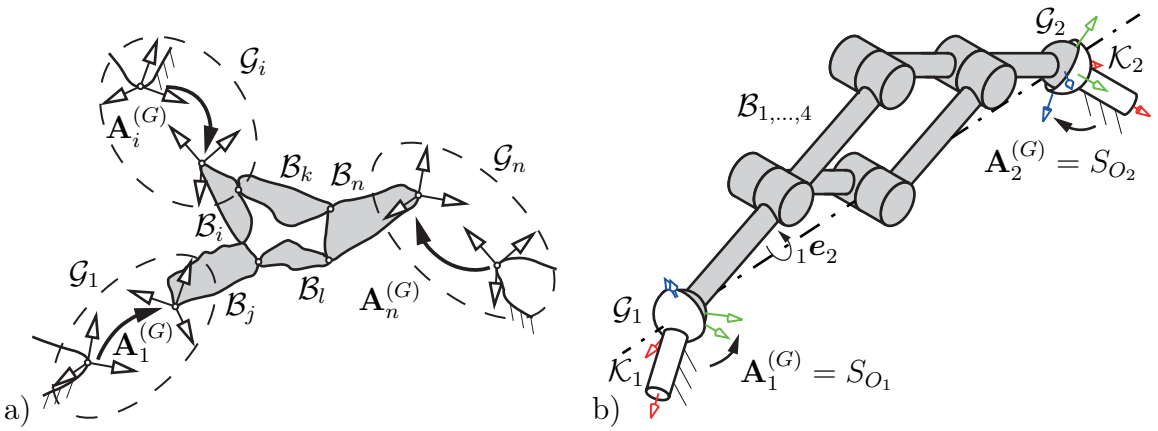

Figure 5.3: a) A compound of connected links with attached joints $\mathcal{G}_1$ to $\mathcal{G}_n$ and an example in b) where such a compound features a structurally isolated degree of freedom

matic chain as a proper degree of freedom, it does not affect the relative poses of links within each component. On the other hand, characteristic properties such as points and axes of the subgroup associated with the structurally isolated degree of freedom are subject to change by motions within the components.

An example of a structurally isolated degree of freedom is given in fig. 5.3 b). Here, a kinematic chain is partitioned into two components highlighted in white and gray by cuts at joints $\mathcal{G}_1$ and $\mathcal{G}_2$, for which

$$f^{\mathrm{iso(G)}} = \mathcal{G}_1{}^{(\mathrm{G})} \cap \mathcal{G}_2{}^{(\mathrm{G})} = S_{O_1} \cap \ S_{O_2} = R_{{}_1\boldsymbol{e}_2, O_1} \ , \tag{5.3}$$

where ${}_1\boldsymbol{e}_2$ is the direction vector from spherical joint $\mathcal{G}_1$ to $\mathcal{G}_2$. Clearly, if the gray component "contracts," the axis ${}_1\boldsymbol{e}_2$ changes with respect to the poses of bodies $\mathcal{B}_1, \mathcal{B}_2, \mathcal{B}_3$, and $\mathcal{B}_4$. On the other side, the respective inner configurations within both components are invariant to the rotation described by the isolated degree of freedom. Therefore, this degree of freedom will be disregarded, when searching for rigid subsystems, as only the distance between both spherical joints defined by the gray component contributes to the relative kinematics of the white component. Against this background, a fully isolated degree of freedom can be seen as a special case of a structurally isolated degree of freedom where one of the two components comprises only a single link.

5.2 Identification and Transmission of Isolated Degrees of Freedom

In sec. 4.3 the concept of decomposing a closed kinematic chain into a system of kinematic loops that are coupled at shared joints was presented forming a kinematic network. With this representation as a starting point, the search for isolated degrees of freedom is first independently performed for each individual kinematic loop. This simplifies the search as only two joints need to be cut in a loop in order to partition the chain into two distinct subchains. Though, since there are coupling conditions introduced at shared joints, degrees of freedom that are isolated in one kinematic loop may turn out to be proper degrees of freedom in another connected loop. Therefore two steps will be conducted:

1. Detect isolated degrees of freedom within each closed kinematic chain
2. Track and classify isolated degrees of freedom within the network

Both steps will be further elaborated within the next two sections.

5.2.1 Detection of Isolated Degrees of Freedom in a Kinematic Loop

The task of detecting fully isolated degrees of freedom within a kinematic loop is straightforward: Check for each link $\mathcal{B}_k$ and its incident joints $\mathcal{G}_i$ and $\mathcal{G}_j$ within the kinematic loop, whether the intersection of the associated groups ${\mathcal{G}_i}^{(\mathrm{G})}$ and ${\mathcal{G}_j}^{(\mathrm{G})}$ feature an isolated degree of freedom according to eq. 5.1. All detected isolated degrees of freedom will be enumerated and labeled by the cut joints

$$f_a^{\mathrm{iso}} : \underbrace{\{\mathcal{G}_i, \mathcal{G}_j\}}_{joint\ set} , \tag{5.4}$$

where the *joint set* contains the cut joints, and a is an ongoing (global) index. $f_a^{\mathrm{iso(G)}}$ then refers to the displacement subgroup associated with the isolated degree of freedom.

The same labeling is applied to structurally isolated degrees of freedom except that both joints are not required to be incident to the same link. For this reason, the labeling only includes the joints and not the links. The case of identifying all independent structurally isolated degrees of freedom is not trivial. For example, in a single-loop kinematic chain of n links and n spherical joints, $n \cdot (n-1)/2$ potential structurally isolated degrees of freedom can be identified, as any pair of spherical joints features an

isolated degree of freedom referring to the rotation about their common axis. However, already for $n = 5$ it becomes obvious, that not all isolated degrees of freedom can simultaneously coexist, as there are $f = 6{\cdot}(5-1)-5{\cdot}3 = 9$ degrees of freedom, but $5{\cdot}(5-1)/2 = 10$ potential isolated degrees of freedom. Five of these can directly be associated with the spins, and the remaining isolated degrees of freedom can be interpreted as "foldings" of the kinematic chain. Nevertheless, the choice of the remaining independent structurally isolated degrees of freedom is ambiguous and non-trivial. However, raising no claim to completeness, two general statements can be easily understood:

- All fully isolated degrees of freedom are also independent
- An isolated degree of freedom with both cut joints within the same structurally isolated subchain of a single-loop kinematic chain is independent of the structurally isolated degree of freedom and vice versa.

The first statement follows directly from the definition that a fully isolated degree of freedom leaves the relative kinematics of the surrounding kinematic chain invariant. Therefore, any other fully isolated degree of freedom must be independent. In the second case, the structurally isolated degree of freedom leaves the internal kinematics of both subchains invariant. On the other hand, as previously stated, characteristic properties of the structurally isolated degree of freedom as axes and points may depend on the internal motion within the subchains. However, as an isolated degree of freedom within one of these subchains has no impact on the subchain's overall configuration, it also leaves the characteristic properties of the structurally isolated degree of freedom unchanged, and both degrees of freedom can be assumed as independent.

Clearly, this is not the case for two structurally isolated degrees of freedom whose respective subchains "overlap," as the characteristic properties of one isolated degree of freedom would depend on the isolated motion of the other. Furthermore, the set of structurally isolated degrees of freedom that fulfill the given statements is also not necessarily unique. Nevertheless, in the case of a directed kinematic network, it is of particular interest, whether there exist structurally isolated degrees of freedom that leave dedicated inputs stemming from other kinematic loops within the network invariant. For this reason, the search for structurally isolated degrees of freedom will be limited to those cases.

Fortunately, this can easily be implemented by temporarily regarding all inputs from other kinematic loops fixed. Afterward, the hereby connected subchains are checked for the existence of structurally isolated degrees of freedom. These are then labeled in

the same manner as described above.

5.2.2 Transmission of Isolated Degrees of Freedom

The isolated degrees of freedom detected within a kinematic loop are in the first place *locally* isolated within that loop. Only if these are isolated for all kinematic loops within a closed kinematic chain, the degrees of freedom are also *globally* isolated and then may be disregarded for the detection of rigid structures. Referring to Simroth et al. (2016), locally isolated degrees of freedom that actually transmit motion into another coupled kinematic loop will be termed *transmitted* isolated degrees of freedom. For this classification, the locally isolated degrees of freedom will be tracked along with the coupled kinematic loops. To that end, it is only necessary to analyze the kinematic loops, coupled by joints involved in the isolated degree of freedom, since the remaining joints are left invariant.

In particular, for two kinematic loops that are coupled by a joint which is involved in a locally isolated degree of freedom f_a^{iso} of the first kinematic loop, there must also exist a locally isolated degree of freedom f_b^{iso} of the same (or a superior) displacement subgroup in the second kinematic loop, in order for the locally isolated degree of freedom to be globally isolated. That is, in order for both isolated degrees of freedom to comply, their group intersection

$$f_a^{\mathrm{iso(G)}} \cap f_b^{\mathrm{iso(G)}} \neq E \tag{5.5}$$

must be different from the identity displacement. As each locally isolated degree of freedom involves two joints, there may be more kinematic loops coupled, for which the same condition must hold. As the degree of freedom can be classified as a globally isolated degree of freedom only once, the remaining locally isolated degrees of freedom are marked as transmitted.

For illustration, the example in fig. 5.4 a) is regarded. The kinematic loops L_1 and L_2 are coupled by joint $\mathcal{G}_2$. L_1 features a locally fully isolated degree of freedom $f_1^{\mathrm{iso}} : \{\mathcal{G}_1, \mathcal{G}_2\}$ with $f_1^{\mathrm{iso(G)}} : R_{\mathbf{1}\boldsymbol{e_2},O_1}$, and similarly, L_2 features a locally fully isolated degree of freedom $f_2^{\mathrm{iso}} : \{\mathcal{G}_2, \mathcal{G}_3\}$ with $f_2^{\mathrm{iso(G)}} : R_{\mathbf{2}\boldsymbol{e_3},O_2}$. Since L_1 and L_2 share $\mathcal{G}_2$, for the locally isolated degree of freedom $f_1^{\mathrm{iso(G)}}$ there must also be a locally isolated degree of freedom in L_2 in order for the spin of $\mathcal{B}$ to be globally isolated. This is indeed the case since $f_1^{\mathrm{iso(G)}} \cap f_2^{\mathrm{iso(G)}} = R_{\mathbf{1}\boldsymbol{e_2},O_1}$, and the isolated spin of $\mathcal{B}$ is globally isolated. The spin of $\mathcal{B}$ can only be assigned once as fully isolated, and for the later inspection, this

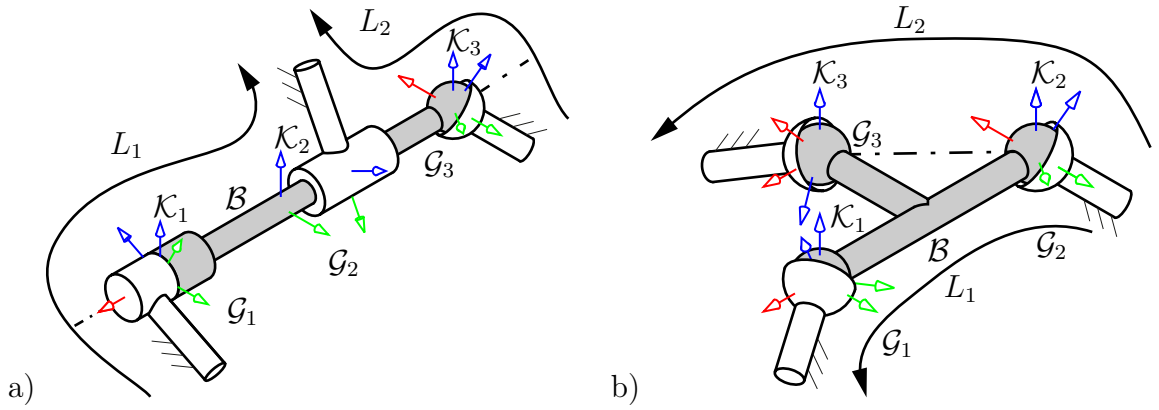

Figure 5.4: a) Fully isolated and b) transmitted isolated degrees of freedom

motion can be thought of as locked. For L_2, the rotation then forms a transmitted isolated degree of freedom, which describes the relative rotation of the links attached to $\mathcal{G}_2$ and $\mathcal{G}_3$.

In fig. 5.4 b), the kinematic loops L_1, and L_2 are also coupled by joint $\mathcal{G}_2$ and feature the locally isolated degrees of freedom $f_1^{\text{iso}} : \{\mathcal{G}_1, \mathcal{G}_2\}$ and $f_2^{\text{iso}} : \{\mathcal{G}_2, \mathcal{G}_3\}$ with $f_1^{\text{iso(G)}} : R_{\mathbf{1}\boldsymbol{e}_{\mathbf{2}},O_1}$ and $f_2^{\text{iso(G)}} : R_{\mathbf{2}\boldsymbol{e}_{\mathbf{3}},O_2}$, respectively. However, even though both loops possess an isolated degree of freedom, which involves $\mathcal{G}_2$, from ${}_1\boldsymbol{e}_2 \nparallel {}_2\boldsymbol{e}_3$ follows that $f_1^{\text{iso(G)}} \cap f_2^{\text{iso(G)}} = E$. Therefore, there is no globally isolated degree of freedom, but instead, the motion of f_1^{iso} from L_1 is transmitted to L_2, where it acts as a proper degree of freedom.

5.2.3 Example: Transmission of Isolated Degrees of Freedom

In sec. 2.5 the concepts of fully, structurally, and transmitted isolated degrees of freedom were introduced and shall now be applied to the example of the tetrahedron shown in fig. 5.5a). There are three independent closed kinematic chains L_1, L_2, and L_3, which are coupled through the mutual spherical joint coupling D. In this case, coupling D is of particular importance for the transmission of isolated degrees of freedom and shall be examined in more detail from a qualitative point of view. Hence, before applying the previously introduced group-based concepts, the next section is dedicated to couplings arising at multiple spherical joints which is a revised version from (Simroth et al., 2016).

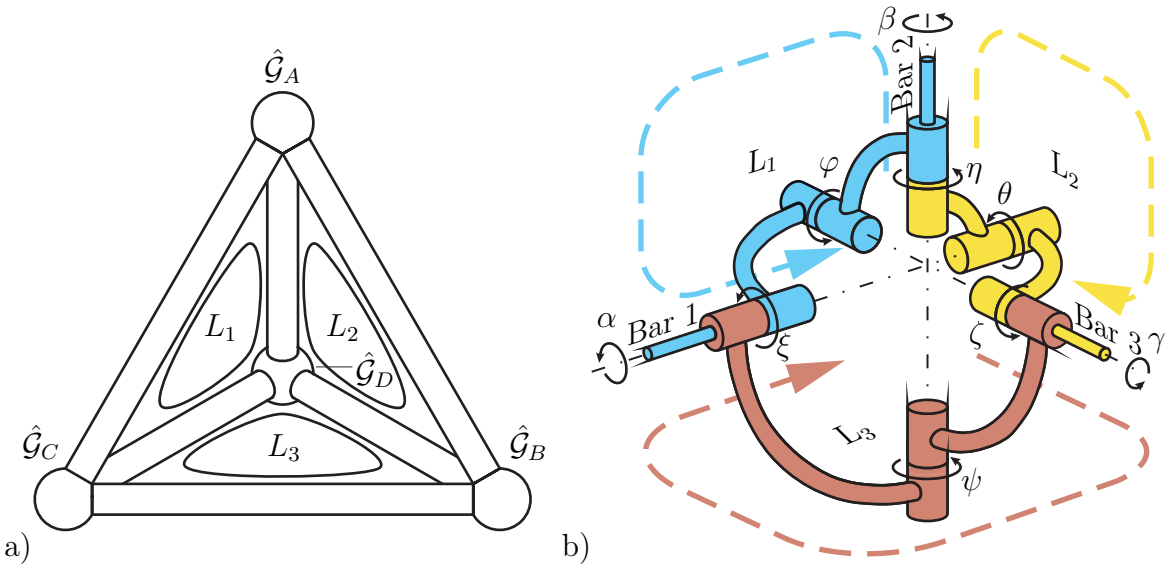

Figure 5.5: a) Tetrahedron with isolated degrees of freedom and b) the decomposed multiple joint $\hat{\mathcal{G}}_D$

Loop coupling conditions at a spherical joint

When multiple loops coincide at one spherical joint, the product of rotation matrices of the relative rotations over all incident loops must yield unity, thus producing 3 independent coupling conditions. Furthermore, when multiple bars coincide in a spherical joint, one can always decompose the relative rotation between the bars within a loop into two terminal rotations about the connecting bars, and one intermediate rotation about some arbitrary axis, which should however be warranted never to become parallel to one of the bars over the complete motion. In this way, one obtains loop couplings at a spherical joint between two isolated bar spin degrees of freedom and one proper aperture angle for each loop incident to that joint. An example is given in fig. 5.5b). Here, the loop coupling equation between the three loops L_1, L_2 and L_3 can be expressed as

$$\mathbf{R}_3(\xi, \psi, \zeta) = \mathbf{R}_1(\alpha, \varphi, \beta) \cdot \mathbf{R}_2(\eta, \theta, \gamma) \ , \tag{5.6}$$

where $\mathbf{R}(\cdot, \cdot, \cdot)$ denotes the rotation matrix in terms of (z-x-z) Euler angles in the order of the arguments. The coupling equation can be interpreted such that the three internal rotations ξ, ψ, ζ of loop L_3 result numerically as a (non-linear) function of the three internal rotations α, φ, β and η, θ, γ of loops L_1 and L_2, respectively. Topologically, this coupling has particular properties due to the implicitly assumed isolated degrees of freedom about the bars that are incident to the spherical joint, which can be described qualitatively without resorting to the explicit resolution of the spatial loop coupling conditions in terms of the output angles ξ, ψ, ζ, as discussed next.

Assuming that the other ends in fig. 5.5b) (not shown) of the bars are also attached to spherical joints, which is the case for the tetrahedron, the bars will be allowed to spin about their longitudinal axis. However, only one rotation per bar can be regarded as truly fully isolated: If a loop "registers" one isolated spin as fully isolated, then for the neighboring loop this rotation becomes transmitted. This is shown by the chosen colors in fig. 5.5b): Assuming that the spin of bars 1 and 2 have been registered as fully isolated in loop L_1, these can be regarded as immaterial spinnings of the pins within the sleeves of the joints of bars 1 and 2, denoted by angles α and β, respectively; however, the rotation within loop L_3 about bar 1, denoted by ξ, is then not fully isolated anymore, and actually "pushes" apart or together the legs of loop L_3 as when unfolding two faces of an origami at the edge folded along the axis of bar 1. Thus, the angle ξ is a transmitted isolated degree of freedom. Similarly, the rotation within loop L_2 about bar 2, denoted by η, rotates the yellow chain within loop L_2 about the axis of bar 2, and is thus again a transmitted isolated degree of freedom. Finally, the rotation γ of the inner pin of the revolute joint along bar 3 can be regarded again as a fully isolated degree of freedom once, which in the case of fig. 5.5b) has been arbitrarily assigned to loop L_2. This makes the rotation about bar 3 within loop L_3, denoted by ζ, again a transmitted isolated degree of freedom.

By the loop coupling conditions, one can recognize that, if loop L_3 is the "output" of the coupling conditions according to eq. 5.6, then two of the incoming variables of loop L_3, namely ξ and ζ, are transmitted isolated degrees of freedom that do not affect the inner kinematics of loop L_3, but the third one, namely ψ, is a proper transmission angle which regulates the relative orientation of bars 1 and 3 with respect to each other. This angle is a function of the opening angles φ and θ of loops L_1 and L_2, respectively, but also of the transmitted isolated degree of freedom η of loop L_2, which thus becomes material. If the three loops L_1, L_2, L_3 are assumed to be triangles with spherical joint nodes (as it is the case for the regarded mechanism), then the angles φ, θ, ψ must remain constant, which means that loop L_3 induces an implicit constraint equation for the transmitted isolated degree of freedom η of loop L_2. This kind of tracking of transmitted isolated degree of freedom up to locations of implicit constraint equations will prove useful for detecting rigid and movable substructures in multiple spherical-spherical bar mechanisms.

Group-based tracking and classification of isolated degrees of freedom

Based on the idea developed above "by inspection" for tracking isolated degrees of freedom for the multiple spherical joint, next, all isolated degrees of freedom for the tetrahedron will be systematically detected and tracked based on the associated displacement subgroups. The directed kinematic network shown in fig. 5.6a), which can be derived following the steps in sec. 4.3.2, serves as a starting point for the classification. As already shown in sec. 5.2.3, L_3 "receives" three joint variables from D, of which the opening angle is already determined by the inner loop closure conditions. In addition, an external input for the spin of the bar not shared with L_1 and L_2 is necessary, from which follows that L_3 is overconstrained by one. At this point, when adding up all external inputs and subtracting the degrees by which L_3 is overconstrained, a degree of freedom of $f = 6$ corresponding to the six bar spins results. In the next step, these bar spins shall be detected as fully isolated degrees of freedom and classified according to the following procedure, such that the tetrahedron can be identified as a structure.

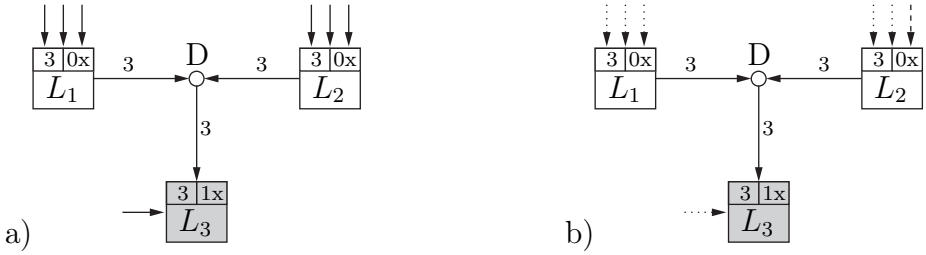

Figure 5.6: a) Directed kinematic network of the tetrahedron before and b) after classification of isolated degrees of freedom

The method is initialized with two lists. One list determines the order in which the loops are handled and naturally defaults to the total order described in sec. 4.3.2 as it also resembles the order in which the loop kinematics are processed. In this way, isolated degrees of freedom are marked as fully isolated at the place of their first occurrence within the solution flow, while for the remaining loops "downstream" they appear as transmitted isolated degrees of freedom. In a second list, locally isolated degrees of freedom within all loops are detected and enumerated according to sec. 5.2.1. Throughout the process, these are successively declared either fully or transmitted isolated and once classified, are removed from the list of locally isolated degrees of freedom.

Similar to the examples in fig. 5.4, a degree of freedom that is locally isolated for a specific loop is only fully isolated for the considered kinematic chain, if the associated

motion within the joints also leaves the relative kinematics within the loops coupled through these joints invariant. Therefore, the goal of the following procedure is to check consecutively for each locally isolated degree of freedom whether there exists at least one "compatible" locally isolated degree of freedom with a common displacement subgroup in the loops connected by the joints performing this particular motion. If not, it can directly be regarded as a transmitted degree of freedom. Iterating through all loops, starting with the first loop within the total order, for each locally isolated degree of freedom f_i^{iso}, the following steps are conducted:

1. Find all unvisited loops coupled by at least one of the joints involved in f_i^{iso} and mark these as visited for f_i^{iso} (loops can be revisited for other degrees of freedom)
2. For each of the coupled loops, check if there is at least one "compatible" locally isolated degree of freedom, i. e., one whose intersection with $f_i^{\text{iso(G)}}$ yields a displacement subgroup other than the identity displacement
3. Recursively apply steps 1 and 2 to the "compatible" isolated degrees of freedom until no further coupled loops are found.
4. Classify f_i^{iso} as fully isolated if there is at least one compatible locally isolated degree of freedom for each coupled loop and else mark f_i^{iso} as transmitted
5. Mark the "compatible" degrees of freedom as transmitted and remove from list

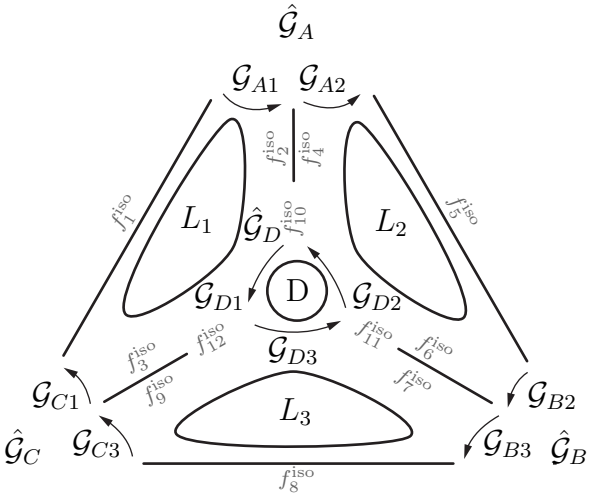

L_i	f_i^{iso}	$f_i^{\text{iso(G)}}$
L_1	$f_1^{\text{iso}} : \{\mathcal{G}_{C1}, \mathcal{G}_{A1}\}$	$R_{\boldsymbol{Ce_A}, O_A}$
L_1	$f_2^{\text{iso}} : \{\mathcal{G}_{A1}, \mathcal{G}_{D1}\}$	$R_{\boldsymbol{Ae_D}, O_D}$
L_1	$f_3^{\text{iso}} : \{\mathcal{G}_{D1}, \mathcal{G}_{C1}\}$	$R_{\boldsymbol{De_C}, O_C}$
L_2	$f_4^{\text{iso}} : \{\mathcal{G}_{D2}, \mathcal{G}_{A2}\}$	$R_{\boldsymbol{De_A}, O_A}$
L_2	$f_5^{\text{iso}} : \{\mathcal{G}_{A2}, \mathcal{G}_{B2}\}$	$R_{\boldsymbol{Ae_B}, O_B}$
L_2	$f_6^{\text{iso}} : \{\mathcal{G}_{B2}, \mathcal{G}_{D2}\}$	$R_{\boldsymbol{Be_D}, O_D}$
L_3	$f_7^{\text{iso}} : \{\mathcal{G}_{D3}, \mathcal{G}_{B3}\}$	$R_{\boldsymbol{De_B}, O_B}$
L_3	$f_8^{\text{iso}} : \{\mathcal{G}_{B3}, \mathcal{G}_{C3}\}$	$R_{\boldsymbol{Be_C}, O_C}$
L_3	$f_9^{\text{iso}} : \{\mathcal{G}_{C3}, \mathcal{G}_{D3}\}$	$R_{\boldsymbol{Ce_D}, O_D}$
D	$f_{10}^{\text{iso}} : \{\mathcal{G}_{D1}, \mathcal{G}_{D2}\}$	S_{O_D}
D	$f_{11}^{\text{iso}} : \{\mathcal{G}_{D2}, \mathcal{G}_{D3}\}$	S_{O_D}
D	$f_{12}^{\text{iso}} : \{\mathcal{G}_{D3}, \mathcal{G}_{D1}\}$	S_{O_D}

Figure 5.7: Locally isolated degrees of freedom in the tetrahedron

These steps are now applied to the directed kinematic network in fig. 5.6 a) of the tetrahedron for which one possible total order is given by the sequence ($L_1 \rightarrow L_2 \rightarrow$

D $\rightarrow L_3$). For better tracking, the multiple joints were decomposed in fig. 5.7 and were indexed by joint and loop numbers for which the relative poses are defined. The table in fig. 5.7 lists all locally isolated degrees of freedom that were identified within the loops and couplings.

Starting with L_1 and f_1^{iso} of the three locally isolated degrees of freedom, according to step 1, no loops are coupled to joints $\mathcal{G}_{C1}$ and $\mathcal{G}_{A1}$, thus steps 2 and 3 can be skipped. In step 4, f_1^{iso} can directly be marked as fully isolated and is removed from the list. As no coupled, locally isolated degrees of freedom exist, step 5 is also omitted. Repeating step 1 for f_2^{iso}, the coupling loop D is found to be coupled by $\mathcal{G}_{D1}$. Following step 2, the two isolated degrees of freedom f_{10}^{iso} and f_{12}^{iso} share joint $\mathcal{G}_{D1}$ and due to $f_2^{\text{iso(G)}} \cap f_{10}^{\text{iso(G)}} = f_2^{\text{iso(G)}} \cap f_{12}^{\text{iso(G)}} = R_{\boldsymbol{A}\boldsymbol{e}_{\boldsymbol{D}},O_D}$ both are compatible. The previous steps are now repeated for both compatible isolated degrees of freedom of which at least one needs to be compatible in order for f_2^{iso} to be fully isolated: For f_{10}^{iso} L_2 is coupled by $\mathcal{G}_{D2}$, and of the three locally isolated degrees of freedom f_4^{iso} is compatible as $f_2^{\text{iso(G)}} \cap f_{10}^{\text{iso(G)}} \cap f_4^{\text{iso(G)}} = R_{\boldsymbol{A}\boldsymbol{e}_{\boldsymbol{D}},O_D}$ due to ${}_A\boldsymbol{e}_D \parallel {}_D\boldsymbol{e}_A$ and both points O_A, O_D being elements of the same rotation axis. For f_4^{iso}, there are no further unvisited coupled loops to check. Applying the same procedure to f_{10}^{iso}, which is coupled to L_3 by $\mathcal{G}_{D3}$, no compatible locally isolated degree of freedom can be found. In conclusion, for f_2^{iso} compatible locally isolated degrees of freedom were found in all coupled loops such that f_4^{iso} is marked fully isolated. The compatible degrees of freedom f_{10}^{iso} and f_4^{iso} on the other side are marked as transmitted and altogether are removed from the list of locally isolated degrees of freedom.

In the same manner, the remaining isolated degree of freedom f_3^{iso} in L_1 is tracked and found to be fully isolated, and the compatible degrees of freedom f_{12}^{iso} and f_9^{iso} will be marked as transmitted.

The next item within the total order is L_2 for which only f_5^{iso} and f_6^{iso} remain listed as locally isolated degrees of freedom, both being fully isolated, whereas f_{11}^{iso} and f_7^{iso} being transmitted by f_6^{iso}. For D, all locally isolated degrees of freedom were already classified, and for L_3 only f_8^{iso} is left to be assigned as fully isolated. The resulting classification of the external inputs has been visualized within the kinematic network in fig. 5.6b).

5.3 Identifying Rigid Subsystems

Before proceeding to the detection of rigid subsystems with isolated degrees of freedom, the general method based on Xia et al. (2012) will be illustrated for the kinematic chain shown in fig. 5.8 a). For the analysis of the dependencies among the kinematic loops within the kinematic network in fig. 5.8 b), a *loop connection graph* is introduced, to which the kinematic network is mapped as depicted in fig. 5.8 c).

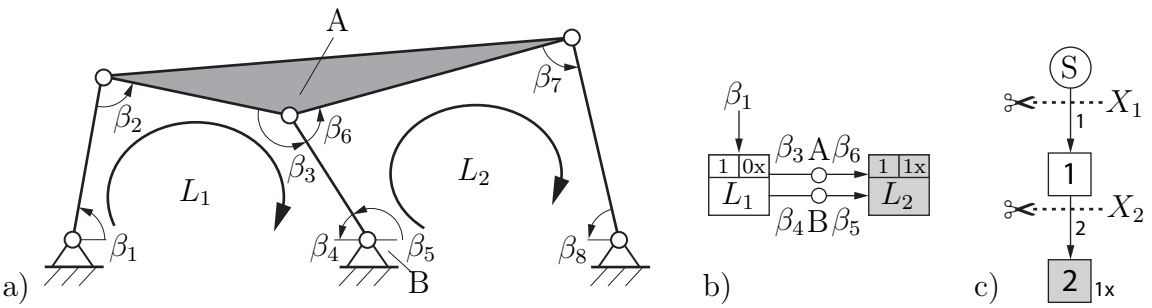

Figure 5.8: a) Rigid double four-bar structure, b) its associated kinematic network, and c) its corresponding loop connection graph

5.3.1 Elements of the Loop Connection Graph

The loop connection graph visualizes the "solution flow" of the previously established directed kinematic network as a layered acyclic directed graph, which eases the application of standard graph-theoretic tools. For this reason, the kinematic transformers are mapped as nodes, retaining only the loop index as well as an annotation denoting the degree by which the number of inputs exceeds the node's degree of freedom, in case this degree is greater than zero. The latter nodes are also highlighted in gray.

Multiple edges within the kinematic network are merged into single weighted edges, with a weight w corresponding to the number of transmitted joint variables. In addition, a source node is added, which symbolizes the origin of any external input for the regarded system. The elements of the loop connection graph are summarized in tab. 5.1 and are compared to those of the kinematic network. The nodes of the loop connection graph are arranged in layers, expressing the level of dependency, with elements of the lower layers being dependent on elements of the upper layers. Consequently, the source node, which is independent of any kinematic transformer, is positioned at the

Table 5.1: Elements of a loop connection graph (LCG) adapted from Xia et al. (2012)

LCG	Kinematic network	Description
		Kinematic transformer
		Kinematic transformer overdetermined by d
	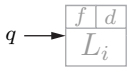	Source of external inputs
	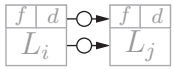	Edge with weight w corresponding to the number of joint variables
	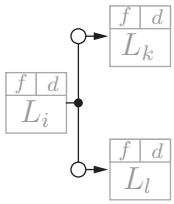	Branching with weight w corresponding to the number of joint variables
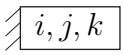	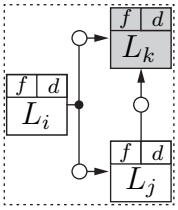	Reduced rigid subsystem
		From left to right: Fully, transmitted, and structurally isolated degrees of freedom

top. For a recursively solvable system, then the path from the source to an individual loop node points out the sequence in which the loops have to be solved.

5.3.2 Search for "Rigid" Cuts

The loop connection graph can be analyzed by performing directed "cuts" X, separating the loop connection graph into an *upstream* component containing the source node and a *downstream* component, such that all cut edges are directed from the upstream to the downstream component.

The sum of the annotated degrees of the loop nodes in the downstream part is termed *absorbing degree* d_X of the cut X, and the *weight* w_X of a cut X is determined by the accumulated weights of the cut edges. With these definitions, the *cut degree of freedom* f_X is defined as the difference of cut weight and absorbing degree

$$f_X = w_X - d_X \tag{5.7}$$

and is an indicator of the degree of freedom of the subsystem formed by the downstream part. Its meaning is similar to the Chebyshev-Grübler-Kutzbach formula if only the elements comprised in the subsystem were regarded. Indeed, the cut directly underneath the source node returns the result from the Chebyshev-Grübler-Kutzbach formula of the regarded kinematic chain.

For a better understanding of absorbing degree and cut weight, it is recalled that the elements within the downstream component of the cut represent a system of equations with the joint variables being the unknowns to be solved for. The absorbing degree then resembles the balance between the total number of joint variables and the number of (constraint) equations introduced by loop closures, couplings, as well as prescribed inputs. Consequently, an absorbing degree greater than zero indicates that the system of equations is overdetermined, and some of the inputs lose their independence. If the absorbing degree is greater or equal to the number of overall inputs entering the regarded subsystem, all inputs lose their independence. As a result, these can be determined solely from the constraints imposed by the subsystem, which can then be regarded as rigid. Thus, the search for a rigid subsystem mainly consists of the search for cuts with a degree of freedom of zero or less.

For illustration, the system displayed in fig. 5.8a) is regarded, which is composed of two coupled planar four-bar mechanisms, featuring one degree of freedom each. The corresponding kinematic network and loop connection graph are shown in fig. 5.8b) and c). There are two possible cuts, of which cut X_2 features $f_{X_2} = 2 - 1 = 1$ degree of freedom, corresponding to the single degree of freedom of the subsystem comprising only the four-bar represented by L_2. Thus, one of the two inputs denoted by the cut depends on the other. However, X_1 with $f_{X_1} = 1 - 1 = 0$ indicates that the regarded system of both four-bars is a rigid structure. The Jacobian matrix of the underlying constraint equations illustrates the dependencies, where an x indicates the non-zero partial derivatives:

$$\mathbf{J}_\beta = \frac{\partial \boldsymbol{g}}{\partial \underline{\beta}} = \begin{array}{c} \\ \beta_1 \\ \uparrow \\ L_1 \\ \downarrow \\ A \\ B \\ \uparrow \\ L_2 \\ \downarrow \end{array} \begin{array}{c} \begin{array}{cccccccc} \beta_1 & \beta_2 & \beta_3 & \beta_4 & \beta_5 & \beta_6 & \beta_7 & \beta_8 \end{array} \\ \begin{pmatrix} 1 & & & & & & & \\ \mathrm{x} & \mathrm{x} & & & & & & \\ \mathrm{x} & \mathrm{x} & \mathrm{x} & & & & & \\ \mathrm{x} & \mathrm{x} & \mathrm{x} & \mathrm{x} & & & & \\ & & & -1 & 1 & & & \\ & & -1 & & & 1 & & \\ & & & & \mathrm{x} & \mathrm{x} & & \\ & & & & \mathrm{x} & \mathrm{x} & \mathrm{x} & \\ & & & & \mathrm{x} & \mathrm{x} & \mathrm{x} & \mathrm{x} \end{pmatrix} \end{array}$$

Each of the two kinematic transformers introduces three closure equations. In addition, there is one input equation defining β_1 and two coupling equations arising from the shared joints. The resulting overdetermined system of nine equations and eight unknowns implies that the input equation defining β_1 can be omitted as β_1 is determined by solving the remaining equations.

Though, as depicted in the introductory example in fig. 2.4, some degrees of freedom may be "conceiled" by some overdetermined subsystem. Therefore, the cut with the most negative degree of freedom, thus indicating the most overdetermined subsystem, is concerned first, and the identified subsystem is replaced by a single element symbolized as depicted in tab. 5.1. As no inputs are required, it will be located at the top layer of the loop connection graph. This implies that former inputs from elements within the loop connection graph are now outputs of the reduced rigid subsystem, and the degrees of the connected elements have to be updated accordingly. The procedure of cutting and pruning is then repeated for the new reduced loop connection graph until no further rigid subsystems are detected.

5.3.3 Limiting the Search Space to Pruned Graphs

Proceeding from a general loop connection graph usually, the number of nodes can be significantly reduced if recursively solvable subsystems are present. For these systems, the number of inputs directly equals the degree of freedom, as there are no overdetermined elements. These subsystems are readily identified within the loop connection graph as non-overdetermined pendant nodes, which can be removed from the loop connection graph. In addition, further reduction rules may be applied to the loop connection graph, as listed in (Xia et al., 2012).

For the remaining loop connection graph, all pendant nodes (termed "sinks") are overdetermined to some degree. The search then confines to "pruned graphs" (Xia et al., 2012) for each of these sinks, which consist only of the sink itself as well as all its predecessors on the path to the source node. In general, besides the pruned graphs themselves, also the graphs generated by their combinations have to be regarded, thus potentially leading to a large number of systems that need to be analyzed. Fortunately, not all combinations yield distinct subsystems, such that the search space can be limited by the following two rules (Simroth et al., 2015b):

Rule 1: A pruned graph for a pendant sink node covers all combinations of that sink node with all other sink nodes contained in the pruned graph.

Rule 2: Pruned graphs that have no other node in common but the source node does not need to be combined.

The procedure depicted in the previous sections will also be applied to systems with isolated degrees of freedom, though a more detailed inspection of the subsystems regarding the classification and transmission of isolated degrees of freedom is necessary, which is the subject of the next section.

5.4 Detection of Rigid Systems with Isolated Degrees of Freedom

The challenge of applying this approach to systems with isolated degrees of freedom resides in the determination of the cut weights. Reverting to the tetrahedron example with its loop connection graph depicted in fig. 5.9 a), all relevant subsystems can be identified by performing directed cuts as introduced before, whereby each of the downstream components represents a subsystem with the cut edges as its inputs. An algorithm for enumerating all minimal cut-sets is provided in Abel and Bicker (1982). The possible cuts are displayed in fig. 5.9 b) of which none has a degree of freedom less or equal to zero since the isolated bar spins are included. In order to disregard isolated bar spins for the detection of rigid subsystems, the hereby identified subsystems can be extracted, and the inputs are classified as fully, structurally, or transmitted isolated. For the cut X_1 that describes the entire tetrahedron, this classification has already been performed in sec. 5.2.3 and the external inputs will now be labeled according to the notation in tab. 5.1.

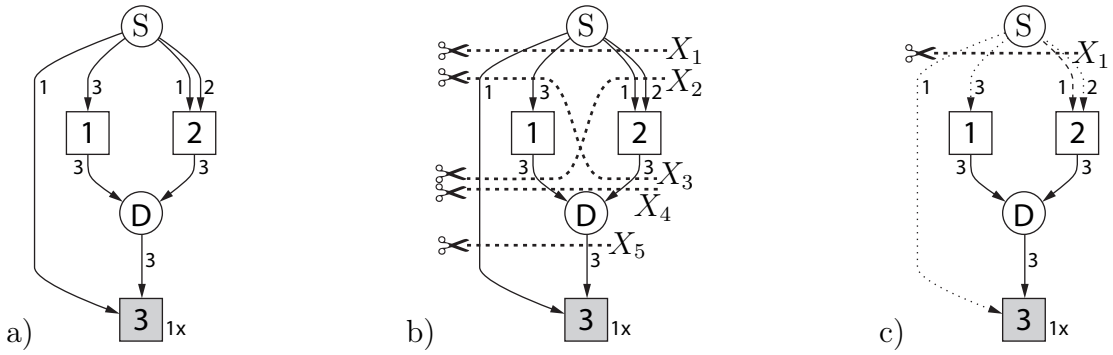

Figure 5.9: a) The loop connection graph of the tetrahedron, b) with potential directed cuts, and c) highlighted isolated degrees of freedom

In this sense, the external input edges of the loop connection graph shown in fig. 5.9 c) are declared as follows: For L_1, all three isolated degrees of freedom f_1^{iso}, f_2^{iso}, and f_3^{iso}, were classified as fully isolated, such that all three external input edges will be marked by dotted lines. For L_2, two isolated degrees of freedom f_5^{iso} and f_6^{iso} were found to be fully isolated, while f_4^{iso} corresponds to the shared link with L_1 and therefore was classified as transmitted and is marked by a dashed line. For coupling D, no external input edges that need to be marked exist. In L_3, f_7^{iso} and f_9^{iso} are transmitted by the internal input edge corresponding to $\mathcal{G}_{D3}$. The external input edge is then associated with the fully isolated degree of freedom f_8^{iso}.

For the evaluation of the cut X_1, now the edges marked as fully isolated will be accounted for with a weight of 0, effectively removing the fully isolated degrees of freedom for the rigidity detection. As a result, the degree of freedom of the cut X_1

$$f_{X_1} = w_{X_1} - d_{X_1} = 1 - 1 = 0 \tag{5.8}$$

indicates that the tetrahedron is a structure that features six fully isolated degrees of freedom.

For a better overview, the individual stages of the overall procedure are summarized in fig. 4.11. When starting from a general kinematic chain, a topological graph is derived. To this end, the relations between the links which are described by sequences of elementary transformations are analyzed, and multiple joints are identified. The topological graph is then used to find a minimum cycle basis. Each cycle is then regarded as a kinematic transformer, which incorporates the underlying kinematics. Regular joints and multiple joints are resolved into couplings, which, together with the kinematic transformers, lead to a kinematic network. By use of a simple greedy algorithm, a sequence by which the elements may be solved efficiently is determined. Afterward,

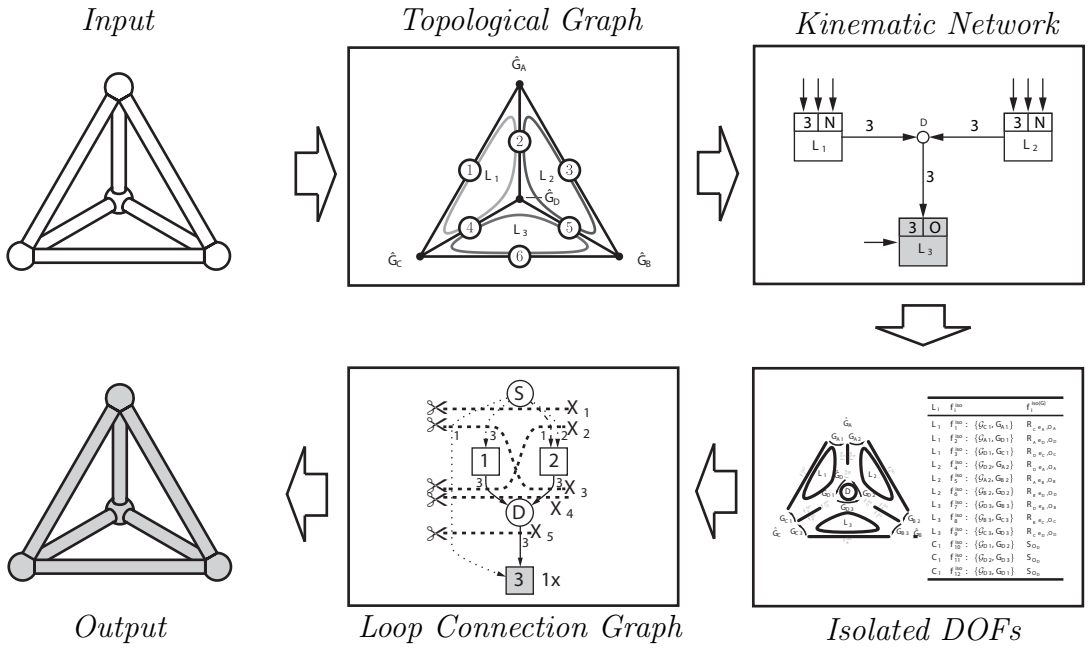

Figure 5.10: General stages of the described approach for detecting rigid subsystems

all kinematic loops are traversed in this order and locally isolated degrees of freedom are identified. The dependencies within the kinematic network are illustrated in a loop connection graph, in which potentially rigid subsystems are identified through evaluating directed cuts. For the hereby depicted subsystems, isolated degrees of freedom among the inputs are classified as fully, structurally, or transmitted isolated. By this means, it is possible to disregard isolated degrees of freedom for the rigidity search, such that overdetermined subsystems that were previously "hidden" by the presence of isolated degrees of freedom are found. After merging these subsystems, general conclusions about the real degree of freedom as well as links forming a rigid component can be made.

6 Applications

In this chapter, the previously derived concepts and methods shall be applied to the well-known "double banana" paradoxical example as well as to the more recently published "7 roofs" challenge. A solution to the first problem applying the methodologies of the present work was published in (Simroth et al., 2015c, 2016) while the latter challenge was approached in (Simroth et al., 2015a,b). In the following two sections, some portions of the published work are adopted and will be further elaborated.

6.1 Solving the "Double Banana" Paradoxical Example

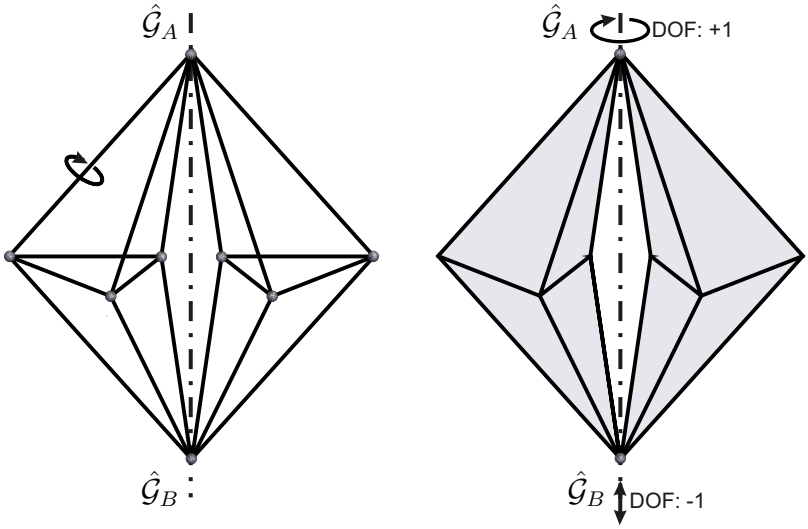

Figure 6.1: Counterexample of mobility criteria known as the "double banana" which features isolated bar spins (Simroth et al., 2016, p. 108)

The kinematic chain in fig. 6.1 is commonly referred to as the "double banana" and has puzzled researchers for many decades (Rojas and Thomas, 2013). Many algorithms for rigidity detection have been provided so far, but the automatic detection of rigid substructures involving *implied hinges*, as indicated by the dot-dashed line, remains a challenge.

The double banana can be seen as a system comprised of 18 bars connected by 8 multiple spherical joints, which could equivalently be decomposed into 28 binary spherical joints with 3 degrees of freedom each. As a result, eq. 2.1 yields an overall degree of freedom of 18, implicating the 18 isolated bar spins. Thus, after subtraction of those, it implies the system to be rigid with a degree of freedom of 0.

However, one can clearly "see" in fig. 6.1 that the double banana structure consists of two rigid bipyramids, one at the left and one at the right, which are coupled together by two spherical joints ($\hat{\mathcal{G}}_A$ and $\hat{\mathcal{G}}_B$). Thus, the segment $\overline{\hat{\mathcal{G}}_A\hat{\mathcal{G}}_B}$ is an *implied hinge* (Cheng et al., 2009) about which the two halves can rotate with respect to each other, while the longitudinal direction is equally defined by the left and the right compound and therefore is overconstrained with a degree of freedom of -1. This implied degree of freedom also remains undetected by the famous test equation for rigidity according to Maxwell's rule proposed in (Maxwell, 1864), which states that a statically and kinematically determined framework with $n_{\mathcal{B}}$ links and $n_{\mathcal{G}}$ joints follows the equation

$$n_{\mathcal{B}} = 3 \cdot n_{\mathcal{G}} - 6 \ . \tag{6.1}$$

It is evident that a bipyramid (single banana), with 9 bars and 5 joints correctly satisfies the condition of Maxwell's rule. However, also the double banana structure obeys Maxwell's rule, although it is obviously not rigid. Thus, this structure is a classical non-trivial example of a mechanism satisfying Maxwell's rule of a statically and kinematically determined framework, which is nevertheless generically able to move, and which has thus attracted considerable attention in literature: Fowler and Guest (2002) analyzed the symmetry of the structure and presented the result of the symmetry of multiple banana mechanisms; Cheng et al. (2009) studied the rigidity of the 3D structure with the double banana as an example, and Rojas and Thomas (2013) proposed the double banana closure conditions as a paradigm for position analysis in robots.

The cause for the double banana paradox consists in the existence of isolated degrees of freedom in the mechanism (e. g., the bar spin between two spherical joints) which create an own level of transmission kinematics, and which thus need to be tracked in order to be able to detect which substructures are rigid and which are movable. For this reason, in a first step, a topological graph for the double banana is derived. The graph corresponding to the left bipyramid is depicted in fig. 6.2 where the connected bars of the right bipyramid are indicated by dashed lines. The bodies are enumerated as 1-3, 4-6, and 7-9 with respect to the upper, middle, and the lower triplet of bars. Since there are only spherical joints present, within the topological graph, all edge weights equal 3/2 for the given case of multiple joint edges. As the resulting graph is already 2-edge connected, no further subdivisions into components of closed kinematic chains are necessary and one can directly proceed with the detection of a minimum cycle basis.

According to eq. 2.3 there exist $n_L = 28 - 18 + 1 = 11$ independent loops. Here, a minimum cycle basis was detected such that every bipyramid contains 5 triangular

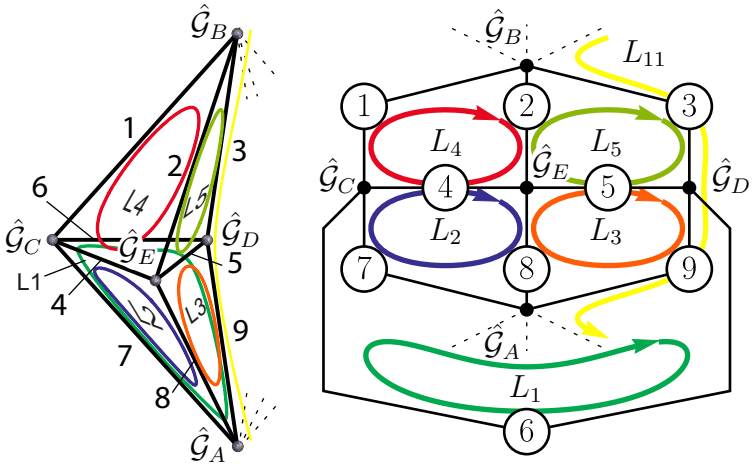

Figure 6.2: Topological graph for the left single banana

loops with one quadrilateral loop connecting both parts.

Next, the multiple joints are resolved into couplings, according to fig. 6.3. It can easily be verified by eq. 4.15 that the condition for the existence of a coupling is not fulfilled at joints $\hat{\mathcal{G}}_B$ and $\hat{\mathcal{G}}_C$, while $\hat{\mathcal{G}}_D$ and $\hat{\mathcal{G}}_E$ (and their respective counterparts in the right bipyramid) give rise to one coupling each and from $\hat{\mathcal{G}}_A$ two couplings A_1 and A_2 originate. Obviously, referring to the coupling graph of $\hat{\mathcal{G}}_A$, both couplings A_1 and A_2 are independent. Since representing spherical joints, each coupling gives rise to three coupling conditions such that for each coupling three joint variables can be determined as a function of the remaining joint variables. In the given case, two of these can be interpreted as isolated spins of two bars while the third one defines the angle between both bars. Based on the derived elements, a kinematic network is established shown

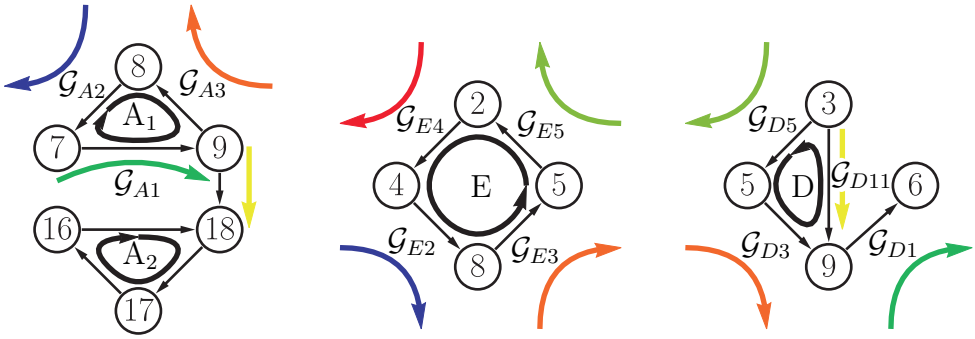

Figure 6.3: Resulting couplings A_1, A_2, E, and D of the left bipyramid

in fig. 6.4 a). All loops feature a spatiality of six such that $L_1, ..., L_{10}$ with nine joint variables stemming from the three spherical joints, have a degree of freedom of three each. These degrees of freedom can be understood as isolated spins of the respective

bars. L_{11} then features six degrees of freedom, of which four can directly be associated with the bar spins.

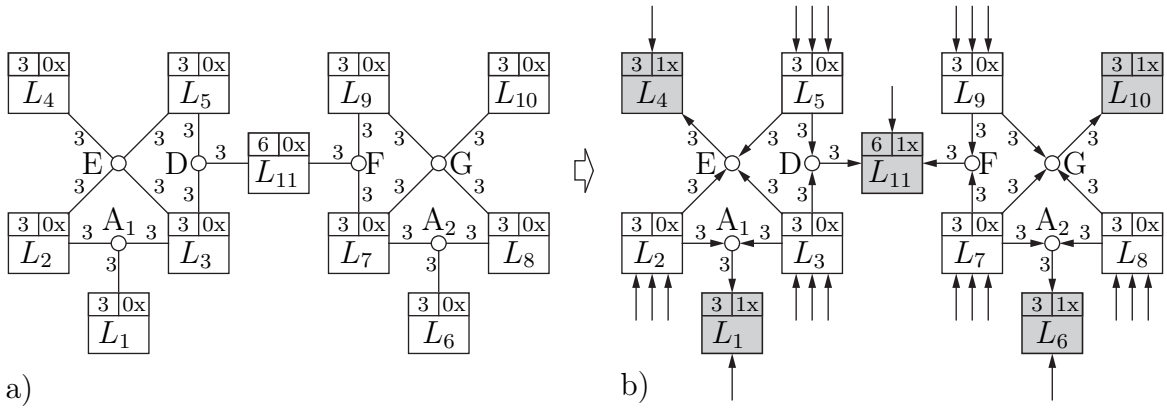

Figure 6.4: a) Undirected kinematic network and b) associated solution flow

In order to find a suitable solution flow for the kinematic network, elements that are least overdetermined when prepended to the topological order are sought subsequently. Indeed, all of the elements L_1, L_4, L_6, L_{10}, and L_{11} possess a degree of freedom greater or equal to the accumulated weight of incident edges, such that these can be positioned at the end of the topological order, orienting the edges into these elements. From the remaining elements, the couplings $\mathrm{A}_1, \mathrm{A}_2, \mathrm{D}, \mathrm{E}, \mathrm{F}$, and G can be prepended next, effectively directing all edges into the couplings that are not incident to the previously added elements. At last, L_2, L_3, L_5, and L_7, L_8, L_9 are added to the beginning of the topological ordering without yielding any overdetermined elements. Afterward, each element is checked for compatibility of chosen inputs and the requirement of additional external inputs. Apparently, the inputs for L_1, L_4, L_6, and L_{10} from the multiple joint couplings also include the aperture angle of the involved triangles, which is likewise defined by the inner geometry of the kinematic loops. As a result, these loops introduce an implicit constraint equation with which the inputs have to comply. Furthermore, these kinematic loops require an additional external input for the spin of the bar not included in any of the other loops. Similarly, the aperture angles of the left and right side of L_{11} introduced by both bipyramids depend on one another, thus introducing one implicit constraint, while the spin about the implied hinge forms an external input. Also, the respective three bar spins in L_2, L_3, L_5 and L_7, L_8, L_9 have to be supplemented by external inputs. A cross-check of the kinematic network with respect to eq. 2.5 with a total sum of 36 degrees of freedom in loops $L_{1,\ldots,11}$ and 18 coupling conditions verifies the consistency with the previously determined degree of freedom of 18.

In the next step, the dependencies among the elements are expressed in the loop con-

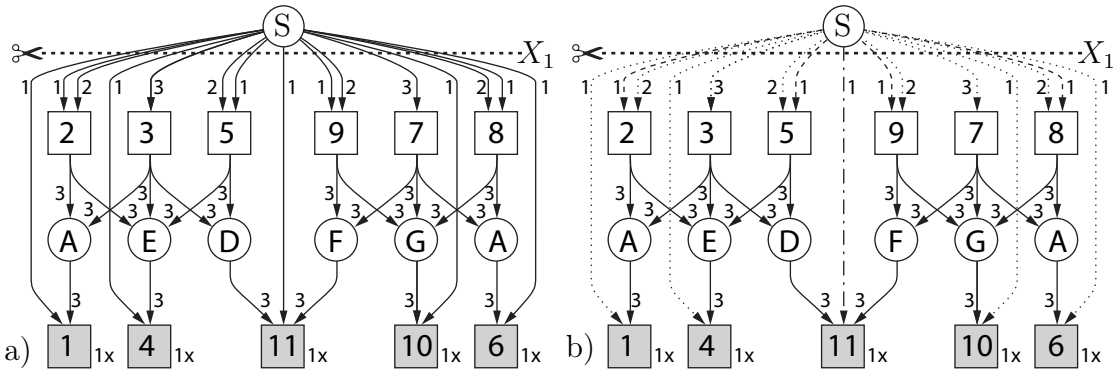

Figure 6.5: a) The loop connection graph for the double banana and b) with highlighted isolated degrees of freedom

nection graph shown in fig. 6.5 a). For each subsystem, isolated degrees of freedom are classified into fully, transmitted, and structurally isolated as described in sec. 5.4. For this reason, all locally isolated degrees of freedom are enumerated and subsequently tracked among the elements in alignment with the total order. The result can easily be verified by inspection: Each isolated spin of a bar is declared only once as fully isolated and for all other elements is regarded as transmitted. In L_{11}, a structurally isolated degree of freedom corresponding to the rotation about the implied edge between $\hat{\mathcal{G}}_A$ and $\hat{\mathcal{G}}_B$ is detected, which leaves the kinematic loop's inputs invariant.

For the loop connection graph in fig. 6.5 a), the degree of freedom of cut X_1 can be derived by counting 23 inputs and an absorbing degree of 5 such that $f_{X_1} = 23-5 = 18$, which suggests the double banana to be rigid if the 18 bar spins are excluded. However, the system is identified to be overconstrained by a degree of freedom of $f_{X_1} = -1$ if the fully isolated spins in fig. 6.5 b) are omitted.

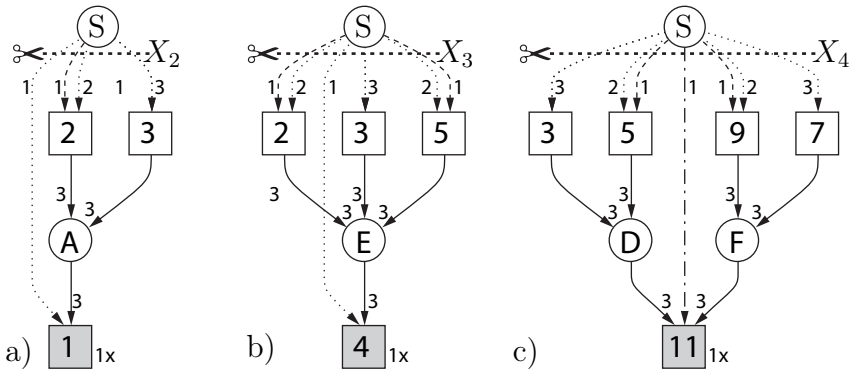

Figure 6.6: Pruned graphs resulting from the loop connection graph with highlighted isolated degrees of freedom

In order to resolve this ambiguity, the rigid parts need to be identified, for which the

pruned graphs in fig. 6.6 are analyzed. Of these, only the pruned graph depicted in a) contains a non-positive cut. Indeed, the corresponding subsystem of a tetrahedron was already addressed and found to be rigid in sec. 5.4. The subsystem is then replaced by a single rigid compound retaining only fully isolated degrees of freedom as all other degrees of freedom are locked due to its inherent constraints and the procedure is restarted. Next, within the subsystem in fig. 6.7 a) a zero degree of freedom cut is found and the corresponding subsystem is again replaced by a single compound yielding the graph in fig. 6.7 b). Here, both bipyramids are already detected as rigid structures with isolated degrees of freedom. For the remaining system, there are only isolated degrees of freedom entering, one of which structurally isolated. It can again be replaced retaining all isolated degrees of freedom such that the implicit condition is dissolved and the graph shown in fig. 6.7 c) is obtained. A cut now reveals that there are 19 degrees of freedom in total, of which 18 are fully isolated corresponding to the bar spins and one is structurally isolated representing the rotation of both bipyramids about the implied hinge.

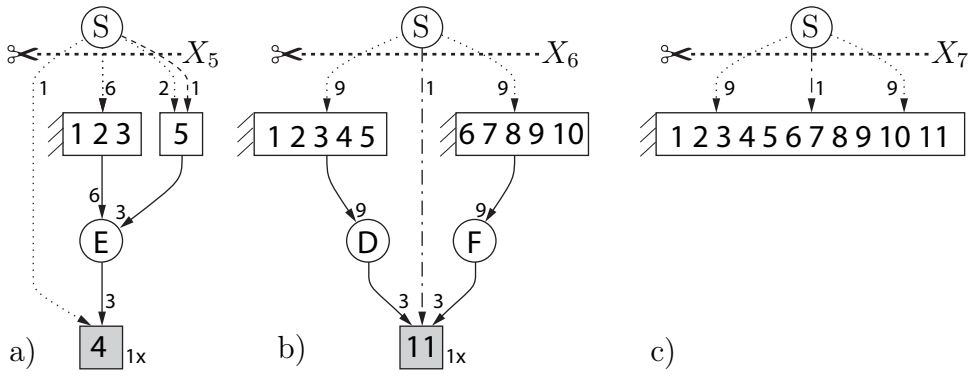

Figure 6.7: Step-by-step replacement of rigid subsystems

6.2 Solving the "Seven-Roof" Paradoxical Example

Cheng et al. (2009) introduced a *nucleation-free* kinematic chain, which is composed of seven "roofs," as depicted in fig. 6.8. In contrast to the previous example, it does not contain any overconstrained subsystems, but instead, the peculiarity consists of the detection of rigid substructures, which are mobile when detached. The solution approach was previously published in Simroth et al. (2015b), of which some of the following passages are reproduced. Each of the seven topologically identical modules is comprised of eight bars, connected by five multiple spherical joints. The hereby formed triangles have one common multiple spherical joint at their center and can

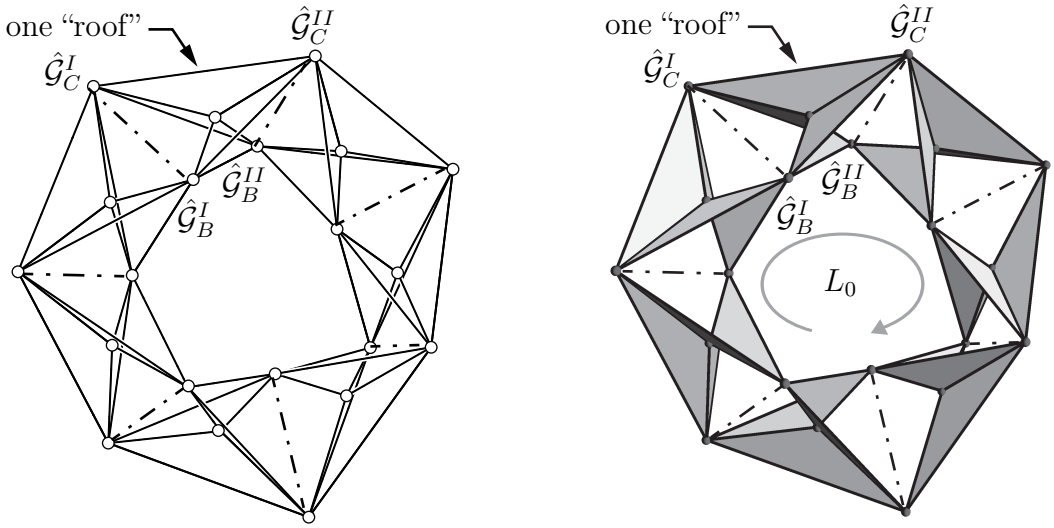

a) b)

Figure 6.8: a) The seven-roof kinematic chain as a system of 56 bars and b) with shaded rigid components (Simroth et al., 2015b, p. 386)

rotate about the bars shared with the neighboring triangles. The roofs are connected by the alternating pairs of spherical joints, which are not directly connected by bars, resulting in a cyclic structure. Overall, the system consists of $n_{\mathcal{B}} = 56$ bars and $n_{\mathcal{G}} = 91$ binary spherical joints, yielding according to eq. 2.1

$$f = 6 \cdot (56 - 1) - 91 \cdot 3 = 57 \tag{6.2}$$

degrees of freedom. Of these, 56 degrees of freedom can be regarded as isolated spins of the bars about their longitudinal axes, while a single proper degree of freedom remains for the internal mobility of the ring structure, which is to be detected.

By inspection, the triangles can be recognized as rigid faces similar to those of an origami-type mechanism, and each roof forms a spherical four-bar with a single proper degree of freedom if regarded detached from the remaining circle. The roofs can rotate relative to each other about *implied edges* displayed as dot-dashed lines in fig. 6.8 b). After closing the cycle, the internal motion of each roof is locked, and the remaining loop L_0 hence becomes a simple 7R spatial loop with one proper degree of freedom.

The analysis will be demonstrated for a single roof embedded into the overall system. Due to the repetitive scheme, all bar, loop, and coupling labels are kept the same for each roof, and where necessary, are enumerated by roman numberings indicating the respective roof. In the first step, the topological graph is established, as shown in

fig. 6.9, such that precisely three multiple spherical joints $\hat{\mathcal{G}}_A$, $\hat{\mathcal{G}}_B$, and $\hat{\mathcal{G}}_C$ are associated with each roof while the corresponding uniform edge weights were omitted for better readability. The numbers 1 to 3 and 6 to 8 denote the upper and lower triplet of bars, and 4 and 5 denote the intermediate bars, respectively. Here, the succeeding roof is indicated by dashed, and the preceding roof by dotted lines. As the system cannot be further subdivided into open and closed kinematic chains, one can proceed with the establishment of a minimum cycle basis.

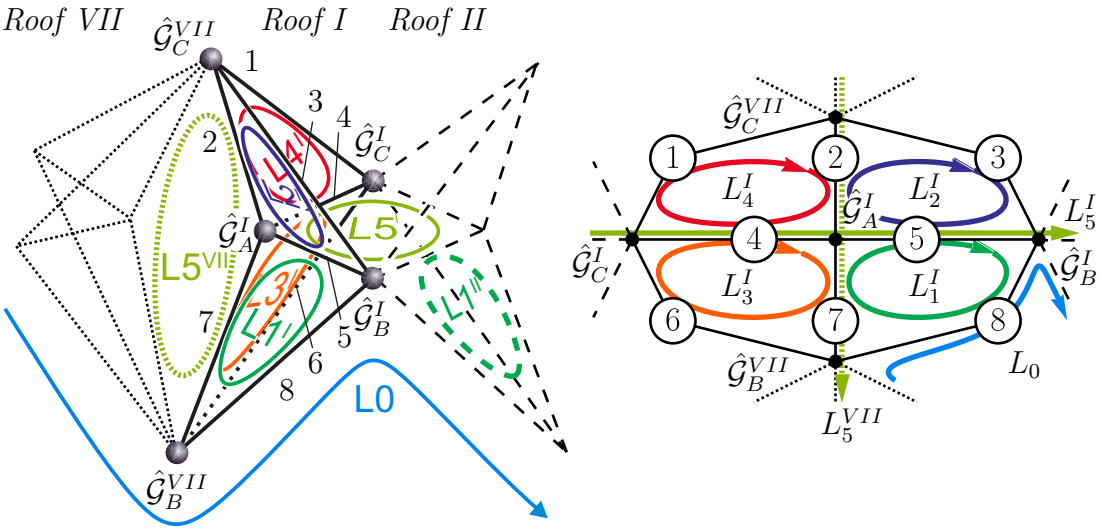

Figure 6.9: Topological graph for the embedded roof I

The total number of required loops is stated by eq. 2.3 to be $n_L = 91 - 56 + 1 = 36$, and one possible minimum cycle basis can be obtained in a way, that each roof features four triangular loops $L_1, ..., L_4$, seven quadrilateral loops L_5 in between the roofs, and a spanning loop L_0 which traverses through one bar of each roof. At Joint $\hat{\mathcal{G}}_C$, the number of incident loops is not sufficient to form any coupling conditions, such that this joint can directly be decomposed into binary spherical joints. The couplings arising at joints $\hat{\mathcal{G}}_A$ and $\hat{\mathcal{G}}_B$ are depicted in fig. 6.10.

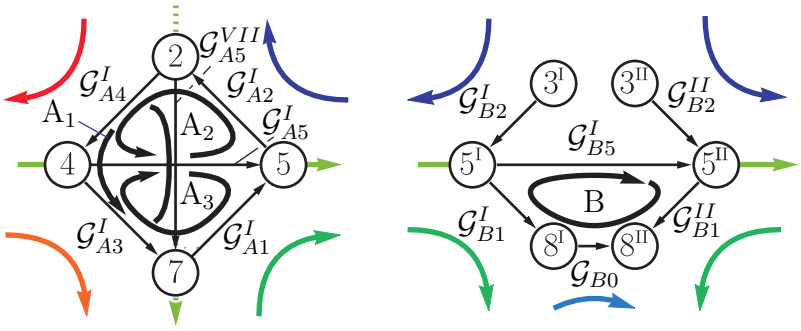

Figure 6.10: Resulting couplings A_1, A_2, A_3, and B at the embedded roof I

Notably, the three couplings A_1, A_2, and A_3 emerge at joint $\hat{\mathcal{G}}_A$, for which additionally the joint edges contributed by the involved loops form branchings, while at $\hat{\mathcal{G}}_B$ only a single coupling B results. Analogously to the previous example, each of these couplings gives rise to three coupling conditions. The next step consists of setting up the kinematic network and finding an appropriate solution flow.

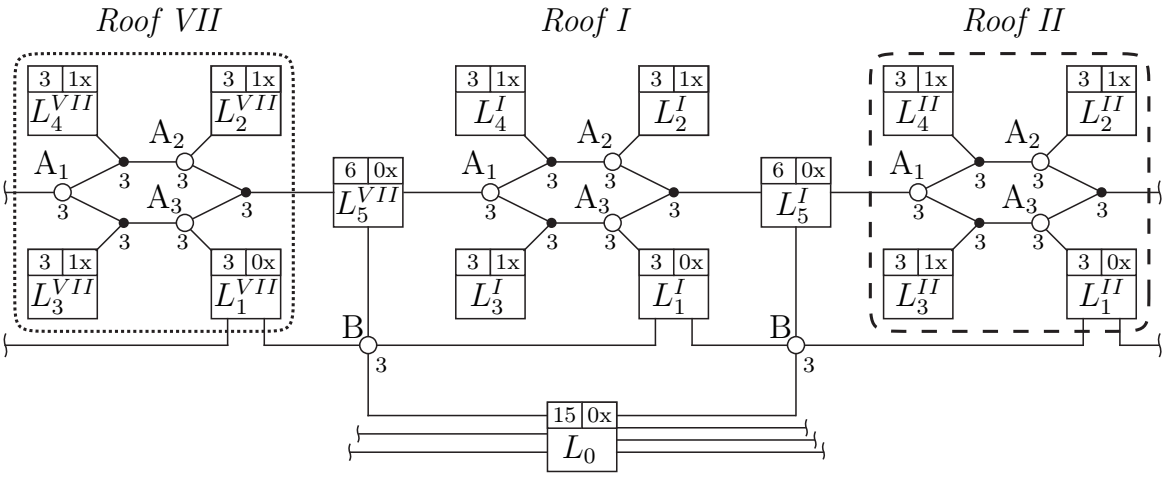

Figure 6.11: Undirected kinematic network of the seven-roof kinematic chain depicted for an embedded roof

Within the resulting kinematic network illustrated in fig. 6.11, loops $L_1, ..., L_4$ render three degrees of freedom each, L_5 renders six, and L_0 comprises 15 degrees of freedom, of which three, four, and seven can directly be associated with the spins of the involved bars, respectively. When searching for a recursive solution flow, first, the loops L_2, L_3, and L_4 are found not to be overdetermined if all internal edges were directed into these elements and thus will be prepended to the solution sequence. This directly brings A_2 as the next element, followed by A_1 and A_3 in that order. After the same order is found for all roofs analogously, there is only one unassigned edge incident to L_5 left, such that L_5 is prepended next, followed by B and consequently L_1. At last, only L_0 remains, which will be the first element within the topological order. At this point, the determined solution sequence actually appears to be potentially recursively solvable. Though, when traversing through the elements, identifying the additionally required external inputs, loops $L_2, ..., L_4$ are found to be overdetermined, as the aperture angle of the triangle transmitted through coupling A is already defined by the inner loops' geometry. The resulting oriented kinematic network with its external inputs is shown in fig. 6.12. Again, the network can be verified by summing up the degrees of freedom of all loops and subtracting the number of coupling conditions according to eq. 2.5 which yields $141 - 84 = 57$ degrees of freedom as determined before. On this basis, the

loop connection graph can be derived for the detection of rigid substructures.

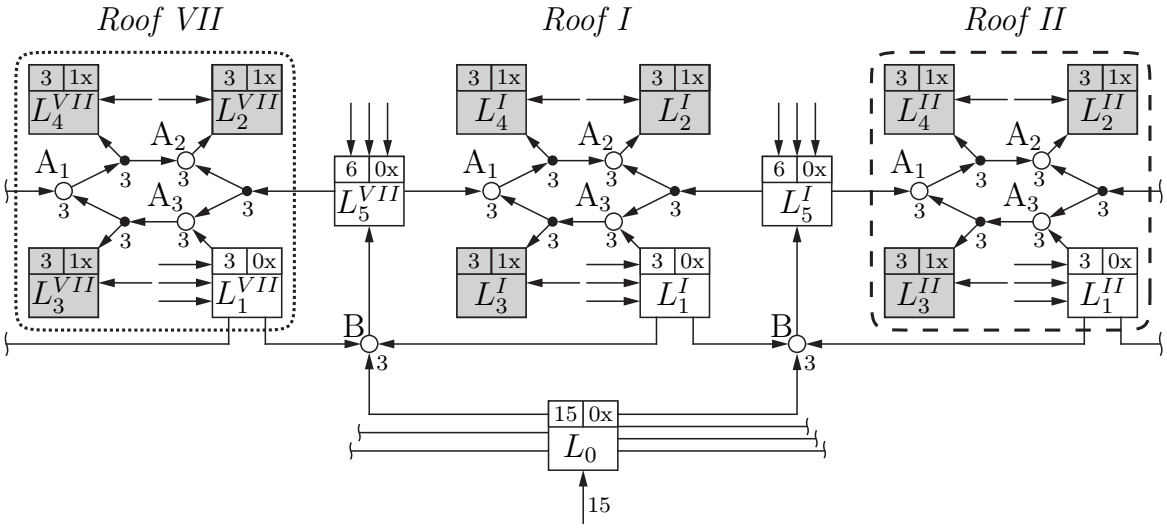

Figure 6.12: The directed kinematic network of the seven-roof kinematic chain depicted for an embedded roof

The dependencies among the elements of the kinematic network are depicted in the loop connection graph in fig. 6.13 a). Here, the subgraph shaded in gray highlights the elements associated with a single roof and the connections to its neighboring roofs. Of all possible directed cuts, in this case, two are of particular interest and will be further examined.

X_1, which separates the source node from the remaining graph, indicates the previously determined 57 degrees of freedom of the seven-roof determined through its cut weight of $w_{X_1} = 15 + 7 \cdot 9 = 78$ reduced by an absorbing degree of $d_{X_1} = 7 \cdot 3 = 21$. The proper degree of freedom of the system will be revealed after classifying the isolated degrees of freedom into fully and transmitted degrees of freedom. At this point, instead of providing an exhaustive list of locally isolated degrees of freedom, the tracking is explained by inspection, and the result for X_1 is shown in fig. 6.13 b). As each roof is comprised of eight bars that are able to spin freely between the spherical joints, there are eight fully isolated degrees of freedom that can be assigned for each roof. These fully isolated inputs will be assigned in order of occurrence within the topological order as follows. Starting with loop L_0, the isolated spin of bar 8 (compare fig. 6.9) can be classified as fully isolated. Following the solution sequence, the spin of the same bar is marked as transmitted in loop L_1, while the remaining two spins of bars 5 and 7 are registered again as fully isolated. Of the three external inputs for L_5, two correspond to spins of bar 2 within the two incident roofs and are marked as fully isolated. Indeed, the remaining input can be regarded as structurally isolated for L_5 between joints

$\hat{\mathcal{G}}_A$. However, it is clearly not isolated within the remaining system, and therefore, is marked as transmitted. The remaining loops L_3, L_4, and L_2 possess one bar not shared with any other loop, such that the corresponding spins are marked as fully isolated. As a result, the degree of freedom of X_1 omitting the isolated spins yields $f_{X_1} = (8 + 7 \cdot 2) - 7 \cdot 3 = 1$.

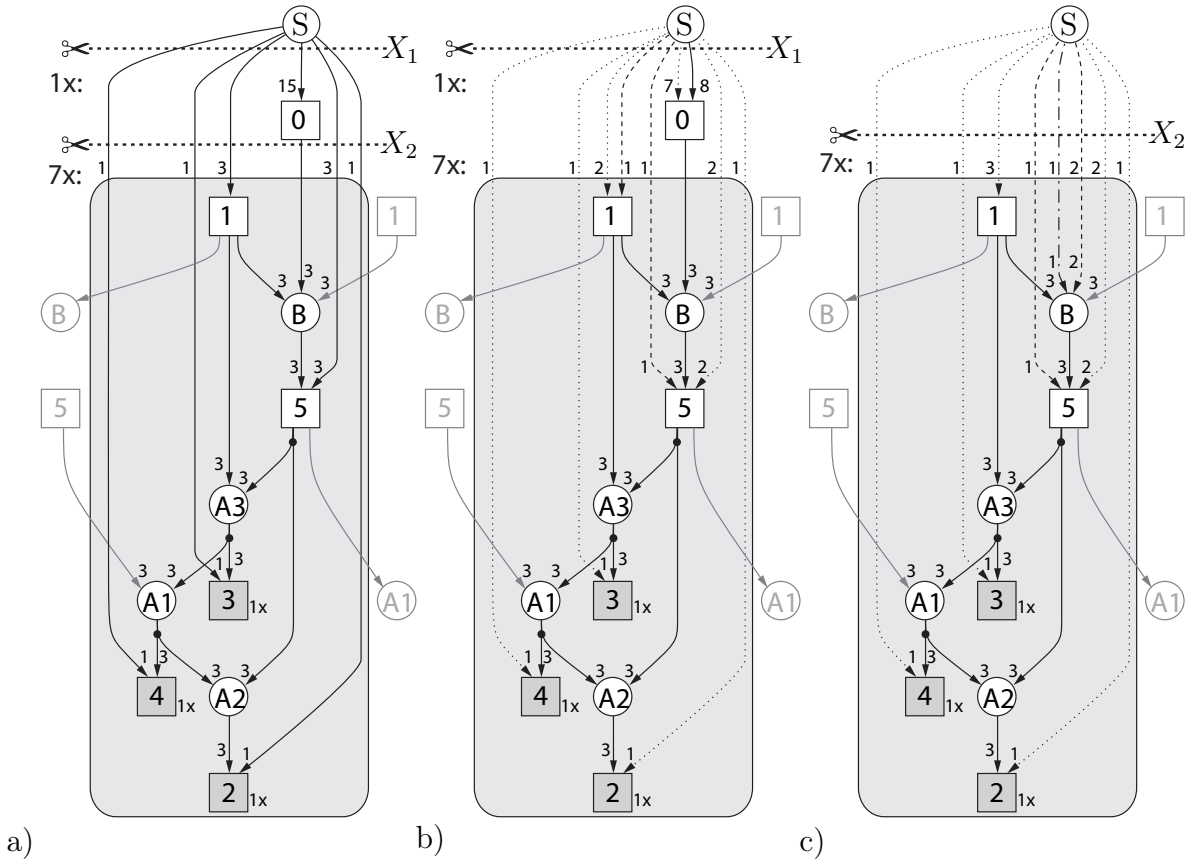

Figure 6.13: a) The loop connection graph of the seven-roof kinematic chain, b) for which cut X_1 yields one degree of freedom, and c) X_2 yields zero degrees of freedom

Though, it remains to detect that the embedded roofs form rigid substructures for which reason X_2 shown in fig. 6.13 c) will be analyzed. The classification of isolated degrees of freedom follows analogously to cut X_1, except that due to the absence of L_0, now the spin of bar 8 is registered as fully isolated for L_1. The case arising at coupling B will be inspected in more detail. Referring to fig. 6.10, coupling B receives $\mathcal{G}^I_{B1}$ and $\mathcal{G}^{II}_{B1}$ from loops L^I_1 and L^{II}_1 as inputs, such that in B according to sec. 5.2.1 a structurally isolated degree of freedom $f^{\text{iso}} : \{\mathcal{G}^I_{B5}, \mathcal{G}_{B0}\}$ with $f^{\text{iso(G)}} = S_B$ is detected: The rotation of the detached triangles formed by bars 5, 7, and 8 about joint $\hat{\mathcal{G}}_B$ leaves the internal kinematics of L^I_1 and L^{II}_1 invariant. However, within the coupled loop L^I_5 only the rotation about the implied edge between joints $\hat{\mathcal{G}}^I_B$ and $\hat{\mathcal{G}}^I_C$ is isolated, such

that by group intersection actually $f^{\mathrm{iso(G)}} = R_{\boldsymbol{B}\boldsymbol{e}_{\boldsymbol{C}},B}$ with $\mathtt{dim}(R_{\boldsymbol{B}\boldsymbol{e}_{\boldsymbol{C}},B}) = 1$. Thus, only one input for coupling B is marked as structurally isolated, while the remaining two inputs are transmitted. Now, omitting the fully and structurally isolated degrees of freedom, the degree of freedom of X_2 with a weight of $w_{X_2} = 7 \cdot 3 = 21$ and an equal absorbing degree of $d_{X_2} = 7 \cdot 3 = 21$ is zero and therefore indicates that the described subsystem containing the 7 individual roofs is rigid with isolated degrees of freedom. In Simroth et al. (2015b), the same conclusion was achieved for a different solution sequence for which L_0 was set as the most dependent element.

7 Summary and Outlook

Within the present work, a systematic approach for the detection of rigid subsystems with isolated degrees of freedom is presented, including some non-trivial cases featuring implied edges in kinematic chains. For this purpose, three new types of isolated degrees of freedom are introduced, which are tracked throughout the kinematic chain.

The approach is based on regarding a multibody system as a network of coupled kinematic loops acting as individual transmission elements. For determining the respective spatiality as well as an efficient solution to the kinematics of each of these elements, a method utilizing isotropy groups is provided, extending the approach of Kecskeméthy and Hiller (1992). By analysis of the topological graph associated with the kinematic chain, the system is dissected into components of closed kinematic chains. For each component, independent kinematic transmission elements are determined by finding a minimum cycle basis. To this end, multiple joints are considered as integral entities, which are afterward decomposed into linear or non-linear coupling conditions.

The resulting kinematic network forms the basis for detecting rigid subsystems and tracking isolated degrees of freedom. For each of its elements, isolated degrees of freedom are enumerated for which insights on the identification and transmission are elaborated, referring to displacement subgroups as presented initially in Hervé (1978). To this end, an automated method to associate joints represented by combinations of elementary joints to displacement subgroups is provided. By this means, isolated degrees of freedom of subsystems are classified according to the proposed types, whereby fully isolated degrees of freedom are disregarded for the detection of rigid subsystems. Subsystems in which all remaining degrees of freedom are locked, i. e., are determined by the subsystems' internal constraints such that they are constant over time, will be regarded as rigid, and are replaced by a single element. In this manner, overconstrained subsystems are resolved, and inconsistencies with respect to the classical degree of freedom counting rules can be overcome.

The method is successfully applied to two non-trivial examples of spherical-spherical bar systems of which one is overconstrained, and the other one is "nucleation-free," i. e., it contains rigid subsystems which are mobile if regarded independently but become rigid and form "implied hinges" when embedded in a specific system. By regarding a kinematic chain as a system of connected kinematic loops, subsystems of different spatiality can easily be mixed in a uniform way, and through the loop-wise consideration, the detection of implied edges is possible. As all properties and dimensions can be

managed symbolically, the solution does not depend on any numeric values.

However, even though many of the steps within the described procedure can be accomplished by standard graph-theoretic algorithms, others take more effort, for example, verifying if conditions for displacement subgroup inclusion are satisfied in case of non-trivial (non-rectilinear) characteristic directions. Also, some questions as the independence of the solution with respect to the choice of the cycle basis and respective solution sequence could not conclusively be answered and state indications for future research.

References

Abel, U. and Bicker, R. (1982). Determination of all minimal cut-sets between a vertex pair in an undirected graph. *IEEE Transactions on Reliability*, 2:167–171.

Agrawal, V. P. and Rao, J. S. (1987a). Fractionated freedom kinematic chains and mechanisms. *Mechanism and Machine Theory*, 22(2):125–130.

Agrawal, V. P. and Rao, J. S. (1987b). The mobility properties of kinematic chains. *Mechanism and Machine Theory*, 22(5):497–504.

Amaldi, E., Iuliano, C., Jurkiewicz, T., Mehlhorn, K., and Rizzi, R. (2009). Breaking the $O(m^2n)$ barrier for minimum cycle bases. In Fiat, A. and Sanders, P., editors, *Algorithms – ESA 2009*, volume 5757 of *Lecture Notes in Computer Science*, pages 301–312, Copenhagen, Denmark. Springer.

Angeles, J. (1982). *Spatial Kinematic Chains: Analysis Synthesis Optimization*. Springer, 1st edition.

Angeles, J. (1988). *Rational Kinematics*, volume 34 of *Springer Tracts in Natural Philosophy*. Springer.

Angeles, J. and Gosselin, C. (1988). Détermination du degré de liberté des chaines cinématique. *Transactions of the Canadian Society for Mechanical Engineering*, 12(4):219–226.

Artobolevskii, I. I. (1951). *Theory of Mechanisms and Machines (in Russian)*. Gosudarstv. Izdat. Tehn.-Teor.

Assur, L. V. (1913). Investigation of plane hinged mechanisms with lower pairs from the point of view of their structure and classification (in Russian): Part I, II. *Bulletin of the Petrograd Polytechnical Institute*, 20:329–386.

Bedi, D. and Chakraborty, B. (2018). Analyzing the rigidity of force networks in jammed granular packings. In *APS March Meeting Abstracts*, volume 63 of *APS Meeting Abstracts*, Los Angeles, United States. American Physics Society.

Berge, C. (1976). *Graphs and Hypergraphs*, volume 6 of *North-Holland Mathematical Library*. North-Holland Publishing Company, 2nd edition.

Berger, M. (2010). *Geometry Revealed: A Jacob's Ladder to Modern Higher Geometry*. Springer.

Bottema, O. and Roth, B. (1990). *Theoretical Kinematics*. Dover Publications.

Campos, A., Budde, C., and Hesselbach, J. (2008). A type synthesis method for hybrid robot structures. *Mechanism and Machine Theory*, 43(8):984–995.

Carretero, J. A., Podhorodeski, R. P., Nahon, M. A., and Gosselin, C. M. (2000). Kinematic analysis and optimization of a new three degree-of-freedom spatial parallel manipulator. *Journal of Mechanical Design*, 122(1):17–24.

Cayley, A. (1889). A theorem on trees. *Quarterly Journal of Mathematics*, 23:376–378.

Chebyshev, P. L. (1854). Théorie des mécanismes connus sous le nom de parallélogrammes, 2 éme partie. *Mémoires présentésa l'Académie impériale des sciences de Saint-Pétersbourg par divers savants*.

Cheng, J., Sitharam, M., and Streinu, I. (2009). Nucleation-free 3D rigidity. In *Proceedings of the 21st Annual Canadian Conference on Computational Geometry*, pages 71–74, Vancouver, Canada.

Chubynsky, M. V. and Thorpe, M. F. (2007). Algorithms for three-dimensional rigidity analysis and a first-order percolation transition. *Physical Review E*, 76(4):11–35.

Connelly, R. (2005). Generic global rigidity. *Discrete & Computational Geometry*, 33(4):549–563.

Crapo, H. (1990). On the generic rigidity of plane frameworks. Research Report RR-1278, Institut National de Recherche en Informatique et en Automatique.

Davies, T. H. (1983). Mechanical networks—II: Formulae for the degrees of mobility and redundancy. *Mechanism and Machine Theory*, 18(2):103–106.

Deo, N. (1974). *Graph Theory With Applications to Engineering and Computer Science*. Prentice-Hall.

Deo, N., Prabhu, G., and Krishnamoorthy, M. S. (1982). Algorithms for generating fundamental cycles in a graph. *ACM Transactions on Mathematical Software*, 8(1):26–42.

Diez-Martínez, C. R., Rico, J. M., Cervantes-Sanchez, J. J., and Gallardo, J. (2006). Mobility and connectivity in multiloop linkages. In Lennarčič, J. and Roth, B., editors, *Advances in Robot Kinematics*, pages 455–464. Springer.

Ding, H. (2015). *Automatic Structural Synthesis of Planar Mechanisms and its Application to Creative Design*. Doctoral dissertation, Universität Duisburg-Essen, Duisburg, Germany.

Ding, H., Huang, Z., and Mu, D. (2008). Computer-aided structure decomposition theory of kinematic chains and its applications. *Mechanism and Machine Theory*, 43(12):1596–1609.

Ding, H., Yang, W., Huang, P., Ma, L., and Kecskeméthy, A. (2013). Generation of planar kinematic chains with one multiple joint. In *Proceedings of the ASME 2013 IDETC/CIEC: 37th Mechanisms and Robotics Conference*, volume 6A of *International Design Engineering Technical Conferences and Computers and Information in Engineering Conference*, page V06AT07A053, Portland, United States. American Society of Mechanical Engineers.

Dong, C., Liu, H., Yue, W., and Huang, T. (2018). Stiffness modeling and analysis of a novel 5-dof hybrid robot. *Mechanism and Machine Theory*, 125:80–93.

Fanghella, P. (1988). Kinematics of spatial linkages by group algebra: A structure-based approach. *Mechanism and Machine Theory*, 23(3):171–183.

Fanghella, P. and Galletti, C. (1994). Mobility analysis of single-loop kinematic chains: An algorithmic approach based on displacement groups. *Mechanism and Machine Theory*, 29(8):1187–1204.

Farre, J., Kleinschmidt, H., Sidman, J., St. John, A., Stark, S., Theran, L., and Yu, X. (2016). Algorithms for detecting dependencies and rigid subsystems for CAD. *Computer Aided Geometric Design*, 47:130–149.

Feng, S. and Sen, P. N. (1984). Percolation on elastic networks: New exponent and threshold. *Physical Review Letters*, 52(3):216–219.

Foufou, S. and Michelucci, D. (2012). Interrogating witnesses for geometric constraint solving. *Information and Computation*, 216:24–38. Special Issue: 8th Conference on Real Numbers and Computers.

Fowler, P. W. and Guest, S. D. (2002). Symmetry analysis of the double banana and related indeterminate structures. In Drew, H. R. and Pellegrino, S., editors, *New Approaches to Structural Mechanics, Shells and Biological Structures*, volume 104 of *Solid Mechanics and its Applications*, pages 91–100. Springer.

Franzblau, D. (2000). Generic rigidity of molecular graphs via ear decomposition. *Discrete Applied Mathematics*, 101(1):131–155.

Gabow, H. N. and Westermann, H. H. (1992). Forests, frames, and games: Algorithms for matroid sums and applications. *Algorithmica*, 7(5):465–497.

Gogu, G. (2005). Mobility of mechanisms: A critical review. *Mechanism and Machine Theory*, 40(9):1068–1097.

Gogu, G. (2008). *Structural Synthesis of Parallel Robots Part 1: Methodology*, volume 149 of *Solid Mechanics and its Applications*. Springer.

Gondran, M. and Minoux, M. (1984). *Graphs and Algorithms*. Wiley-interscience series in discrete mathematics. John Wiley & Sons.

Gronowicz, A. (1981). Identifizierungsmethode der Zwanglaufbedingungen von kinematischen Ketten. *Mechanism and Machine Theory*, 16(2):127–135.

Grübler, M. (1883). Allgemeine Eigenschaften der zwangläufigen ebenen kinematischen Ketten: I. *Civilingenieur*, 29:167–200.

Grübler, M. (1917). *Getriebelehre: Eine Theorie des Zwanglaufes und der ebenen Mechanismen*. Springer.

Haller, K., John, A. L.-S., Sitharam, M., Streinu, I., and White, N. (2012). Body-and-cad geometric constraint systems. *Computational Geometry*, 45(8):385–405.

Hariharan, R., Kavitha, T., and Mehlhorn, K. (2006). A faster deterministic algorithm for minimum cycle bases in directed graphs. In Bugliesi, M., Preneel, B., Sassone, V., and Wegener, I., editors, *Automata, Languages and Programming: 33rd International Colloquium, ICALP 2006*, pages 250–261, Venice, Italy. Springer.

Hendrickson, B. (1992). Conditions for unique graph realizations. *SIAM Journal on Computing*, 21(1):65–84.

Hervé, J. M. (1978). Analyse structurelle des mécanismes par groupe des déplacements. *Mechanism and Machine Theory*, 13(4):437–450.

Hervé, J. M. (1992). Group mathematics and parallel link mechanisms. In *Proceedings of the IMACS SICE International Symposium on Robotics, Mechatronics and Manufacturing Systems*, pages 459–464, Kobe, Japan. International Association for Mathematics and Computers in Simulation.

Hervé, J. M. (1999). The Lie group of rigid body displacements, a fundamental tool for mechanism design. *Mechanism and Machine Theory*, 34(5):719–730.

Hilgert, J. and Neeb, K.-H. (2012). *Structure and Geometry of Lie Groups*. Springer Monographs in Mathematics. Springer.

Hiller, M. and Anantharaman, M. (1989). Systematische Strukturierung der Bindungsgleichungen mehrschleifiger Mechanismen. *Journal for Applied Mathematics and Mechanics*, 69(5):303–305.

Hiller, M. and Kecskeméthy, A. (1989). Equations of motion of complex multibody systems using kinematical differentials. *Transactions of the Canadian Society for Mechanical Engineering*, 13(4):113–121.

Hiller, M., Kecskeméthy, A., and Woernle, C. (1986). A loop-based kinematical analysis of spatial mechanisms. ASME paper 86-DET-184. In *Proceedings of the 19th Biennial ASME Mechanisms Conference*, Columbus, United States. American Society of Mechanical Engineers.

Hiller, M. and Woernle, C. (1988). The characteristic pair of joints – an effective approach for the inverse kinematic problem of robots. In *Proceedings of the 1988 IEEE International Conference on Robotics and Automation*, pages 846–851, Los Alamitos, United States. Institute of Electrical and Electronics Engineers Computer Society.

Horton, J. D. (1987). A polynomial-time algorithm to find the shortest cycle basis of a graph. *SIAM Journal on Computing*, 16(2):358–366.

Hsu, K. S., Karkoub, M., Tsai, M.-C., and Her, M. G. (2004). Modelling and index analysis of a delta-type mechanism. *Proceedings of the Institution of Mechanical Engineers, Part K: Journal of Multi-body Dynamics*, 218(3):121–132.

Hunt, K. H. (1978). *Kinematic Geometry of Mechanisms*. The Oxford Engineering Science Series. Clarendon Press.

Hwang, W.-M. and Hwang, Y.-W. (1991). An algorithm for the detection of degenerate kinematic chains. *Mathematical and Computer Modelling*, 15(11):9–15.

Imai, H. (1985). On combinatorial structures of line drawings of polyhedra. *Discrete Applied Mathematics*, 10(1):79–92.

Ionescu, T. (2003). Terminology for mechanisms and machine science. *Mechanism and Machine Theory*, 38(7):597–1111.

Isaksson, M., Eriksson, A., Watson, M., Brogårdh, T., and Nahavandi, S. (2015). A method for extending planar axis-symmetric parallel manipulators to spatial mechanisms. *Mechanism and Machine Theory*, 83:1–13.

Jackson, B. and Jordán, T. (2005). Connected rigidity matroids and unique realizations of graphs. *Journal of Combinatorial Theory, Series B*, 94(1):1–29.

Jackson, B. and Owen, J. C. (2016). A characterisation of the generic rigidity of 2-dimensional point–line frameworks. *Journal of Combinatorial Theory, Series B*, 119:96–121.

Jacobs, D. J. and Hendrickson, B. (1997). An algorithm for two dimensional rigidity percolation: The pebble game. *Journal of Computational Physics*, 137(2):346–365.

Jacobs, D. J., Kuhn, L. A., and Thorpe, M. F. (2002). Flexible and rigid regions in proteins. In Thorpe, M. F. and Duxbury, P., editors, *Rigidity Theory and Applications*, Fundamental Materials Research, pages 357–384. Springer.

Jacobs, D. J., Rader, A. J., Kuhn, L. A., and Thorpe, M. F. (2001). Protein flexibility predictions using graph theory. *Proteins: Structure, Function, and Bioinformatics*, 44(2):150–165.

Jain, A. and Rodriguez, G. (1993). An analysis of the kinematics and dynamics of underactuated manipulators. *IEEE Transactions on Robotics and Automation*, 9(4):411–422.

Jinkui, C. and Weiqing, C. (1998). Systemics of Assur groups with multiple joints. *Mechanism and Machine Theory*, 33(8):1127–1133.

Kaveh, A. and Roosta, G. R. (1994). Revised greedy algorithm for formation of a minimal cycle basis of a graph. *Communications in Numerical Methods in Engineering*, 10(7):523–530.

Kavitha, T., Liebchen, C., Mehlhorn, K., Michail, D., Rizzi, R., Ueckerdt, T., and Zweig, K. A. (2009). Cycle bases in graphs characterization, algorithms, complexity, and applications. *Computer Science Review*, 3(4):199–243.

Kavitha, T., Mehlhorn, K., Michail, D., and Paluch, K. (2004). A faster algorithm for minimum cycle basis of graphs. In Díaz, J., Karhum aki, J., Lepist o, A., and

Sannella, D., editors, *Automata, Languages and Programming: 31st International Colloquium, ICALP 2004*, volume 3142 of *Lecture Notes in Computer Science*, pages 846–857, Turku, Finland. Springer.

Kecskeméthy, A. (1993a). *Objektorientierte Modellierung der Dynamik von Mehrkörpersystemen mit Hilfe von Übertragungselementen*, volume 88 of *Fortschritt-Berichte VDI Reihe 20, Rechnerunterstützte Verfahren*. VDI-Verlag.

Kecskeméthy, A. (1993b). On closed form solutions of multiple-loop mechanisms. In Angeles, J., Hommel, G., and Kovács, P., editors, *Computational Kinematics*, volume 28 of *Solid Mechanics and its Applications*, pages 263–274. Springer.

Kecskeméthy, A. and Hiller, M. (1992). Automatic closed-form kinematics-solutions for recursive single-loop chains. In Kinzel, G. L., editor, *Proceedings of the 22nd Biennial ASME Mechanisms Conference on Flexible Mechanisms, Dynamics, and Analysis*, volume 47, pages 387–393, Scottsdale, United States. American Society of Mechanical Engineers.

Kecskeméthy, A., Krupp, T., and Hiller, M. (1997). Symbolic processing of multiloop mechanism dynamics using closed-form kinematics solutions. *Multibody System Dynamics*, 1(1):23–45.

Kitson, D. and Power, S. C. (2018). The rigidity of infinite graphs. *Discrete & Computational Geometry*, 60(3):531–557.

Kosmann-Schwarzbach, Y. (2010). *Groups and Symmetries: From Finite Groups to Lie Groups*. Universitext. Springer.

Kramer, G. A. (1992). *Solving Geometric Constraint Systems: A Case Study in Kinematics*. Artificial Intelligence Series. MIT Press.

Krupp, T. D. (1999). *Symbolische Gleichungen für Mehrkörpersysteme mit kinematischen Schleifen*. Berichte aus der Softwaretechnik. Shaker Verlag.

Kruskal, J. B. (1956). On the shortest spanning subtree of a graph and the traveling salesman problem. *Proceedings of the American Mathematical Society*, 7(1):48–50.

Kutzbach, K. (1929). Mechanische Leitungsverzweigung, ihre Gesetze und Anwendungen. *Maschinenbau*, 8(21):710–716.

Laman, G. (1970). On graphs and rigidity of plane skeletal structures. *Journal of Engineering Mathematics*, 4(4):331–340.

Lee, A. (2008). *Geometric Constraint Systems With Applications in CAD and Biology*. Doctoral dissertation, University of Massachusetts Amherst, Amherst, United States.

Lee, C.-C. and Hervé, J. M. (2002). Discontinuous mobility of one family of spatial 6R mechanisms through the group algebraic structure of displacement set. In Howell, L. L., editor, *Proceedings of the ASME 2002 DETC/CIEC: 27th Biennial Mechanisms and Robotics Conference*, volume 5 of *International Design Engineering Technical Conferences and Computers and Information in Engineering Conference*, pages 645–653, Montreal, Canada. American Society of Mechanical Engineers.

Lee, H.-J. and Yoon, Y.-S. (1992). Detection of rigid structure in enumerating basic kinematic chain by sequential removal of binary link string. *JSME International Journal*, 35(4):647–651.

Lee-St. John, A. and Sidman, J. (2013). Combinatorics and the rigidity of CAD systems. *Computer-Aided Design*, 45(2):473–482.

Liu, H., Huang, T., Kecskeméthy, A., and Chetwynd, D. G. (2014). A generalized approach for computing the transmission index of parallel mechanisms. *Mechanism and Machine Theory*, 74:245–256.

Liu, H., Kecskeméthy, A., and Huang, T. (2017). An automatic approach for identification of natural reciprocal screw systems of serial kinematic chains based on the invariance properties matrix. *Mechanism and Machine Theory*, 107:352–368.

Manolescu, N. I. (1979). A unified method for the formation of all planar jointed kinematic chains and baranov trusses. *Environment and Planning B: Planning and Design*, 6(4):447–454.

Manolescu, N. I. and Manafu, V. (1963). Sur la détermination du degré de mobilité des mécanismes. *Bulletin of the Polytechnical Institute Bucharest*, 25:45–66.

Maxwell, J. C. (1864). XLV. On reciprocal figures and diagrams of forces. *Philosophical Magazine and Journal of Science*, 27(182):250–261.

Mazzone, A., Spagno, C., and Kunz, A. (2003). A haptic feedback device based on an active mesh. In *Proceedings of the ACM Symposium on Virtual Reality Software and Technology*, pages 188–195, Osaka, Japan. Association for Computing Machinery.

Meng, J., Liu, G., and Li, Z. (2007). A geometric theory for analysis and synthesis of sub-6 DOF parallel manipulators. *IEEE Transactions on Robotics*, 23(4):625–649.

Merlet, J.-P. (2005a). Jacobian, manipulability, condition number, and accuracy of parallel robots. *Journal of Mechanical Design*, 128(1):199–206.

Merlet, J.-P. (2005b). Kinematics and synthesis of cams-coupled parallel robots. In Ceccarelli, M., editor, *Proceedings of CK2005, International Workshop on Computational Kinematics*, Cassino, Italy. International Federation for the Promotion of Mechanism and Machine Science.

Merlet, J.-P. (2006). *Parallel Robots*, volume 128 of *Solid Mechanics and its Applications*. Springer, 2nd edition.

Michelucci, D. and Foufou, S. (2006). Geometric constraint solving: The witness configuration method. *Computer-Aided Design*, 38(4):284–299.

Mitsi, S., Bouzakis, K.-D., Mansour, G., and Popescu, I. (2003). Position analysis in polynomial form of planar mechanisms with assur groups of class 3 including revolute and prismatic joints. *Mechanism and Machine Theory*, 38(12):1325–1344.

Moinet, M., Mandil, G., and Serre, P. (2014). Defining tools to address over-constrained geometric problems in computer aided design. *Computer-Aided Design*, 48:42–52.

Moroskine, Y. F. (1954). General analysis of the theory of mechanisms. *Teorii Masini Mekhanizmov*, 14:25–50.

Moukarzel, C. (1996). An efficient algorithm for testing the generic rigidity of graphs in the plane. *Journal of Physics A: Mathematical and General*, 29(24):8079–8098.

Müller, A. (2007). Generic mobility of rigid body mechanisms: On the existence of overconstrained mechanisms. In *Proceedings of the ASME 2007 IDETC/CIEC: 31st Mechanisms and Robotics Conference, Parts A and B*, volume 8 of *International Design Engineering Technical Conferences and Computers and Information in Engineering Conference*, pages 457–465, Las Vegas, United States. American Society of Mechanical Engineers.

Müller, A. and Maißer, P. (2003). A Lie-group formulation of kinematics and dynamics of constrained MBS and its application to analytical mechanics. *Multibody System Dynamics*, 9(4):311–352.

Nixon, A., Schulze, B., Sljoka, A., and Whiteley, W. (2014). Symmetry adapted Assur decompositions. *Symmetry*, 6(3):516–550.

Orin, D. E. and Schrader, W. W. (1984). Efficient computation of the Jacobian for robot manipulators. *The International Journal of Robotics Research*, 3(4):66–75.

Pennock, G. R. and Kamthe, G. M. (2006). Study of dead-centre positions of single-degree-of-freedom planar linkages using Assur kinematic chains. *Journal of Mechanical Engineering Science*, 220(7):1057–1074.

Phillips, J. (1984). *Freedom in Machinery: Introducing Screw Theory*, volume 1. Cambridge University Press.

Prim, R. C. (1957). Shortest connection networks and some generalizations. *The Bell System Technical Journal*, 36(6):1389–1401.

Razmara, N., Kohli, D., and Dhingra, A. K. (2000). On the degrees of freedom of motion of planar-spatial mechanisms. In Wang, Y. M., Kazmer, D., and Regli, W. C., editors, *Proceedings of the ASME 2000 IDETC/CIEC: 5th Design for Manufacturing Conference*, volume 7 of *International Design Engineering Technical Conferences and Computers and Information in Engineering Conference*, Baltimore, United States. American Society of Mechanical Engineers.

Renaud, M. (1981). Geometric and kinematic models of a robot manipulator: Calculation of the Jacobian matrix and its inverse. In *Proceedings of the 11th International Symposium on Industrial Robots*, pages 757–763, Tokio, Japan. Japan Robot Association.

Reuleaux, F. (1875). *Theoretische Kinematik: Grundzüge einer Theorie des Maschinenwesens*, volume 1 of *Lehrbuch der Kinematik*. Vieweg Verlag.

Rico Martínez, J. M., Gallardo, J., and Ravani, B. (2003). Lie algebra and the mobility of kinematic chains. *Journal of Robotic Systems*, 20(8):477–499.

Rico Martínez, J. M. and Ravani, B. (2003). On mobility analysis of linkages using group theory. *Journal of Mechanical Design*, 125(1):70–80.

Rico Martínez, J. M. and Ravani, B. (2004). Mobility of spatial multi-loop and mixed linkages. In Lenarčič, J. and Galletti, C., editors, *On Advances in Robot Kinematics*, pages 133–142. Springer.

Rojas, N. and Thomas, F. (2012). On closed-form solutions to the position analysis of Baranov trusses. *Mechanism and Machine Theory*, 50:179–196.

Rojas, N. and Thomas, F. (2013). The closure condition of the double banana and its application to robot position analysis. In *Proceedings of the IEEE International Conference on Robotics and Automation*, pages 4641–4646, Karlsruhe, Germany. Institute of Electrical and Electronics Engineers.

Rolland, L. (1999). The Manta and the Kanuk: Novel 4-dof parallel mechanisms for industrial handling. In *Proceedings of ASME Dynamic Systems and Control Division IMECE*, volume 99, pages 831–844, Nashville, United States. American Society of Mechanical Engineers.

Samin, J.-C. and Fisette, P. (2003). *Symbolic Modeling of Multibody Systems*, volume 112 of *Solid Mechanics and its Applications*. Springer.

Sarrus, P. T. (1853). Note sur la transformation des mouvements rectilignes alternatifs, en mouvements circulaires: Et réciproquement. *Comptes Rendus des Séances de l'Académie des Sciences de Paris*, 36:1036–1038.

Schmidt, J. M. (2013). A simple test on 2-vertex-and 2-edge-connectivity. *Information Processing Letters*, 113(7):241–244.

Servatius, B. and Servatius, H. (2010). Rigidity, global rigidity, and graph decomposition. *European Journal of Combinatorics*, 31(4):1121–1135.

Servatius, B., Shai, O., and Whiteley, W. (2010a). Combinatorial characterization of the Assur graphs from engineering. *European Journal of Combinatorics*, 31(4):1091–1104.

Servatius, B., Shai, O., and Whiteley, W. (2010b). Geometric properties of Assur graphs. *European Journal of Combinatorics*, 31(4):1105–1120.

Shai, O. and Müller, A. (2013). A novel combinatorial algorithm for determining the generic/topological mobility of planar and spherical mechanisms. In *Proceedings of ASME 2013 IDETC/CIEC: 37th Mechanisms and Robotics Conference*, volume 6B of *International Design Engineering Technical Conferences and Computers and Information in Engineering Conference*, Portland, United States. American Society of Mechanical Engineers.

Shai, O., Sljoka, A., and Whiteley, W. (2013). Directed graphs, decompositions, and spatial linkages. *Discrete Applied Mathematics*, 161(18):3028–3047.

Sharma, C. S. and Purohit, K. (2006). *Theory of Mechanisms and Machines*. Prentice-Hall of India.

Shigley, J. E. and Uicker, J. J. (1995). *Theory of Machines and Mechanisms*. McGraw-Hill, 2nd edition.

Shiriaev, A. S., Freidovich, L. B., and Gusev, S. V. (2010). Transverse linearization for controlled mechanical systems with several passive degrees of freedom. *IEEE Transactions on Automatic Control*, 55(4):893–906.

Simroth, F., Ding, H., and Kecskeméthy, A. (2015a). Detecting rigid substructures in spatial nucleation free spherical-spherical bar mechanisms based on kinematical loops. In *Proceedings of the First IFToMM DA-CH Conference*, pages 68–69, Dortmund, Germany. International Federation for the Promotion of Mechanism and Machine Science.

Simroth, F., Ding, H., and Kecskeméthy, A. (2015b). A loop-based approach for the detection of rigid substructures in spatial nucleation-free spherical-spherical bar mechanisms. In *Proceedings of the 14th IFToMM World Congress*, pages 382–391, Taipei, Taiwan. International Federation for the Promotion of Mechanism and Machine Science.

Simroth, F., Ding, H., and Kecskeméthy, A. (2015c). A novel, loop-based approach for rigidity detection for systems with multiple spherical–spherical bars: The "double-banana" case. In Flores, P. and Viadero, F., editors, *New Trends in Mechanism and Machine Science*, volume 24 of *Mechanisms and Machine Science*, pages 91–98. Springer.

Simroth, F., Ding, H., and Kecskeméthy, A. (2016). Solving the double-banana rigidity problem: A loop-based approach. *Mechanical Sciences*, 7(1):107–117.

Sljoka, A., Shai, O., and Whiteley, W. (2011). Checking mobility and decomposition of linkages via pebble game algorithm. In *Proceedings of the ASME 2011 IDETC/CIEC: 35th Mechanisms and Robotics Conference, Parts A and B*, volume 6 of *International Design Engineering Technical Conferences and Computers and Information in Engineering Conference*, pages 493–502, Washington, United States. American Society of Mechanical Engineers.

Somov, P. O. (1887). On the degree of freedom of the motion of kinematic chains (in Russian). *Russian Journal of Physical Chemistry*, 19(9):7–25.

Stelzle, W., Kecskeméthy, A., and Hiller, M. (1995). A comparative study of recursive methods. *Archive of Applied Mechanics*, 66(1):9–19.

Sugihara, K. (1980). On redundant bracing in plane skeletal structures. *Bulletin of the Electrotechnical Laboratory*, 44(5):376–386.

Sunkari, R. P. (2006). *Structural Synthesis and Analysis of Planar and Spatial Mechanisms Satisfying Grübler's Degrees of Freedom Equation*. Doctoral dissertation, University of Maryland, College Park, United States.

Sunkari, R. P. and Schmidt, L. C. (2005). Critical review of existing degeneracy testing and mobility type identification algorithms for kinematic chains. In *Proceedings of the ASME 2005 IDETC/CIEC: 29th Mechanisms and Robotics Conference, Parts A and B*, volume 7 of *International Design Engineering Technical Conferences and Computers and Information in Engineering Conference*, pages 255–263, Long Beach, United States. American Society of Mechanical Engineers.

Sylvester, J. J. (1875). On recent discoveries in mechanical conversion of motion. *Van Nostrand's Eclectic Engineering Magazine*, 12(76):313–321.

Tarjan, R. E. (1972). Depth-first search and linear graph algorithms. *SIAM Journal on Computing*, 1(2):146–160.

Tarjan, R. E. (1974). A note on finding the bridges of a graph. *Information Processing Letters*, 2(6):160–161.

Tay, T.-S. (1984). Rigidity of multi-graphs. I. Linking rigid bodies in n-space. *Journal of Combinatorial Theory, Series B*, 36(1):95–112.

Thomas, F. and Torras, C. (1988). A group-theoretic approach to the computation of symbolic part relations. *IEEE Journal on Robotics and Automation*, 4(6):622–634.

Thorpe, M. F. (1985). Rigidity percolation in glassy structures. *Journal of Non-Crystalline Solids*, 76(1):109–116.

Togashi, J., Matsuda, T., and Mitobe, K. (2014). A low cost and lightweight wire driven robot arm by using elastic strings. In *Proceedings of the 2014 IEEE/SICE International Symposium on System Integration*, pages 436–440, Tokyo, Japan. Institute of Electrical and Electronics Engineers.

Tsai, L.-W. (2001). *Mechanism Design: Enumeration of Kinematic Structures According to Function*. Mechanical Engineering Series. CRC Press LLC.

Tuttle, E. R. (1996). Generation of planar kinematic chains. *Mechanism and Machine Theory*, 31(6):729–748.

Voinea, R. and Atanasiu, M. (1960). Contribution á l'étude de la structure des chaines cinématiques. *Bulletin of the Polytechnical Institute Bucharest*, 21(1):29–77.

Waldron, K. J. (1973). A study of overconstrained linkage geometry by solution of closure equations – Part 1. Method of study. *Mechanism and Machine Theory*, 8(1):95–104.

Waldron, K. J. (1982). Geometrically based manipulator rate control algorithms. *Mechanism and Machine Theory*, 17(6):379–385.

Wang, J. and Gosselin, C. M. (1998). Kinematic analysis and singularity loci of spatial four-degree-of-freedom parallel manipulators using a vector formulation. *Journal of Mechanical Design*, 120(4):555–558.

Whiteley, W. (2005). Counting out to the flexibility of molecules. *Physical Biology*, 2(4):116–126.

Wittenburg, J. (2008). *Dynamics of Multibody Systems*. Springer, 2nd edition.

Woernle, C. (1988). *Ein systematisches Verfahren zur Aufstellung der geometrischen Schließbedingungen in kinematischen Schleifen mit Anwendung bei der Rückwärtstransformation für Industrieroboter*, volume 59 of *Fortschritt-Berichte VDI; Reihe 18, Mechanik/Bruchmechanik*. VDI-Verlag.

Woernle, C. (2016). *Mehrkörpersysteme: Eine Einführung in die Kinematik und Dynamik von Systemen starrer Körper*. Springer, 2nd edition.

Wolfram Research, Inc. (2019). Mathematica, version 12.0.

Xia, S., Ding, H., and Kecskeméthy, A. (2012). A loop-based approach for rigid subchain identification in general mechanisms. In Lenarčič, J. and Husty, M., editors, *Latest Advances in Robot Kinematics*, pages 19–26. Springer.

Yan, H.-S. and Hsu, C.-H. (1988). Contracted graphs of kinematic chains with multiple joints. *Mathematical and Computer Modelling*, 10(9):681–695.

Yang, D.-C., Xiong, J., and Yang, X.-D. (2008). A simple method to calculate mobility with Jacobian. *Mechanism and Machine Theory*, 43(9):1175–1185.

Yang, T.-L., Liu, A.-X., Shen, H.-P., Luo, Y.-F., Hang, L.-B., and Jin, Q. (2015). Composition principle based on SOC unit and coupling degree of BKC for general spatial mechanisms. In *Proceedings of the 14th IFToMM World Congress*, pages

437–446, Taipei, Taiwan. International Federation for the Promotion of Mechanism and Machine Science.

DOI: 10.17185/duepublico/73524
URN: urn:nbn:de:hbz:464-20201210-155357-7